

Environmental Impact of New Chemical Agents for Fire Suppression

Robert E. Huie

Physical & Chemical Properties Division
National Institute of Standards & Technology
Gaithersburg, MD 20899-8381

Final Report

Sponsored by:

The Department of Defense
Strategic Environmental Research and Development Program
MIPR Number W74RDV73243630

“The views and conclusions contained in this document are those of the authors and should not be interpreted as representing the official policies, either expressed or implied, of the Strategic Environmental Research and Development Program, the National Institute of Standards & Technology, or any other part of the U. S. Government.”

DISTRIBUTION STATEMENT A
Approved for Public Release
Distribution Unlimited

20031121 109

REPORT DOCUMENTATION PAGE

Form Approved
OMB No. 0704-0188

The public reporting burden for this collection of information is estimated to average 1 hour per response, including the time for reviewing instructions, searching existing data sources, gathering and maintaining the data needed, and completing and reviewing the collection of information. Send comments regarding this burden estimate or any other aspect of this collection of information, including suggestions for reducing the burden, to Department of Defense, Washington Headquarters Services, Directorate for Information Operations and Reports (0704-0188), 1215 Jefferson Davis Highway, Suite 1204, Arlington, VA 22202-4302. Respondents should be aware that notwithstanding any other provision of law, no person shall be subject to any penalty for failing to comply with a collection of information if it does not display a currently valid OMB control number.

PLEASE DO NOT RETURN YOUR FORM TO THE ABOVE ADDRESS.

1. REPORT DATE (DD-MM-YYYY) 28-08-2003		2. REPORT TYPE Final		3. DATES COVERED (From - To) October 1997 - August 2002	
4. TITLE AND SUBTITLE Environmental Impact of New Chemical Agents for Fire Suppression 4B/3/8901				5a. CONTRACT NUMBER W74RDV73243630	
				5b. GRANT NUMBER	
				5c. PROGRAM ELEMENT NUMBER	
6. AUTHOR(S) Robert E. Huie				5d. PROJECT NUMBER	
				5e. TASK NUMBER	
				5f. WORK UNIT NUMBER	
7. PERFORMING ORGANIZATION NAME(S) AND ADDRESS(ES) National Institute of Standards and Technology Stop 8381 Gaithersburg, MD 20899-8381				8. PERFORMING ORGANIZATION REPORT NUMBER	
9. SPONSORING/MONITORING AGENCY NAME(S) AND ADDRESS(ES) Department of Defense Strategic Environmental Research and Development Office 901 North Stuart Street, Suite 303 Arlington, Virginia 22203				10. SPONSOR/MONITOR'S ACRONYM(S) SERDP	
				11. SPONSOR/MONITOR'S REPORT NUMBER(S)	
12. DISTRIBUTION/AVAILABILITY STATEMENT Unlimited					
13. SUPPLEMENTARY NOTES					
14. ABSTRACT The environmental impact of chemical agents is intimately tied to the environmental transformations these chemicals undergo. In this project, the most important transformations for various classes of proposed fire suppression agents were investigated and, for the important case of hydrogen abstraction by hydroxyl radicals, a computational screening tool was developed. Rate constants for hydroxyl radical reactions with hydrofluoroethers, perfluorinated alkenes, bromine-containing fluoroalkenes and fluoroalkanes, were determined. By using the computational tool developed in the project, rate constants and atmospheric lifetimes for several bromine-containing halomethanes were calculated. In addition, the reactivity of several alkyl phosphates with free radicals in water were measured and the solubility of a series of fluoroalkylamines were calculated.					
15. SUBJECT TERMS Chemical agents; fire suppression; atmospheric lifetime; environmental fate; ozone depletion potential; computational chemistry; hydroxyl radical					
16. SECURITY CLASSIFICATION OF:			17. LIMITATION OF ABSTRACT	18. NUMBER OF PAGES 10	19a. NAME OF RESPONSIBLE PERSON Robert E. Huie
a. REPORT U	b. ABSTRACT U	c. THIS PAGE U			19b. TELEPHONE NUMBER (Include area code) 301-975-2559

Environmental Impact of New Chemical Agents for Fire Suppression

Robert E. Huie

Physical & Chemical Properties Division
National Institute of Standards & Technology
Gaithersburg, MD 20899-8381

Final Report

Sponsored by:
The Department of Defense
Strategic Environmental Research and Development Program
MIPR Number W74RDV73243630

“The views and conclusions contained in this document are those of the authors and should not be interpreted as representing the official policies, either expressed or implied, of the Strategic Environmental Research and Development Program, the National Institute of Standards & Technology, or any other part of the U. S. Government.”

Environmental Impact of New Chemical Agents for Fire Suppression

Robert E. Huie

Physical & Chemical Properties Division
National Institute of Standards & Technology
Gaithersburg, MD 20899-8381

Abstract

The environmental impact of chemical agents is intimately tied to the environmental transformations these chemicals undergo. In this project, the most important transformations for various classes of proposed fire suppression agents were investigated and, for the important case of hydrogen abstraction by hydroxyl radicals, a computational screening tool was developed. Rate constants for hydroxyl radical reactions with hydrofluoroethers, perfluorinated alkenes, bromine-containing fluoroalkenes and fluoroalkanes, were determined. By using the computational tool developed in the project, rate constants and atmospheric lifetimes for several bromine-containing halomethanes were calculated. In addition, the reactivity of several alkyl phosphates with free radicals in water were measured and the solubility of a series of fluoroalkylamines were calculated.

Introduction

Although the bromofluorocarbon compounds known as halons are excellent fire suppressants, their production is being phased out due to the considerable danger they pose to the Earth's ozone layer. To replace these compounds, both bromine-containing and non-bromine-containing substitutes have been proposed. Central to the acceptance of any alternative compound is the environmental consequences associated with its introduction. If the replacement contains an element known to be active towards ozone depletion – chlorine, bromine, or iodine – then the possible transport of these elements to the stratosphere must be considered. For other substances, the environmental fate is important in order to ascertain if there might be unintended consequences of its use. In this project, we have carried out kinetic and photochemical studies related to these questions, with a particular emphasis on developing screening tools that can be applied to estimate environmental lifetimes and fates.

Since most of the proposed replacement compounds are volatile, the major concern in these studies has been with atmospheric lifetimes. Generally, the atmospheric lifetime is controlled by reaction with hydroxyl radicals, which are generated at a low level in the

atmosphere. Thus, the rate constants for the reactions of these compounds with OH are of paramount importance. In this project, we have measured rate constants for the reactions of the OH radical for a number of compounds, including a bromine-containing fluoroether, bromine-containing fluoroalkenes, 1- and 2-bromopropane, and a series of perfluoroalkenes. From these measurements, we calculated atmospheric lifetimes and estimated, where appropriate, ozone depletion potentials.

The direct measurement of OH rate constants is quite labor intensive. Therefore, we initiated a project to develop a computational method to calculate these rate constants for those compounds for which hydrogen abstraction would be expected to be the dominant reaction mechanism. This method was developed utilizing a set of compounds for which reliable experimental data were available, which allowed us to establish its reliability. It was then applied to a set of bromine-containing halomethanes for which no data had been reported, leading to estimated lifetimes and ozone depletion potentials.

The photolysis of the compounds in the ultraviolet region of the solar spectrum also can be of importance, particularly when the ozone depletion potential of the compound is required. Thus, for all the compounds for which we have carried out kinetic measurements we have also measured uv absorption spectra down to 160 nm. These data, in addition to being reported in standard publications, have also been gathered together with other far-UV and infrared spectra taken by this Group, and made available on the internet at: <http://nist.gov/kinetics/spectra/spectraindex.htm>. The infrared spectra are required to calculate global warming potentials for various compounds.

Finally, some suggested fire suppressants are not volatile but their environmental fate is still of concern. This was particularly true of the phosphate esters. For these compounds, we have measured rate constants in water for their reactions with the hydroxyl radical, the sulfate radical, and the carbonate radical.

Results and Discussion

A Screening Tool for the Environmental Impact of New Fluids

The objective of this activity was to develop a screening tool, based on quantum mechanics, for the prediction of the environmental impact of new classes of halogenated compounds. Experimental studies had demonstrated that the reactivity of the hydroxyl radical toward halogenated organic compounds is not adequately correlated by simple structure-activity relationships. This was particularly evident when an ether linkage was introduced, where even the relative order of reactivity among the various ethers could not be predicted correctly. This implied that it would be necessary to measure rate constants for a large number of members of any new class of reactants in order to predict the environmental impact of these possible new solvents, refrigerants, or fire suppressants. A better method of screening candidate molecules was clearly needed.

The basic idea underlying this activity was to establish a level of theory that would predict the reactivity of the hydroxyl radical with a series of simple molecules, seeking the lowest possible degree of computational difficulty. This level of theory would then

be applied to more complex molecules and, ultimately, applied to the new class of interest. The results may then be validated by a limited number of experimental determinations, but extensive experimentation and synthesis could be avoided. In the initial study, several levels of theory were explored for the reaction of OH with CH_2Br_2 . This study included the treatment of tunneling, making use of three different methods of approximating this correction. The molecule CH_2Br_2 was chosen both because of the importance of bromine as a fire suppressant and because the relatively large electron system of the molecule makes this reaction a serious test of the various levels of theory. Building on the results of this study, the reactions of OH with the other halogen-substituted methanes, up to bromine, were investigated. From these studies, we chose a level of theory and applied it bromine-containing for which there had been no experimental determinations. Subsequently, we have been investigating computationally the reactions of OH with several fluoroethanes and the ethers derived from them. These pairs were chosen to represent the extremes of behavior observed experimentally: an increase in reactivity upon addition of the ether linkage; a reduction in reactivity; and a small change in reactivity upon addition of the ether linkage. Theory has been able to reproduce the observed trends, with predictions in absolute reactivity within a factor of three. For bis-(difluoromethyl) ether, we have carried out a more exhaustive theoretical analysis of the reaction surface in order to better understand these reactions in general. At the present, we are further refining this approach, with a particular emphasis on better tunneling corrections and the use of pseudo-potentials. Calculations are being extended up to ethers with several carbons and containing fluorine and one or more bromine atoms. In order to verify these calculations, a sample of 1-bromo-2,2-difluoroethyl methyl ether was synthesized for us and used in an experimental determination of the rate constant.

This activity has resulted in three peer-reviewed publications in the *Journal of Physical Chemistry A* and a report in *Halon Options Technical Working Conference: Proceedings*, which are attached and may be consulted for additional details.

Experimental Determinations of OH Reactivity

The reactivity of the OH radical towards organic compounds proposed as possible fire suppressants was determined by the use of the flash photolysis-resonance fluorescence technique. This method, originally developed at NIST in the 1960s, has been incrementally improved to the point that it is routinely capable of obtaining a measurement imprecision of better than 3%. This capability allows sensitive tests to be performed to ascertain the accuracy of the measurements and allows considerable confidence in the results and the derived atmospheric lifetimes. Our initial work involved the measurement of the reactivity of some hydrofluoroethers in order to develop some predictive capability for use in evaluating the reactivity of proposed bromine-containing hydrofluoroethers. The reactivity patterns for these ethers did not show clear trends, leading to our computational studies discussed elsewhere in this report. An important part of this effort was to have a hydrofluorobromoether synthesized in order to measure its reactivity and UV spectrum. After several tries, this was accomplished for $\text{CH}_3\text{OCF}_2\text{CH}_2\text{Br}$. To further refine our understanding of the role of bromine in hydrogen-abstraction reactions, rate constants were also measured for the reactions of OH

with propane and both bromopropanes. These studies were carried out over the temperature range 210 to 480 K.

Rate constants for the reactions of OH with unsaturated alkenes are not presently amenable to reliable theoretical estimation. Since these compounds are under active consideration as fire suppressants, particularly those containing Br in addition to F, we have carried out a number of studies of these reactions as part of this project. The role of halogenation on reactivity is quite complicated. Generally, this role can be summarized by saying that at room temperature, asymmetric fluorination lessens reactivity whereas further fluorination, leading to more symmetric substitution, tends to restore the reactivity. Bromination of an olefinic carbon located between the double bond and a fluorinated group increases the reactivity, whereas bromine on a remote location has little effect. Recent work we carried out after the completion of this project suggests that the substitution of bromine on a carbon opposite the double bond from a fluoroalkyl group substantially reduces the reactivity.

The effect of temperature on the reactivity of perfluoroalkenes is quite complicated. For the simplest alkene, perfluoroethene, there was simple negative temperature dependence. Upon substitution of a $-\text{CF}_3$ (or C_2F_5) about the double bond, the rate constant was found to increase with temperature at the higher temperatures. In all cases, the substitution led to a significant decrease in the rate constant at room temperature.

This activity has resulted in three peer-reviewed publications in the *Journal of Physical Chemistry A*, two manuscripts in preparation, and a report in *Halon Options Technical Working Conference: Proceedings* (Compact Disk), which are attached and may be consulted for additional details.

Reactivity of Alkyl Phosphates towards Radicals in Water

Alkyl phosphates are a class of chemicals that have been extensively investigated as fire suppression agents. They have very low volatility and are unlikely to be degraded in the atmosphere. They are, however, soluble in water and their environmental fate is likely to involve reactions in this medium. As part of this project, we have measured the rate constants for their reactions with radicals important in aqueous phase degradation processes: the carbonate radical, CO_3^- , and the dichloride radical, Cl_2^- . The reactivity towards the sulfate radical, SO_4^- , was also measured for comparison. The procedure used was pulse radiolysis, in which a high-energy electron pulse is utilized to generate the radicals, whose temporal history is monitored by the use of optical absorption.

Although the sulfate radical reacted at a measurable rate with all the compounds, only upper limits could be obtained for the reactions of the two other radicals. The results seemed to indicate that both hydrogen abstraction and electron transfer reactions took place for the very strong oxidant SO_4^- , but that the reduction potentials of CO_3^- and Cl_2^- are not high enough to react with these phosphates and neither of these radicals has a strong propensity for hydrogen abstraction. The reactions of the two radicals, CO_3^- and

Cl_2^- , are too slow for this degradation mechanism to be of importance in the environment. The results of this study are presented in the table below (in units of $\text{L mol}^{-1} \text{s}^{-1}$)

	SO_4^-	Cl_2^-	CO_3^-
Triethyl Phosphate	1.6×10^6	$<7 \times 10^4$	$<1 \times 10^4$
Diethyl Phosphate	8.7×10^6		$<1 \times 10^4$
Trimethyl Phosphate	1.3×10^5	$<4 \times 10^4$	$<3 \times 10^3$
Dimethyl Phosphate	7×10^4		

Henry's Law Constants for Fluoroalkylamines

Fluorinated alkyl amines have been proposed as possible fire suppressants. In this case, a possible atmospheric loss mechanism was considered dissolution into atmospheric droplets and subsequent rainout. To investigate the likelihood of this process, we have calculated Henry's Law constants for a series of fluoroalkylamines, using the SM5.42 solvation model at the PM3 level of theory. Based on comparisons of the results of calculations for similar alkylamines with experiment, we estimate that these results are valid to within a factor of three. Based on these results, rainout is likely not to be a very effective removal mechanism for the more highly fluorinated species.

Amine	del G kJ/mol	Kh M/Atm	exp Kh
NH ₃	-10.24	62.29	61
NH ₂ CH ₃	-9.82	52.52	89
NH(CH ₃) ₂	-8.47	30.45	56
N(CH ₃) ₃	-4.99	7.49	9.5
NH ₂ CF ₃	-14.08	292.79	
NH(CF ₃) ₂	-5.46	9.06	
N(CF ₃) ₃	13.01	5.3E-03	
N(CH ₃) ₂ (CH ₂ CF ₃)	-5.87	10.69	
NCH ₃ (CF ₃) ₂	0.79	0.73	
N(CF ₃) ₂ (CH ₂ CHF ₂)	2.35	0.39	
N(CF ₃) ₂ (CH ₂ CF ₃)	3.80	0.22	
N(CF ₃) ₂ (CH ₂ CH ₃)	4.39	0.17	
N(CF ₃) ₂ (CF ₂ CF ₃)	20.69	2.4E-04	
N(CF ₃)(CF ₂ CF ₃) ₂	30.07	5.4E-06	
N(CF ₂ CF ₂) ₃	35.11	7.1E-07	

experimental from Christie & Crisp, 1967

Important findings and conclusions

An early finding in this program was the discovery that simple estimation tools were not adequate to predict the rate constants for hydrogen abstractions reactions by hydroxyl radicals for such classes as halogenated ethers. Because of this, we explored the possibility that the application of more advanced computational tools might prove fruitful. Indeed, we did find this to be the case and have demonstrated the utility of such a tool. Of particular interest is the observation that a simple bond-strength correlation, based on simpler theoretical calculations, might prove adequate. It seems apparent that this should be explored further. Experimental studies of addition reactions of the hydroxyl radical also have shown simple concepts are not necessarily adequate. For some of these reactions, the rate constant may both decrease and increase with temperature, depending on the temperature region. Recent observations on the effect of bromine substitution were surprising. It would probably be useful to carry out some computational studies on these reactions. Since the theory for addition reactions is not as well advanced as for abstraction reactions, simple correlations based on such parameters as electron density should probably be explored first.

Publication List

1. Orkin, V. L., Villenave, E., Huie, R. E., and Kurylo, M. J., "Atmospheric Lifetimes and Global Warming Potentials of Hydrofluoroethers: Reactivity Toward OH, UV Spectra, and IR Absorption Cross Sections", *J. Phys. Chem. A*, **103**, 9770-9779 (1999).
2. Louis, F., Gonzalez, C., Huie, R. E., and Kurylo, M. J., "An *ab Initio* Study of the Reaction of Halomethanes with the Hydroxyl Radical. Part 1: CH_2Br_2 ", *J. Phys. Chem. A*, **104**, 2931-2938 (2000).
3. Louis, F., Gonzalez, C., Huie, R. E., and Kurylo, M. J., "An *Ab Initio* Study of the Kinetics of the Reactions of Halomethanes with the Hydroxyl Radical. Part 2: A Comparison between Theoretical and Experimental Values of the Kinetic Parameters for 12 Partially Halogenated Substituted Methanes.", *J. Phys. Chem. A*, **104**, 8773-8778 (2000).
4. Huie, R. E., Louis, F., Gonzalez, C. A., and Kurylo, M. J., "An *Ab initio*-Based Screening Tool for the Atmospheric Lifetimes of Halon Replacements", *Halon Options Technical Working Conference: Proceedings*, pp. 87-92, Albuquerque, (2000).
5. Louis, F., Gonzalez, C., Huie, R. E., and Kurylo, M. J., "An *Ab Initio* Study of the Kinetics of the Reactions of Halomethanes with the Hydroxyl Radical. Part 3. Reactivity Trends and Kinetics Parameter Predictions for the Potential Halon Replacements CH_2FBr , CHFBr_2 , CHFCIBr , CHCl_2Br , and CHClBr_2 ", *J. Phys. Chem. A*, **105**, 1599-1604 (2001).
6. Huie, R. E., Orkin, V. L., Louis, F., Kozlov, S. N., and Kurylo, M. J. "Effect of Bromine Substitution on the Lifetimes and Ozone Depletion Potentials of Organic Compounds", *Proceedings of HOTWC-2002. 12th Halon Options Technical Working Conference*, NIST Special Publication 984, R. G. Gann and P. A. Reneke, Eds. (Compact Disk) (2002).
7. Orkin, V. L., Louis, F., Huie, R. E., and Kurylo, M. J., "Photochemistry of Bromine-Containing Fluorinated Alkenes: Reactivity toward OH and UV Spectra", *J. Phys. Chem. A*, **106**, 10195-10199 (2002).
8. Kozlov, S. N., Orkin, V. L., Huie, R. E., and Kurylo, M. J., "OH Reactivity and UV Spectra of Propane, n-Propyl Bromide, and Isopropyl Bromide", *J. Phys. Chem. A*, **107**, 1333-1338 (2003).
9. Orkin, V. L., Huie, R. E., and Kurylo, M. J., "OH Reactivity and UV Spectra of Perfluorinated Alkenes", in preparation.
10. Orkin, V. L., Huie, R. E., and Kurylo, M. J., "OH Reactivity and UV Spectra of $\text{CH}_3\text{OCF}_2\text{CH}_2\text{Br}$ ", in preparation.

Technical Publications

Atmospheric Lifetimes and Global Warming Potentials of Hydrofluoroethers: Reactivity toward OH, UV Spectra, and IR Absorption Cross Sections

Vladimir L. Orkin,^{*,†} Eric Villenave,[‡] Robert E. Huie, and Michael J. Kurylo

Physical and Chemical Properties Division, National Institute of Standards and Technology, Gaithersburg, Maryland 20899

Received: May 26, 1999; In Final Form: September 28, 1999

The rate constants for the reactions of OH radicals with the fluorinated ethers, CHF₂-O-CHF₂ (HFOC-134) and CF₃CH₂-O-CH₂CF₃ (HFOC-356mff), were measured using the flash photolysis resonance fluorescence technique over the temperature range 277-370 K to give the following Arrhenius expressions: $k_{\text{HFOC-134}}(T) = (0.63^{+0.20}_{-0.16}) \times 10^{-12} \exp\{-(1646 \pm 76)/T\} \text{ cm}^3 \text{ molecule}^{-1} \text{ s}^{-1}$, $k_{\text{HFOC-356mff}}(T) = (2.32^{+0.46}_{-0.41}) \times 10^{-12} \exp\{-(790 \pm 47)/T\} \text{ cm}^3 \text{ molecule}^{-1} \text{ s}^{-1}$. On the basis of the analysis of the available experimental results, the following Arrhenius expression can be recommended for the rate constant of the reaction between OH and HFOC-134: $k_{\text{HFOC-134}}(T) = (0.82^{+0.34}_{-0.24}) \times 10^{-12} \exp\{-(1730 \pm 110)/T\} \text{ cm}^3 \text{ molecule}^{-1} \text{ s}^{-1}$. Atmospheric lifetimes were estimated to be 24.8 years for HFOC-134 (23.8 years based on the results of this study alone) and 0.3 years for HFOC-356mff. Infrared absorption cross sections of HFOC-134, HFOC-356mff, and HFOC-125 (CHF₂-O-CF₃) were measured at $T = 295 \text{ K}$ from 500 to 1600 cm⁻¹ and the global warming potentials of the three compounds were estimated. Ultraviolet absorption spectra of the ethers were measured between 160 and 220 nm. The general pattern of reactivity of hydrofluoroethers toward OH is discussed.

Introduction

Because of the role of chlorofluorocarbons (CFCs) in stratospheric ozone depletion, a large number of replacement compounds, such as hydrochlorofluorocarbons (HCFCs) and hydrofluorocarbons (HFCs), have been selected for industrial applications. The search for CFC alternatives has also focused on oxygen-containing compounds such as partially fluorinated ethers (HFOCs) which, by virtue of not containing any chlorine or bromine, do not contribute to ozone depletion. Nevertheless, the infrared absorbing properties of such fluorinated compounds raise concerns about their role as potential greenhouse gases. The assessment of the global warming potential (GWP) of a compound requires the knowledge of both its atmospheric lifetime and infrared absorption cross sections in the "atmospheric transparency window" between ca. 8 and 12 μm. The atmospheric lifetime of a hydrogen-containing compound is mainly dictated by its reaction with OH radicals in the troposphere. Ultraviolet photolysis can also be important in the case of compounds with low reactivity toward OH however.

In contrast to HCFCs and HFCs, there is very little information on reactivity of partially fluorinated ethers toward hydroxyl radicals.¹⁻⁷ Only a few measurements have been reported on the temperature dependence of such rate constants³⁻⁵ to derive Arrhenius parameters as well as rate constants at the temperatures important for atmospheric calculations. We report here the experimental determinations of the rate constants for the reactions of OH with two symmetrical hydrofluoroethers, CHF₂-O-CHF₂ (HFOC-134) and CF₃CH₂-O-CH₂CF₃ (HFOC-356mff), over the temperature range 277-370 K.

Ultraviolet absorption cross sections of HFOC-134, HFOC-356mff, and HFOC-125 (CHF₂-O-CF₃) were measured over the wavelength range 160-220 nm to ascertain the effect of fluorination on the UV spectra of ethers and to estimate the possible role of UV solar absorption on their atmospheric lifetimes. Infrared spectra between 500 and 1600 cm⁻¹ were measured for HFOC-134, HFOC-356mff, and HFOC-125 (CHF₂-O-CF₃), and integrated band intensities are reported here as well as the estimated global warming potentials (GWPs) of the three compounds.

Experimental Section

Detailed descriptions of the apparatus and the experimental methods employed in the present work are given elsewhere.⁸⁻¹⁰ Thus, only brief overview is given here. Certain commercial equipment, instruments, or materials are identified in this article in order to adequately specify the experimental procedure. Such identification does not imply recognition or endorsement by the National Institute of Standards and Technology, nor does it imply that the material or equipment identified are necessarily the best available for the purpose.

OH Reaction Rate Constant Measurements. The principal component of the flash photolysis/resonance fluorescence (FP/RF) apparatus is a Pyrex reactor (of approximately 50 cm³ internal volume) thermostated via a fluid circulated through its outer jacket. The reaction was studied in argon carrier gas (99.9995% purity) at a total pressure of 13.33 kPa (100.0 Torr). Dry argon, argon bubbled through water thermostated at 276 K, and HFOC-134 (or HFOC-356mff, 2.00% volume fraction in argon) were premixed and flowed through the reactor at a total flow rate of 0.3 cm³ s⁻¹ to 1.4 cm³ s⁻¹, STP. The concentrations of the gases in the reactor were determined by measuring the mass flow rates and the total pressure using a MKS Baratron manometer. Flow rates of both argon and the H₂O/Ar mixture were measured using calibrated Tylan mass

[†] Also associated with the Institute of Energy Problems of Chemical Physics, Russian Academy of Sciences, Moscow, 117829, Russia.

[‡] Present address: Laboratoire de Physico-Chimie Moléculaire CNRS UMR 5803, Université Bordeaux I, 351, Cours de la Libération, 33405 Talence Cedex, France.

TABLE 1: Summary of the Results Obtained for the Reactions of OH with CHF₂-O-CHF₂ (HFOC-134) and CF₃-CH₂-O-CH₂-CF₃ (HFOC-356mff)

temperature, K	[CHF ₂ OCHF ₂], 10 ¹⁶ molecule/cm ³	<i>k</i> _{HFOC-134} × 10 ¹⁵ , ^a cm ³ molecule ⁻¹ s ⁻¹	[CF ₃ CH ₂ OCH ₂ CF ₃], 10 ¹⁴ molecule/cm ³	<i>k</i> _{HFOC-356mff} × 10 ¹³ , ^a cm ³ molecule ⁻¹ s ⁻¹
277	1.1–3.9	1.70 ± 0.15 (2)	1.3–4.9	1.35 ± 0.09 (4)
298	0.57–2.6	2.47 ± 0.12 (4)	0.50–3.5	1.63 ± 0.03 (12)
323	0.60–1.8	3.77 ± 0.35 (1)	1.0–3.2	1.93 ± 0.17 (4)
349	0.35–1.06	5.67 ± 0.52 (1)	0.75–2.7	2.38 ± 0.19 (3)
370	0.25–0.85	7.48 ± 0.45 (2)	0.65–2.3	2.77 ± 0.12 (6)

^a Error bars are levels of confidence of 95% and do not include estimated systematic errors of 4% (see text). Numbers in parentheses indicate the number of experimental measurements.

flow meters, whereas that of the HFOC-134 (or the HFOC-356mff/Ar mixture) was determined by direct measurements of the rate of pressure change in a calibrated volume. The ranges of hydrofluoroethers concentrations are presented in Table 1. The partial pressure of H₂O in the reactor was ca. 0.08 Torr (0.01 kPa) in the experiments presented in Table 1 and up to ca. 2 Torr (0.27 kPa) in some test experiments. Hydroxyl radicals were produced by the pulsed photolysis (0.7–4.2 Hz repetition rate) of H₂O (introduced via the 276 K H₂O/Ar bubbler) using a xenon flash lamp focused into the reactor. The radicals were then monitored by their resonance fluorescence near 308 nm, excited by a microwave-discharge resonance lamp (280 Pa or 2.1 Torr of a ca. 2% volume fraction of H₂O in ultrahigh purity helium) focused into the reactor center. The resonance fluorescence signal was recorded on a computer-based multichannel scanner (channel width 100 μs) as a summation of 1000–22000 consecutive flashes. The radical decay signal at each reactant concentration ([HFOC-134] or [HFOC-356mff]) was analyzed as described by Orkin et al.⁹ to obtain the first-order decay rate due to the reaction under study.

UV Absorption Spectra Measurements. The absorption spectra of several ethers and fluoroethers were measured over the wavelength range of 160–220 nm using a single beam apparatus consisting of a 1 m vacuum monochromator equipped with a 600 lines/mm grating. The radiation source was a Hamamatsu L1385 deuterium lamp, and the detector was a Hamamatsu R166 photomultiplier. Spectra were recorded at increments of either 0.5 or 0.1 nm at spectral slit widths of 0.5 and 0.1 nm. The pressure inside the 16.90 ± 0.05 cm absorption cell was measured using full scale 10 and 1000 Torr MKS Baratron manometers at *T* = 295 ± 1 K. Absorption spectra of the evacuated cell and of the cell filled with a gas sample were alternately recorded several times and the absorption cross sections were calculated from the differences. The complete spectra were constructed from data taken over several overlapping wavelength ranges. Data over each range were obtained at several pressures to verify adherence to the Beer–Lambert absorption law. The spectra were measured at the following compound pressures in the cell: HFOC-134, HFOC-125 (100–900 Torr/13.3–120 kPa); HFOC-356mff (0.5–120 Torr/67 Pa to 16 kPa); dimethyl ether (0.1–900 Torr/13 Pa to 120 kPa); diethyl ether (0.1–400 Torr/13 Pa to 53.3 kPa). The overall instrumental error associated with uncertainties in the path length, pressure, temperature stability, and measured absorbance was estimated to be less than 2% over most of the wavelength range, increasing to approximately 5–10% at the long-wavelength ends of the spectra.

IR Absorption Cross Section Measurements. The spectra were obtained between 500 and 1600 cm⁻¹ using a Bruker IFS-66v Fourier transform spectrophotometer. The spectrophotometer, including the cell compartment, was evacuated to less than 10 mPa using a turbomolecular pump in order to minimize errors due to water vapor absorption. All the data presented were

measured with ca. 0.12 cm⁻¹ spectral resolution. A 20.15 ± 0.05 cm glass absorption cell fitted with KBr windows was used to obtain absorption spectra at the temperature *T* = 295 ± 1 K. Between spectrum measurements, the cell was pumped out down to ca. 10 mPa using a turbomolecular pump and filled with the gas to be studied two to three times. Sample pressures were measured using full scale 10 and 1000 Torr MKS Baratron manometers. Data over each absorption band range were obtained at several pressures to verify adherence to the Beer–Lambert absorption law. The overall instrumental error associated with uncertainties in the path length, pressure, temperature stability, and the measured absorbance was estimated to be less than 2% over the wavenumber range, increasing below 600 cm⁻¹ for weak bands because of residual water vapor absorption.

Absorption spectra of the evacuated cell and the cell filled with the ether under study were recorded sequentially to calculate the absorption cross sections from their differences at different ether concentrations using the Beer–Lambert law,

$$\sigma_{\text{HFOC}}(\nu) = \frac{2.303}{[\text{HFOC}]L} \{A_{\text{HFOC}}(\nu) - A_0(\nu)\} \quad (1)$$

where $\sigma(\nu)$ is the absorption cross section at wavenumber ν , in units of cm² molecule⁻¹; $A_{\text{HFOC}}(\nu)$ and $A_0(\nu)$ are absorbancies (base 10) in the presence of ether and that of the evacuated cell at wavenumber ν , as measured with the spectrophotometer; [HFOC] is the concentration of the ether under study, in units of molecule/cm³; and *L* is the optical path length in centimeters. A spectrum for each absorption band was recorded at a few different pressures suitable for that band; the maximum absorbance did not exceed $A_{\text{HFOC}}(\nu) = 0.7$. The IR measurements were done at the following sample pressures in the cell: HFOC-134 (0.2–8 Torr/27 Pa to 1.1 kPa); HFOC-356mff (0.2–16 Torr/27 Pa to 2.1 kPa); HFOC-125 (0.4–6 Torr/53 Pa to 0.8 kPa). Linear least-squares fits were applied to all sample pressure measurements in order to obtain absorption cross sections as well as integrated band intensities. Any measured absorption band with an IBI greater than 0.2% of the highest IBI was attributed to the IR absorption spectra of the compound under study.

All the MKS Baratron manometers used for the OH reaction rate constant measurements (measurements of the pressure in the cell and the ether flow rate), UV absorption measurements, and IR absorption measurements were calibrated and intercompared by measuring the same argon pressure to be identical within less than 0.5% over the whole pressure range.

Sample Purity. The sample of CHF₂-O-CHF₂, HFOC-134, was obtained from Hampshire Chemical Co. with a stated purity of 99.97%. Our GC and GC/MS analysis of this sample indicated ca. 99.8% purity with the main impurities, CF₃Cl (ca. 17%), CH₃OH (ca. 0.007%), and CHF₂OCH₂F (ca. 0.027%), with trace amounts of CHF₃ and water. Two samples of CF₃CH₂-O-CH₂CF₃, HFOC-356mff, were obtained from

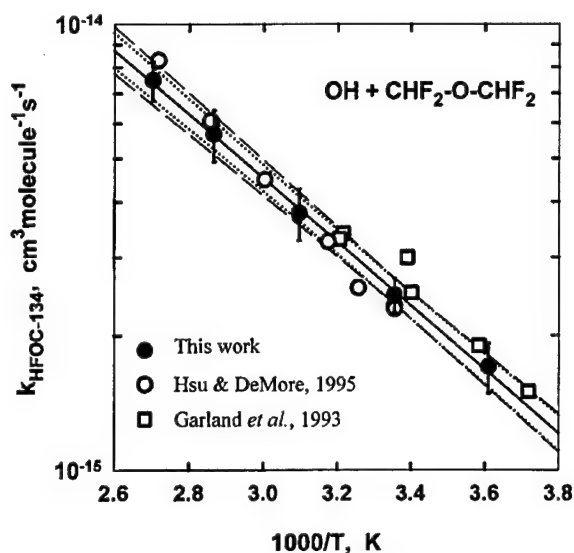


Figure 1. Arrhenius plot showing the average values obtained for $k_{\text{HFOC-134}}$ at each temperature. The error bars at each temperature represent the 95% confidence intervals and include the estimated systematic error. The solid line is a least-squares fit to the individual data points that make up these average values. The dotted lines bracket the 95% confidence intervals rigorously obtained from the statistical fit while the dashed lines are from eqs 2 and 2a in the text; both include our estimate of possible systematic errors.

Aldrich Chemical Co., each with a stated purity of 99.5%+ with $\text{CF}_3\text{CH}_2\text{OH}$ as a main possible impurity. Our analysis of the first sample indicated in ca. 99.87% purity with ca. 0.035% of water, 0.017% of trifluoroethanol, and 0.076% of nonidentified fluorinated impurity, probably a fluoroether. The second sample was ca. 99.7% purity based on our analysis with ca. 0.1% of water and ca. 0.2% of trifluoroethanol as main impurities.

A preparative scale gas chromatograph was used for purification of original samples from the detected impurities. The GC purification of the original samples resulted in no reliably detectable impurities in the purified samples of both HFOC-134 and HFOC-356mff, except residual water, which could also come from a detection system injector. This indicates that the concentrations of all detected impurities were decreased by a factor of at least 20–200.

Results and Discussion

Results of the OH reaction rate constant determinations averaged at each temperature are presented in Table 1 and Figures 1 and 2. Table 2 presents the Arrhenius parameters derived from the fitting to the individual rate constants obtained in our experiments at each temperature as well as the parameters obtained from the fitting of data from other laboratories.

Experiments summarized in Table 1 were performed with GC purified samples of ethers at low flash energy. Test experiments were performed at $T = 298$ K to check possible complications due to any "secondary" chemistry or reactions with impurities. These complications and test experiments are carefully discussed in our previous paper.¹⁰ The initial concentration of OH radicals was changed by either variation of the photolysis flash energy (variation of an electrical energy from 0.3 to 3.3 J) or variation of H_2O concentration in the reactor (a factor of 10). No statistically significant changes in the measured rate constants were obtained. In addition, no dependence of the rate constant on the flash repetition rate by a factor of 4 was discernible. This indicates that "secondary" reactions with

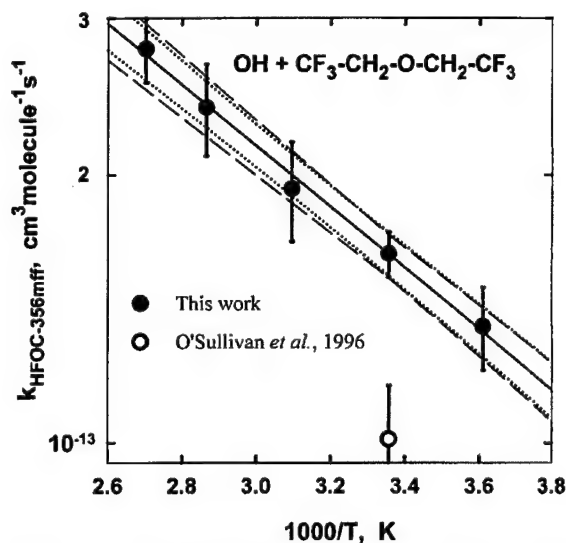


Figure 2. Arrhenius plot showing the average values obtained for $k_{\text{HFOC-356mff}}$ at each temperature. The error bars at each temperature represent the 95% confidence intervals and include the estimated systematic error. The solid line is a least-squares fit to the individual data points that make up these average values. The dotted lines bracket the 95% confidence intervals rigorously obtained from the statistical fit while the dashed lines are from eqs 3 and 3a in the text; both include our estimate of possible systematic errors.

radicals formed either in the reactions under study or due to photolysis of reactants do not affect the results of our measurements.

The possible reactions of OH with reactive impurities in the reagent samples can cause the rate constant overestimation especially for reagents having low reactivity toward OH. The error due to the presence of identified impurities can be estimated based on impurity levels and the rate constant of their reactions with OH. In the case of original HFOC-134 sample such estimation indicates that ca. (5–6)% overestimation of the room temperature rate constant would have occurred. The GC purification of the original sample resulted in no reliably detectable impurities in the purified sample of HFOC-134. Thus, the impurity levels in the GC purified sample are low enough to cause no problems in the rate constant measurements. In addition, 21 experiments were done with the original sample before purification which resulted in $k_{\text{HFOC-134}}(298) = (2.74 \pm 0.08) \times 10^{-15} \text{ cm}^3 \text{ molecule}^{-1} \text{ s}^{-1}$ vs $k_{\text{HFOC-134}}(298) = (2.52 \pm 0.07) \times 10^{-15} \text{ cm}^3 \text{ molecule}^{-1} \text{ s}^{-1}$ in the case of the purified sample. This difference, although only slightly exceeding the overall statistical confidence interval of the measurements, is reasonably consistent with the 5–6% overestimation mentioned above. Hence, the reduction of impurities by more than an order of magnitude should yield results for the purified sample of $\text{CHF}_2\text{O-CHF}_2$ that are free from systematic errors due to impurities.

Although we could not identify all detected impurities in the sample of HFOC-356mff, the higher reactivity of this ether makes impurity effects less important. For example, even the highest level (0.2%) of $\text{CF}_3\text{CH}_2\text{OH}$ could result in ca. 0.2% rate constant overestimation based on its reaction rate constant¹¹ of $1 \times 10^{-13} \text{ cm}^3 \text{ molecule}^{-1} \text{ s}^{-1}$. Similarly, the rate constant for the reaction of OH with diethyl ether,¹² $1.3 \times 10^{-11} \text{ cm}^3 \text{ molecule}^{-1} \text{ s}^{-1}$, can be used to estimate a conservative upper limit for possible errors due to reaction with a fluoroether impurity. Such errors are not expected to exceed 6% for the original sample and become negligible in the case of GC purified one. Therefore, detected impurities could not be a source of

TABLE 2: Summary of Measurements of $k_{\text{HFOC-134}}$ and $k_{\text{HFOC-356mff}}$

molecule (HFOC)	temperature range, K	$A \times 10^{12}$, $\text{cm}^3 \text{ molecule}^{-1} \text{ s}^{-1}$	$E/R \pm \Delta E/R$, K	$k_{\text{HFOC}}(298) \times 10^{14}$, $\text{cm}^3 \text{ molecule}^{-1} \text{ s}^{-1}$	reference
$\text{CHF}_2\text{-O-CHF}_2$ (HFOC-134)	269–312	0.54 ± 0.35^a	1560 ± 200^a	0.29 ± 0.02^a	Garland et al. ³
		$0.55^{+1.1}_{-0.37}^b$	1583 ± 322^b	0.27 ± 0.02^b	Garland et al. ^{3,b}
	298–368	$1.9^{+1.2}_{-0.8}^c$	2007 ± 162^c	0.23 ± 0.013^c	Hsu & DeMore ⁵
	277–370	$0.63^{+0.20}_{-0.16}$	1646 ± 76	0.252 ± 0.017^d	this work
$\text{CF}_3\text{-CH}_2\text{-O-CH}_2\text{-CF}_3$ (HFOC-356mff)	298			10.1 ± 1.5^e	O'Sullivan et al. ⁶
	277–298	$2.32^{+0.46}_{-0.41}$	790 ± 47	16.3 ± 0.9^d	this work

^a All values with their 2 σ error bars are taken from the original paper. ^b Results of our fitting to the data set presented in the original paper. Error bars are 95% confidence intervals from the statistical fitting and do not reflect any systematic error. ^c Error bars were derived by fitting of the data set from the original paper and represent 95% confidence intervals. They include neither any possible systematic error nor any uncertainty associated with the rate constant of the reference reaction between OH and $\text{CH}_3\text{-CCl}_3$. ^d All error bars indicated include estimated systematic errors of 4%. To obtain the rate constant uncertainties at any temperature, eqs 2a or 3a, given in the text, can be used. ^e The result of a relative rate constant measurement. The reference reaction is not reported. The rate constant and its uncertainty are as quoted by authors.

the error in our experiments with HFOC-356mff. In support of this conclusion, we note that nine experiments using the original sample resulted in $k_{\text{HFOC-356mff}}(298) = (1.68 \pm 0.09) \times 10^{-13} \text{ cm}^3 \text{ molecule}^{-1} \text{ s}^{-1}$ (seven measurements) and $k_{\text{HFOC-356mff}}(277) = (1.44 \pm 0.20) \times 10^{-13} \text{ cm}^3 \text{ molecule}^{-1} \text{ s}^{-1}$ (two measurements), statistically the same as in the case of GC purified samples (see Table 1).

The expressions for the rate constants and the uncertainty of the rate constants can be written in the manner chosen by the NASA Panel for Data Evaluation, as we have described previously.⁹ The Arrhenius parameters were obtained from the linear fitting for $\log k_i$ vs $1/T$ data sets (see eqs 2 and 3). Therefore, the uncertainties in thus-determined rate constants should be presented as the uncertainty factors rather than the absolute errors at any temperature. The uncertainty factors can be approximated as given in eqs 2a and 3a:

$$k_{\text{HFOC-134}}(T) = 2.52 \times 10^{-15} \exp\left\{-1646\left(\frac{1}{T} - \frac{1}{298}\right)\right\} \text{ cm}^3 \text{ molecule}^{-1} \text{ s}^{-1} \quad (2)$$

$$f(T)_{\text{HFOC-134}} = 1.028 \exp\left\{76\left|\frac{1}{T} - \frac{1}{298}\right|\right\} + 0.04 \approx 1.068 \exp\left\{76\left|\frac{1}{T} - \frac{1}{298}\right|\right\} \quad (2a)$$

$$k_{\text{HFOC-134}}(T) = 1.62 \times 10^{-13} \exp\left\{-793\left(\frac{1}{T} - \frac{1}{298}\right)\right\} \text{ cm}^3 \text{ molecule}^{-1} \text{ s}^{-1} \quad (3)$$

$$f(T)_{\text{HFOC-356mff}} = 1.017 \exp\left\{47\left|\frac{1}{T} - \frac{1}{298}\right|\right\} + 0.04 \approx 1.057 \exp\left\{47\left|\frac{1}{T} - \frac{1}{298}\right|\right\} \quad (3a)$$

Here we have included an estimated systematic uncertainty of 4% as well as the statistical uncertainty factors $f(298)_{\text{HFOC-134}} = 1.028$ and $f(298)_{\text{HFOC-356mff}} = 1.017$, respectively, at $T = 298$ K obtained from the Arrhenius fitting to the entire data sets. All the uncertainties in both $k_i(298)$ and E/R represent 95% confidence intervals associated with the statistical fitting procedure. The acceptability of the above presentation of the uncertainties (eqs 2a and 3a) is illustrated in Figures 1 and 2 in which we show both the rigorously computed 95% confidence intervals of the regression lines (dotted lines) as well as those approximated using eqs 2a and 3a (dashed lines). Both include the 4% estimated systematic error as a summand. One can see that the uncertainty factors well describe the confidence intervals, especially below room-temperature range, which is important for atmospheric modeling purposes.

The rate constant for the reaction of OH with $\text{CHF}_2\text{-O-CHF}_2$ was measured previously using a flash photolysis/resonance fluorescence technique by Zhang et al.,^{2b} a laser photolysis/laser fluorescence technique by Garland et al.,³ and a relative technique with OH + $\text{CH}_3\text{-CCl}_3$ as a reference reaction by Hsu and DeMore.⁵ Table 2 shows the 95% confidence intervals obtained from an Arrhenius fitting of the data presented in the original papers.^{3,5} We have not included the room-temperature data from ref 2b in the table since the rate constant obtained, $k(296) = 2.5 \times 10^{-14} \text{ cm}^3 \text{ molecule}^{-1} \text{ s}^{-1}$, is an order of magnitude higher than those from other measurements and is most likely due to the presence of unresolved reactive impurities in the ether sample. (Our analysis of the data from ref 3 resulted in slightly different Arrhenius parameters and the rate constant at 298 K than those derived by Garland et al. (see Table 2)). Both the A factor and E/R derived by Hsu and DeMore⁵ are significantly higher than those derived by Garland et al.³ The presence of reactive impurities in the sample used by Garland et al. has been suggested by Hsu and DeMore to be a reason for such a discrepancy.

Similar differences exist between the Arrhenius parameters from the present study and those of Hsu and DeMore. However, we paid particular attention to the sample purity. In fact, differences in Arrhenius parameters derived from sets of rate constant data covering only narrow temperature ranges can be misleading. A comparison of the actual rate constants over the common temperature range of study is more appropriate. This is shown in Figure 1 where one can see that our data are in good agreement (better than 15%) with those obtained in ref 5 over entire common temperature range. In particular, our value at $T = 298$ K is not statistically different from that of ref 5, especially when the uncertainty associated with the reference rate constant used in the relative rate study is included. At the high temperature, however, the relative technique data begin to diverge from those of the present study (becoming about 13% higher at $T = 370$ K and leading to the calculation of larger values for both A and E/R than derived from the present results). This difference cannot be explained by the presence of reactive impurities in our study since impurity contamination would cause greater deviations at the lower temperatures. Thus, the differences in the derived Arrhenius parameters are probably due to data scattering (i.e., random errors) or to some systematic errors in one or both of the studies.

The result presented by O'Sullivan et al.⁶ appears to be the only available measurement of the rate constant for the reaction between OH and $\text{CF}_3\text{-CH}_2\text{-O-CH}_2\text{-CF}_3$. Unfortunately, there is no detailed information on the measurements presented in ref 6 and the reason for the large discrepancy (a factor of 1.6)

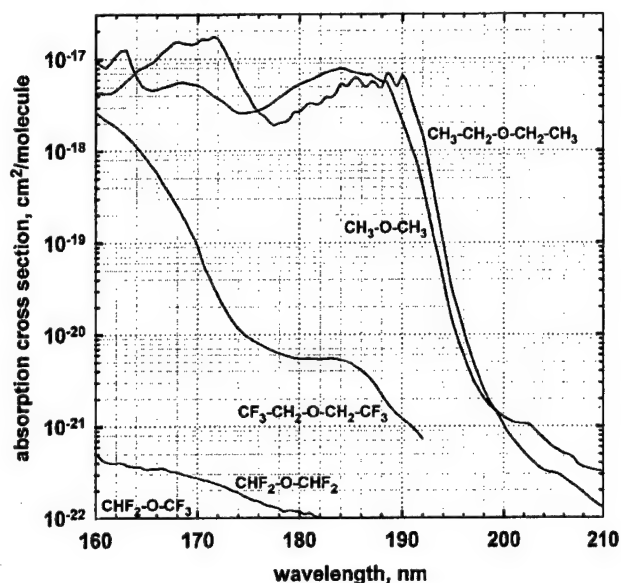


Figure 3. Ultraviolet absorption spectra of several ethers at $T = 295$ K. (The absorption cross sections of $\text{CHF}_2\text{-O-CF}_3$ (HFOC-125) were found to be less than $10^{-22} \text{ cm}^2 \text{ molecule}^{-1}$ over the entire spectral range.)

is not clear. As discussed above, we are confident that our measurements are not complicated by either reaction with impurities in the sample or by secondary chemistry.

UV Absorption Spectra. Measured UV absorption spectra of several ethers are presented in Figure 3. For comparison, we have measured the absorption spectra of nonfluorinated analogues as well.

The measurements of the short-wavelength absorption spectra of both $\text{CHF}_2\text{-O-CF}_3$ and $\text{CHF}_2\text{-O-CHF}_2$ were affected by the residual water vapor absorption. We used low-temperature distillation with a cold trap temperature from -80 to -100 °C in order to remove the residual water from the samples. Thus, we can conclude that the absorption cross sections of $\text{CHF}_2\text{-O-CF}_3$ are below $10^{-22} \text{ cm}^2 \text{ molecule}^{-1}$ over the entire range of measurements. On the basis of this result, as well as on an identical purification procedure, we are reasonably certain that the absorption spectrum obtained for $\text{CHF}_2\text{-O-CHF}_2$ is not affected by an impurity. The reproducibility of $\text{CF}_3\text{-CH}_2\text{-O-CH}_2\text{-CF}_3$ absorption measurements at wavelengths longer than ca. 190 nm was poor, possibly due to compound adsorption at the optical windows at near saturated vapor pressure. Therefore, we can give only the upper limit of $10^{-21} \text{ cm}^2 \text{ molecule}^{-1}$ for the absorption cross sections over the stratospheric transparency window near 200 nm.

In contrast to alkanes, ethers without fluorine substitution exhibit strong absorption at the wavelengths below 200 nm. This is drastically reduced by fluorination; even fluorination of the carbon atom in the β position with respect to the ether linkage results in a significant decrease of the ether absorptivity. The decrease is more pronounced when the adjacent carbon is fluorinated.

Therefore, fluorinated ethers do not appreciably absorb ultraviolet radiation in the spectral range above 190 nm that can be important for atmospheric implications. The negligible absorbance of fluorinated ethers in the spectral range important for atmospheric implications was also indicated by Orkin et al.^{4b}

IR Absorption Cross Sections. The high-resolution infrared spectra of fluorinated ethers obtained in this work did not exhibit any evidence of well-resolved fine rotational structure that could

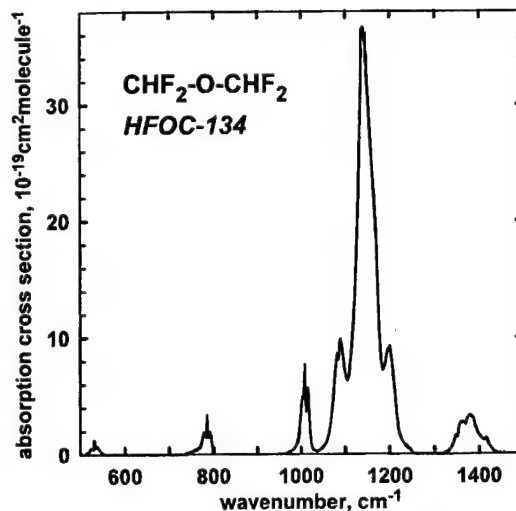


Figure 4. Infrared absorption cross sections of $\text{CHF}_2\text{-O-CHF}_2$ (HFOC-134) at $T = 295$ K.

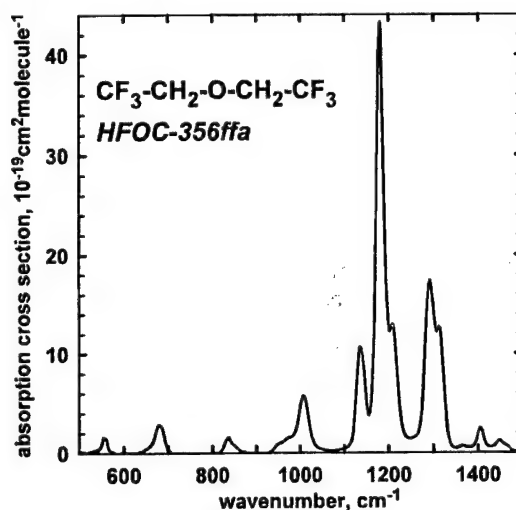


Figure 5. Infrared absorption cross sections of $\text{CF}_3\text{-CH}_2\text{-O-CH}_2\text{-CF}_3$ (HFOC-356ffa) at $T = 295$ K.

affect the accuracy of the absorption cross section or band intensity measurements. This is not an unexpected result for the compounds containing few heavy halogen atoms in the molecule as will be discussed in a subsequent publication.¹³ The integrated band intensities for such molecules can thus be measured without any special spectrum broadening procedure.¹³

The IR spectra measured for three fluorinated ethers are shown in Figures 4–6. Table 3 lists the integrated band intensities of the main features of the measured IR absorption spectra. The integrated band intensities (IBI) were calculated as follows:

$$\text{IBI}_{\text{HFOC}}(\nu_1 - \nu_2) = \int_{\nu_1}^{\nu_2} \sigma_{\text{HFOC}}(\nu) d\nu \quad (4)$$

The units of IBI are $\text{cm}^2 \text{ molecule}^{-1} \text{ cm}^{-1}$. The indicated band intervals were chosen simply to separate spectral features and compare the IBI with those available from the literature. The absorption cross sections as well as integrated band intensities for the spectral regions were determined from plots of the integrated areas versus hydrofluoroether concentrations. Figure 7 shows examples of such dependencies for the most intense absorption bands.

TABLE 3: Integrated Band Intensities of HFOC-134, HFOC-125, HFOC-356mff

molecule (compound)	integration limits, cm ⁻¹	IBI, 10 ⁻¹⁷ cm ² molecule ⁻¹ cm ⁻¹			
		this work ^a	ref 15	ref 16	
CHF ₂ -O-CHF ₂ (HFOC-134)	515-552	0.193 ± 0.006			
	600-710	0.047 ± 0.015			
	741-803	0.531 ± 0.008		0.39 ± 0.05	
	965-1035	1.315 ± 0.009			
	1035-1253	21.728 ± 0.030	{24.90 ± 0.03}	{25.18 ± 0.41}	
	1322-1443	1.855 ± 0.011			
CF ₃ -CH ₂ -O-CH ₂ -CF ₃ (HFOC-356mff)	500-600	0.307 ± 0.007			
	600-740	0.798 ± 0.019			
	780-900	0.389 ± 0.013			
	900-1070	2.328 ± 0.017			
	1070-1250	15.605 ± 0.062			
	1250-1350	7.130 ± 0.035			
	1350-1600	1.162 ± 0.032			
CHF ₂ -O-CF ₃ (HFOC-125)	555-670	0.229 ± 0.009		{0.58 ± 0.02}	
	700-785	0.225 ± 0.015	0.209 ± 0.01		
	785-830	(0.025 ± 0.007) ^b		{0.03 ± 0.01}	
	830-860	(0.009 ± 0.001) ^b			
	860-980	0.962 ± 0.020	0.949 ± 0.01	0.93 ± 0.04	
	980-1143	5.746 ± 0.027			
	1143-1184	4.465 ± 0.010			
	1184-1266	13.123 ± 0.053	{31.22 ± 0.07}	{32.3 ± 0.40}	{31.3 ± 1.09}
	1266-1343	6.804 ± 0.022			
	1343-1450	0.999 ± 0.022			
	1450-1510	0.080 ± 0.008			

^a IBI values and their 95% confidence intervals shown in the table were obtained from the linear fitting of the integrated absorption areas versus hydrofluoroether pressure and do not include the estimated systematic error of ca. 2%. ^b The weak absorption band was not originally included in Table 3 to be assigned to the IR spectrum of CH₂F₂-O-CF₃. The value is shown to compare with that by Heathfield et al.¹⁶

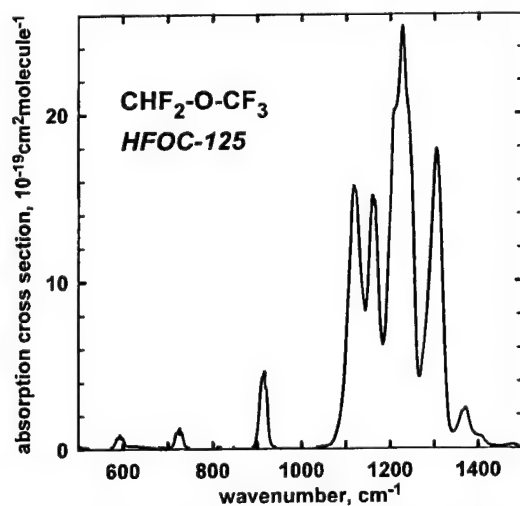


Figure 6. Infrared absorption cross sections of CHF₂-O-CF₃ (HFOC-125) at *T* = 295 K.

There are three papers reporting integrated band intensities measured for these three hydrofluoroethers.¹⁴⁻¹⁶ Only the total integrated absorption intensity of HFOC-125 over the entire range between 450 and 2000 cm⁻¹ measured with a spectral resolution of 0.5 cm⁻¹ is presented in ref 14. The reported value of 29.22 cm² molecule⁻¹ cm⁻¹ is significantly smaller than our total value of 32.64 cm² molecule⁻¹ cm⁻¹ for the same range. Results from two other studies^{15,16} reporting the integrated band intensities for different absorbing bands of HFOC-125 and HFOC-134 are listed in Table 3 for comparison with our data. These two studies of CHF₂-O-CF₃ were performed using different spectral resolutions. Heathfield et al.¹⁵ employed resolutions of 0.03 and 0.1 cm⁻¹ to measure the absorption of nondiluted ether samples. Heathfield et al.¹⁶ used the higher resolution of 0.0032 cm⁻¹ to study the nitrogen-diluted samples.

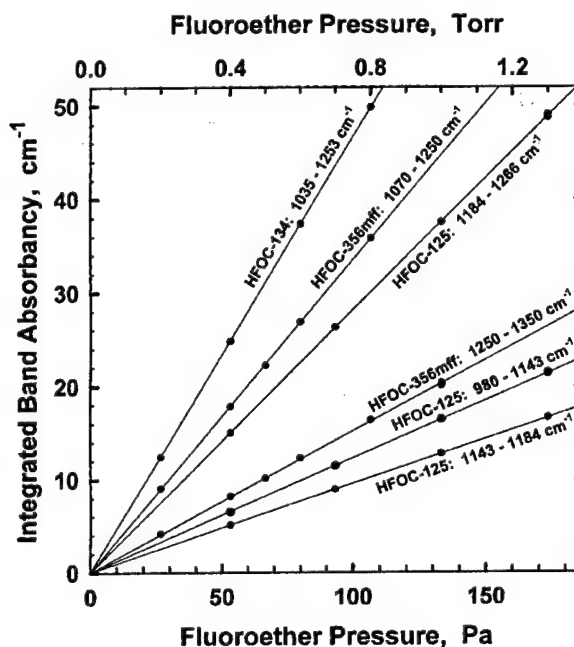


Figure 7. Dependence of the integrated absorption in several of the strongest bands (base 10) on the hydrofluoroether pressure.

One can see the excellent agreement between all measurements for the main absorption bands, while some discrepancies exist for the weakest ones. The agreement confirms our conclusion that neither pressure broadening nor very high resolution are necessary for measuring the midinfrared range absorption spectra of deeply halogenated hydrocarbons.¹³ Note that two bracketed absorption band intensities shown in Table 3 did not meet our 0.2% criteria to be assigned to the absorption spectrum of CHF₂-O-CF₃ (since they were only 0.19% and 0.07% of the strongest 1184-1266 cm⁻¹ band, respectively). They are

TABLE 4: Relative Radiative Forcing ($\text{RRF}_{\text{HFOC}}^{\text{CFC-11}}$), Atmospheric Lifetime, HGWP, and GWP for Hydrofluoroethers

compound (molecule)	$\text{RRF}_{\text{HFOC}}^{\text{CFC-11}}$	atmospheric lifetime, yrs	Global warming potentials at time horizons of:					
			20 years		100 years		500 years	
			HGWP	GWP	HGWP	GWP	HGWP	GWP
CFC-11 (CFCl_3)	1.00	45 ^a	1.0	6300	1.0	4600	1.0	1600
HFOC-134 ($\text{CHF}_2\text{-O-CHF}_2$)	1.77 ^c	24.8	1.75	11000	1.25	5800	1.14	1820
HFOC-356mff ($\text{CF}_3\text{-CH}_2\text{-O-CH}_2\text{-CF}_3$)	1.54 ^c	0.294	0.021	134	0.0086	39	0.0076	12
HFOC-125 ($\text{CHF}_2\text{-O-CF}_3$)	1.80 ^c	165 ^b	2.1	13400	3.4	15600	6.4	10200

^a The calculated atmospheric lifetime of CFC-11 (CFCl_3) and its GWP relative to CO_2 were taken from ref 22. ^b The atmospheric lifetime of $\text{CHF}_2\text{-O-CF}_3$ was calculated using eq 5 and the rate constant for the reaction with OH from ref 19. ^c Heathfield et al.¹⁶ reported $\text{RRF}_{134}^{\text{CFC-11}} = 1.48$ and $\text{RRF}_{125}^{\text{CFC-11}} = 1.40$; Christidis et al.¹⁴ reported $\text{RRF}_{125}^{\text{CFC-11}} = 1.55$; Wallington et al.¹⁷ reported $\text{RRF}_{356\text{mff}}^{\text{CFC-11}} = 1.35$. All data are based on results of radiative transfer modeling for the cloudy sky.

included into the table only to compare with the results presented by Heathfield et al.¹⁶ In any case, such disagreement in the weak long-wavelength band intensities does not affect the estimations of the global warming potentials of the compounds.

Garland et al.³ measured the IR absorption spectrum of HFOC-134 diluted with dry air up to 1 atm total pressure between 770 and 1430 cm^{-1} (the spectral resolution is not reported). Their absorption intensity integrated over the range can be recalculated¹⁶ to give $25.3 \times 10^{-17} \text{ cm}^2 \text{ molecule}^{-1} \text{ cm}^{-1}$ that coincides with our value of $25.4 \times 10^{-17} \text{ cm}^2 \text{ molecule}^{-1} \text{ cm}^{-1}$ obtained by integrating over the same wavenumber interval.

The only available IR spectrum of $\text{CF}_3\text{-CH}_2\text{-O-CH}_2\text{-CF}_3$ is presented in a figure by Wallington et al.¹⁷ Their absorption cross sections appear to agree with our results as best as can be estimated from an analysis of the published figure. The agreement is probably better than 3% at the main absorption peak at 1181.3 cm^{-1} .

Atmospheric Implications

Reactions with hydroxyl radicals in the troposphere are the main removal processes for hydrogen-containing compounds. Following Prather and Spivakovsky,¹⁸ we can estimate the atmospheric lifetime of an HFOC ($\tau_{\text{HFOC}}^{\text{OH}}$) due to reactions with hydroxyl radicals in the troposphere as

$$\tau_{\text{HFOC}}^{\text{OH}} = \frac{k_{\text{MC}}(277)}{k_{\text{HFOC}}(277)} \tau_{\text{MC}}^{\text{OH}} \quad (5)$$

where $\tau_{\text{HFOC}}^{\text{OH}}$ and $\tau_{\text{MC}}^{\text{OH}} = 5.9$ years are the atmospheric lifetimes of HFOC under study and methyl chloroform (MC), respectively, due to reactions with hydroxyl radicals in the troposphere only, and $k_{\text{HFOC}}(277)$ and $k_{\text{MC}}(277) = 6.69 \times 10^{-15} \text{ cm}^3 \text{ molecule}^{-1} \text{ s}^{-1}$ (ref 19) are the rate constants for the reactions of OH with these substances at $T = 277$ K. The value of $\tau_{\text{MC}}^{\text{OH}}$ was obtained following the procedure used by Prinn et al.²⁰ from the measured lifetime of MC, $\tau_{\text{MC}} = 4.8$ years when an ocean loss of 85 years and a stratospheric loss of 37 years are taken into account.

Given our earlier discussion of the differences in the Arrhenius parameters for the reaction between OH and $\text{CHF}_2\text{-O-CHF}_2$ obtained in the present work and reported in ref 5, a fit to the combined data is best recommended. Such a combined fit results in

$$k_{\text{HFOC-134}}(T) = (0.82_{-0.24}^{+0.34}) \times 10^{-12} \exp\{-(1730 \pm 110)/T\} \text{ cm}^3 \text{ molecule}^{-1} \text{ s}^{-1} \quad (6a)$$

$$k_{\text{HFOC-134}}(T) = 2.46 \times 10^{-15} \exp\left\{-1730\left(\frac{1}{T} - \frac{1}{298}\right)\right\} \text{ cm}^3 \text{ molecule}^{-1} \text{ s}^{-1} \quad (6b)$$

$$f(T)_{\text{HFOC-134}} \approx 1.1 \exp\left\{110\left|\frac{1}{T} - \frac{1}{298}\right|\right\} \quad (6c)$$

We did not include the data from ref 3 in this combined fit because of their higher scatter and smaller region of temperature overlap with the other studies. The fit to a data set combined from the results obtained over different temperature ranges can cause additional systematic errors in the Arrhenius parameters.²⁹ The recommended fit to our data and those of ref 5 results in a rate constant $k_{\text{HFOC-134}}(277) = 1.59 \times 10^{-15} \text{ cm}^3 \text{ molecule}^{-1} \text{ s}^{-1}$ that is ca. 14% higher than the current JPL Data Panel recommendation.¹⁹ For the rate constant of the reaction between OH and $\text{CF}_3\text{-CH}_2\text{-O-CH}_2\text{-CF}_3$, we can only recommend expression 3 (which does not include the room-temperature data of ref 6 because of the lack of detailed information on these measurements). The atmospheric lifetimes were thus calculated to be 24.8 years and 0.294 years for HFOC-134 and HFOC-356mff, respectively, based on these recommendations for the rate constants.

All the fluorinated ethers studied here absorb UV radiation in neither the troposphere nor the stratosphere. Therefore, the values of $\tau_{\text{HFOC}}^{\text{OH}}$ are the good estimations of their total atmospheric lifetimes.⁹ The calculated atmospheric lifetimes are presented in Table 4 along with our estimations of the radiative forcing and global warming potentials of the compounds.

The measured infrared absorption cross sections together with the estimated atmospheric lifetimes allowed us to estimate the climate related properties of the fluorinated ethers. The calculation technique we used here will be described in detail by Orkin et al.¹³ Therefore, we present here only the main equations that were used for the calculations. The experimentally obtained spectrum of the Earth's outgoing infrared radiation²¹ was used to calculate the relative radiating forcing of the ether with CFC-11 (CFCl_3) as the reference,

$$\text{RRF}_{\text{HFOC}}^{\text{CFC-11}} = \frac{\int_{\nu_1}^{\nu_2} \sigma_{\text{HFOC}}(\nu) \Phi(\nu) d\nu}{\int_{\nu_1}^{\nu_2} \sigma_{\text{CFC-11}}(\nu) \Phi(\nu) d\nu} \quad (6)$$

where $\Phi(\nu)$ is the intensity of outgoing Earth's radiation. We

TABLE 5: Rate Constants for Reactions between Fluorinated Ethers and Corresponding Alkanes

molecule	$A \times 10^{12}$, $\text{cm}^3 \text{molec}^{-1} \text{s}^{-1}$	E/R , K	$k(298) \times 10^{14}$, $\text{cm}^3 \text{molec}^{-1} \text{s}^{-1}$	reference
CH_3-CH_3	7.9	1030	25.0	27
$\text{CH}_3-\text{O}-\text{CH}_3$	11.0	370	290.0	27
$\text{CH}_3-\text{CH}_2-\text{CF}_3$			4.2	19
$\text{CH}_3-\text{O}-\text{CH}_2-\text{CF}_3$			63.0	2, 6
$\text{CH}_3-\text{CH}_2-\text{O}-\text{C}_4\text{F}_9$			7.0	28
CH_3-CF_3	1.2	2030	0.13	9
$\text{CH}_3-\text{C}_2\text{F}_5$	0.44	1690	0.15	29
$\text{CH}_3-\text{O}-\text{CF}_3$	1.5	1450	1.2	19
$\text{CH}_3-\text{O}-\text{C}_4\text{F}_9$			1.4	30
CH_3-CHF_2	2.4	1260	3.5	19
$\text{CH}_3-\text{O}-\text{CHF}_2$	6.0	1530	3.5	4
$\text{CHF}_2-\text{CHF}_2$	1.6	1680	0.57	19
$\text{CHF}_2-\text{O}-\text{CHF}_2$	0.63	1650	0.25	this work
	1.9	2000	0.23	5
CHF_2-CF_3	0.56	1700	0.19	19
$\text{CHF}_2-\text{O}-\text{CF}_3$	0.47	2100	0.041	19
$\text{CH}_3-\text{CH}_2-\text{CH}_2-\text{CH}_3$	9.0	395	240.0	27
$\text{CH}_3-\text{CH}_2-\text{O}-\text{CH}_2-\text{CH}_3$	5.8	-240	1300.0	12
$\text{CF}_3-\text{CH}_2-\text{CH}_2-\text{CF}_3$	3.0	1800	0.71	19
$\text{CF}_3-\text{CH}_2-\text{O}-\text{CH}_2-\text{CF}_3$	2.3	790	16.2	this work
$\text{CHF}_2-\text{CH}_2-\text{CF}_3$	0.61	1330	0.70	19
$\text{CHF}_2-\text{O}-\text{CH}_2-\text{CF}_3$	2.6	1610	1.2	19

used absorption cross sections of CFC_{11} , $\sigma_{\text{CFC-11}}(\nu)$ obtained by Orkin et al.¹³ for the calculations.

Time-dependent halocarbon global warming potentials, $\text{HGWP}(t)$ (the global warming potential with CFC_{11} as a reference compound), were then calculated¹³ using the compound atmospheric lifetimes presented in Table 4,

$$\text{HGWP}_{\text{HFOC}}(t) =$$

$$\frac{M_{\text{CFC-11}} \int_{\nu_1}^{\nu_2} \sigma_{\text{HFOC}}(\nu) \Phi(\nu) d\nu}{M_{\text{HFOC}} \int_{\nu_1}^{\nu_2} \sigma_{\text{CFC-11}}(\nu) \Phi(\nu) d\nu} \frac{\tau_{\text{HFOC}}}{\tau_{\text{CFC-11}}} \frac{1 - \exp(-t/\tau_{\text{HFOC}})}{1 - \exp(-t/\tau_{\text{CFC-11}})} =$$

$$\text{RRF}_{\text{HFOC}}^{\text{CFC-11}} \frac{M_{\text{CFC-11}}}{M_{\text{HFOC}}} \frac{\tau_{\text{HFOC}}}{\tau_{\text{CFC-11}}} \frac{1 - \exp(-t/\tau_{\text{HFOC}})}{1 - \exp(-t/\tau_{\text{CFC-11}})} \quad (7)$$

where M_{HFOC} and $M_{\text{CFC-11}}$ are molecular weights of the fluoroether and CFC_{11} , respectively. The hydrofluoroethers studied in the present work have no intense absorption bands that overlap the $15 \mu\text{m}$ absorption band of carbon dioxide (ca. $600\text{--}800 \text{ cm}^{-1}$). Therefore, such calculations should result in reasonable and accurate estimations of the radiative forcing and HGWPs of the compounds.¹³

All the atmospheric parameters discussed above τ_{HFOC} , $\text{RRF}_{\text{HFOC}}^{\text{CFC-11}}$, and $\text{HGWP}_{\text{HFOC}}(t)$ are the results of self-consistent estimations made by using only data from laboratory measurements (k_i , $\sigma_i(\nu)$) and field measurements (τ_{MC} , $\Phi(\nu)$). Global warming potentials with CO_2 as a reference (GWP) cannot be accurately calculated in the above-described manner due to the high concentration of carbon dioxide in the real Earth's atmosphere that results in nonlinear absorption of the outgoing radiation by CO_2 molecules.¹³ Therefore, we used the global warming potential of CFC_{11} referenced to CO_2 ($\text{GWP}_{\text{CFC-11}}$) calculated using a radiative transfer model of the atmosphere²² to obtain the GWPs of the ethers presented in Table 4,

$$\text{GWP}_{\text{HFOC}}(t) = \text{HGWP}_{\text{HFOC}}(t) \text{GWP}_{\text{CFC-11}}(t) \quad (8)$$

The latest accepted data for GWPs are presented in the *Scientific Assessment of Ozone Depletion: 1998*.²² Our estimations for

the GWPs of HFOC_{125} presented in Table 4 agree with the recommendations from this assessment to better than 3%. Our estimations for the GWPs of HFOC_{134} differ from those in ref 22 by between 7% and 21% depending on the time horizon. This difference is entirely due to the difference between the lifetime for HFOC_{134} derived here and that used in ref 22. For example, if a lifetime of HFOC_{134} of 29.7 years (i.e., the value in ref 22) were used in our calculations, the GWPs derived would agree with those from ref 22 within 2%.

Reactivity of Hydrofluoroethers

Generally, it has been assumed that ethers are more reactive toward hydrogen abstraction than the parent alkanes due to a decrease in the C—H bond strengths, particularly on the carbon adjacent to the ether linkage. Indeed, evidence has been presented indicating the effect of the ether linkage on increasing the reactivity of C—H bonds^{2a} as far as four carbons removed from the ether function. Increases in reactivity of a corresponding magnitude have not been observed when a second ether function is present.²³ In fact, the presence of a second ether function in a cyclic ether actually decreases the reactivity of the compound (for example, *p*-dioxane vs tetrahydrofuran).²⁴ However, early calculations support the idea that this reactivity pattern correctly reflected the differences in the bond strengths.²⁵ Examination of the current data set for hydrofluoroethers suggests that the inclusion of an ether linkage in a fluoroalkane either does not decrease the C—H bond strength as it does for simple hydrocarbons or that other factors (in addition to C—H bond strength) may be important in determining reactivity patterns.

In Table 5, we present the kinetic parameters for the reactions of OH with hydrofluoroethers and for their parent alkanes. The same results are presented graphically in Figure 8, where the room-temperature rate constants for the alkanes are given on a logarithmic scale on the left and the ethers on the right. The lines drawn connect the corresponding pairs. It is quite evident that the simple assumption of uniform activation of neighboring

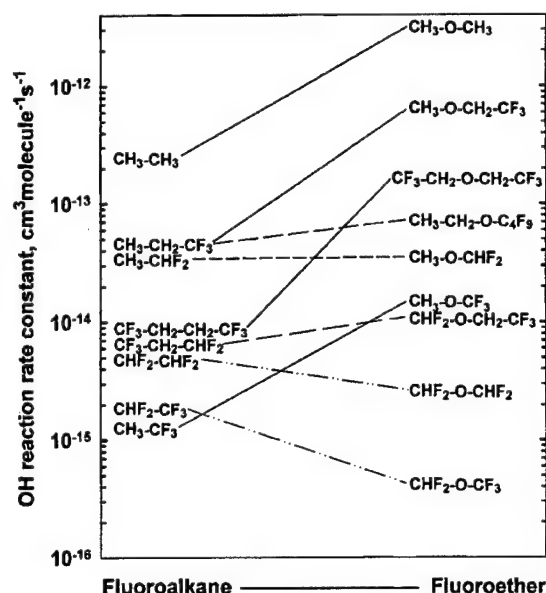


Figure 8. Graph of OH reactivity toward fluoroalkanes and corresponding fluoroethers at $T = 298$ K.

C-H bonds by the ether linkage is not correct. Rather, both activation and deactivation are observed. The net result is that the reactivities of the ethers span a much wider range than the reactivities of the parent alkanes, i.e., an increased spread of about 1.5 orders of magnitude.

It is difficult to discern clear trends from these data. We note that the two hydrofluoroethers, with no fluorine α to the ether linkage, both react significantly faster than their parent alkanes. For ethers where only one of the α carbons is fluorinated, the reactivity ranges from remaining unchanged to increasing by an order of magnitude. On the other hand, decreases in reactivity are observed for the two ethers in which both α carbon atoms are fluorinated. In the absence of a more comprehensive database for hydrofluoroether reactivity, it is difficult to draw conclusions regarding changes in Arrhenius parameters due to the addition of an ether linkage. We are presently performing *ab initio* calculations of the OH + hydrofluoroether reaction system in an attempt to obtain insight into the energetics and mechanisms for such reactions, with the objective of developing a predictive capability for reactivity toward OH.

Rate constants for the reactions between OH and few other hydrofluoroethers not listed in the Table 5 are also available from the literature. O'Sullivan et al.⁶ reported a rate constant of 2.1×10^{-14} cm³ molecule⁻¹ s⁻¹ for the reaction between OH and CH₃-O-CF₂CHF₂. This result is reasonably consistent with the structurally closest reactions in Table 5. Heathfield et al.⁷ reported rate constants of 20, 16.5, 9.4, and 43 ($\times 10^{-14}$ cm³ molecule⁻¹ s⁻¹) for the reactions of OH with CH₃-O-CF₂CHF₂, CH₃-O-CF₂CHFCl, CF₃CH₂-O-CF₂-CHF₂, and CH₃CH₂-O-CF₂CHF₂, respectively, from a pulse radiolysis experiment. On the basis of the reactivity information presented in Table 5, we conclude that all of them (especially first three reactions) are highly overestimated. Indeed, we expect the reactivity of CH₃-O-CF₂CHF₂ to be between that of CH₃-O-CF₃ and CH₃-O-CHF₂, i.e., around 2×10^{-14} cm³ molecule⁻¹ s⁻¹ (see Table 5). On the basis of the reactivity of closely related haloethanes,^{19,26} we conclude that the reactivity of CH₃-O-CF₂CHFCl should be higher than that of CH₃-O-CF₂CHF₂, not vice versa. The reactivity of CF₃CH₂-O-CF₂CHF₂ is probably close to that of CF₃CH₂-O-CHF₂ (see

Table 5). The estimation of the reactivity of CH₃CH₂-O-CF₂-CHF₂ is not as straightforward. It should slightly exceed the reactivity of CH₃CH₂-O-C₄F₉, whereas a factor of 6 (as suggested by the results of Heathfield et al.) seems too high. The presence of reactive impurities in the samples or the reactions with the ether decomposition products in the studies by these authors could be the possible reasons for such overestimation.

Acknowledgment. This work was supported by the Upper Atmosphere Research Program of the National Aeronautics and Space Administration and by the Next Generation Fire Suppression Technology Program, funded by the Department of Defense Strategic Environmental Research and Development Program under MIPR number W74RDV73243630. We thank Dr. Pamela Chu (NIST) for her help in measuring the IR spectra of the compounds.

References and Notes

- (1) (a) Brown, A. C.; Canosa-Mas, C. E.; Parr, A. D.; Pierce, J. M. T.; Wayne, R. P. *Nature* **1989**, *341*, 635-637. (b) Brown, A. C.; Canosa-Mas, C. E.; Parr, A. D.; Wayne, R. P. *Atmos. Environ.* **1990**, *24A*, 2499-2511.
- (2) (a) Wallington, T. J.; Liu, R.; Dagaut, P.; Kurylo, M. J. *Int. J. Chem. Kinet.* **1988**, *20*, 41-49. (b) Zhang, Z.; Saini, R. D.; Kurylo, M. J.; Huie, R. E. *J. Phys. Chem.* **1992**, *96*, 9301-9304.
- (3) Garland, N. L.; Medhurst, L. J.; Nelson, H. H. *J. Geophys. Res.* **1993**, *98*, 23107-23111.
- (4) (a) Orkin, V. L.; Khamaganov, V. G.; Guschin, A. G.; Huie, R. E.; Kurylo, M. J. *The 13th International Symposium on Gas Kinetics*; The University College of Dublin, Dublin, Ireland, September 1994; p D56. (b) Orkin, V. L.; Khamaganov, V. G.; Guschin, A. G.; Kasimovskaya, E. E.; Larin, I. K. *Development of Atmospheric Characteristics of Chlorine-Free Alternative Fluorocarbons, Report on R-134a and E-143a*; Report ORNL/Sub/86X-SL103V prepared for the Oak Ridge National Laboratory, 1993. (c) Orkin, V. L.; Khamaganov, V. G.; Guschin, A. G.; Larin, I. K. Manuscript in preparation.
- (5) Hsu, K.-J.; DeMore, W. B. *J. Phys. Chem.* **1995**, *99*, 11141-11146.
- (6) O'Sullivan, N.; Wenger, J.; Sidebottom, H. In *Proceedings of the 7th European Commission Symposium on Physicochemical Behavior of Atmospheric Pollutants*; Venice, Italy, October, 1996; Larsen, B., Versino, B., Eds.; Office for Official Publications of the European Communities: Luxembourg, 1997; p 77-79.
- (7) Heathfield, A. E.; Anastasi, C.; Pagsberg, P.; McCulloch, A. *Atmos. Environ.* **1998**, *32*, 711-717.
- (8) Kurylo, M. J.; Cornett, K. D.; Murphy, J. L. *J. Geophys. Res.* **1982**, *87*, 3081-3085.
- (9) Orkin, V. L.; Huie, R. E.; Kurylo, M. J. *J. Phys. Chem.* **1996**, *100*, 8907-8912.
- (10) Orkin, V. L.; Khamaganov, V. G.; Guschin, A. G.; Huie, R. E.; Kurylo, M. J. *J. Phys. Chem.* **1997**, *101*, 174-178.
- (11) Wallington, T. J.; Dagaut, P.; Kurylo, M. J. *J. Phys. Chem.* **1988**, *92*, 5024.
- (12) Mellouki, A.; Teton, S.; Le Bras, G. *Int. J. Chem. Kinet.* **1995**, *27*, 791-805.
- (13) Orkin, V. L.; Guschin, A. G.; Larin, I. K.; Huie, R. E.; Kurylo, M. J. Manuscript in preparation.
- (14) Christidis, N.; Hurley, M. D.; Pinnock, S.; Shine, K. P.; Wallington, T. J. *J. Geophys. Res.* **1997**, *102* (D16), 19597-19609.
- (15) Heathfield, A. E.; Anastasi, C.; Ballard, J.; Newnham, D. A.; McCulloch, A. *J. Quant. Spectrosc. Radiat. Transfer* **1998**, *59*, 91-97.
- (16) Heathfield, A. E.; Anastasi, C.; McCulloch, A.; Nicolaisen, F. M. *Atmos. Environ.* **1998**, *32*, 2825-2833.
- (17) Wallington, T. J.; Guschin, A.; Stein, T. N.; Platz, J.; Sehested, J.; Christensen, L. K.; Nielsen, O. J. *J. Phys. Chem. A* **1998**, *102*, 1152-1161.
- (18) Prather, M.; Spivakovsky, C. M. *J. Geophys. Res.* **1990**, *95*, 18723-18729.
- (19) DeMore, W. B.; Sander, S. P.; Golden, D. M.; Hampson, R. F.; Kurylo, M. J.; Howard, C. J.; Ravishankara, A. R.; Kolb, C. E.; Molina, M. J. *JPL Publication 97-4*; Jet Propulsion Laboratory, California Institute of Technology: Pasadena, CA, 1997.

- (20) Prinn, R. G.; Weiss, R. F.; Miller, B. R.; Huang, A.; Alyea, F. N.; Cunnold, D. M.; Fraser, P. J.; Hartley, D. E.; Simmonds, P. G. *Science* **1995**, *269*, 187–192.
- (21) Kunde, V. G.; Conrath, B. J.; Hanel, R. A.; Maguire, W. C.; Prabhakara, C.; Salomonson, V. V. *J. Geophys. Res.* **1974**, *79*, 777–784.
- (22) *Scientific Assessment of Ozone Depletion: 1998*; Global Ozone Research and Monitoring Project, Report No. 44; World Meteorological Organization: Geneva, Switzerland, 1999.
- (23) Dagaut, P.; Liu, R.; Wallington, T. J.; Kurylo, M. J. *Int. J. Chem. Kinet.* **1989**, *21*, 1173–1180.
- (24) Dagaut, P.; Liu, R.; Wallington, T. J.; Kurylo, M. J. *J. Phys. Chem.* **1990**, *94*, 1881–1883.
- (25) Huie, R. E.; Clifton, C. L.; Kafafi, S. A. *J. Phys. Chem.* **1991**, *95*, 9336–9340.
- (26) Guschin, A. G.; Kasimovskaya, E. E.; Khamaganov, V. G.; Orkin, V. L. *Proceedings of the Workshop on the Atmospheric Degradation of HCFCs and HFCs*; Boulder CO, November 17–19, 1993; p 1–51.
- (27) Atkinson, R.; Baulch, D. L.; Cox, R. A.; Hampson, R. F., Jr.; Kerr, J. A.; Rossi, M. J.; Troe, J. *J. Phys. Chem. Ref. Data* **1999**, *28*, 191–393.
- (28) Christensen, L. K.; Sehested, J.; Nielsen, O. J.; Bilde, M.; Wallington, T. J.; Guschin, A.; Molina, L. T.; Molina, M. J. *J. Phys. Chem. A* **1998**, *102*, 4839–4845.
- (29) Orkin, V. L.; Huie, R. E.; Kurylo, M. J. *J. Phys. Chem.* **1997**, *101*, 9118–9124.
- (30) Wallington, T. J.; Schneider, W. F.; Sehested, J.; Bilde, M.; Platz, J.; Nielsen, O. J.; Christensen, L. K.; Molina, M. J.; Molina, L. T. *J. Chem. Phys. A* **1997**, *101*, 8264–8274.

An *ab Initio* Study of the Kinetics of the Reactions of Halomethanes with the Hydroxyl Radical. 1. CH₂Br₂

Florent Louis,* Carlos A. Gonzalez,* Robert E. Huie, and Michael J. Kurylo

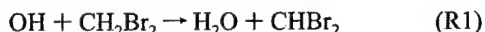
Physical and Chemical Properties Division, National Institute of Standards and Technology,
Gaithersburg, Maryland 20899

Received: March 24, 1999; In Final Form: January 20, 2000

Ab initio calculations were carried out with Møller–Plesset second- and fourth-order perturbation theory (MP2 and MP4), and the coupled cluster method, CCSD(T), on the H atom abstraction reaction from dibromomethane by hydroxyl radical attack. Geometry optimization and vibrational frequency calculations at the MP2 level were performed on reactants, products, and the transition state using the 6-311G(d,p) and 6-311G(2d,2p) basis sets. The geometry parameters optimized at the MP2/6-311G(2d,2p) level of theory were used in single-point energy calculations with increasing basis set sizes, from 6-311G(2d,2p) to 6-311++G-(3df,3pd) at both the MP2 and MP4(SDTQ) levels of theory. Canonical transition-state theory was used to predict the rate constants as a function of the temperature (250–400 K). It was found that the kinetic parameters obtained in this work with the spin-projected method PMP4(SDTQ)/6-311++G-(3df,3pd)/MP2/6-311G(2d,2p) are in reasonable agreement with the experimental values. The prospect of using relatively low level *ab initio* electronic structure calculations aimed at the implementation of inexpensive semiquantitative “screening tools” that could aid scientists in predicting the kinetics of similar processes is also discussed.

Introduction

In this paper, we initiate a systematic study of the application of *ab initio* electronic structure calculations combined with transition-state theory to the kinetics of hydrogen atom abstractions by hydroxyl radicals. This work is part of an ongoing effort at the National Institute of Standards and Technology (NIST) leading to the implementation of efficient and reliable computational chemistry “screening tools” useful in predicting the fate of haloalkanes once they are released into the atmosphere. Our focus is mainly directed to the use of computationally inexpensive *ab initio* molecular orbital methodologies that could be used on a routine basis by both experimentalists and computational chemists so that a reliable semiquantitative picture of the kinetics of these reactions can be obtained with the minimum amount of effort. In this work, we report results for the reaction



We have chosen this reaction as a prototype of processes for which the proposed screening tool will be used. One of the reasons for this choice is the availability of reliable experimental data and because the significant computational difficulty in treating relatively large electronic systems containing bromine atoms makes this reaction a serious test of the applicability of the current quantum chemistry methodologies in such systems. Thus, it is expected that a viable theory level for this reaction should be adequate for other haloalkanes containing bromine or lighter halogen atoms. In addition, bromine is an active agent in fire suppression and inhibition.¹ In the screening for suitability as a fire suppressant, the reactivity of the agent is of important consideration, with regard to both its utility and its environmental acceptability.

There have been some early applications of transition-state theory to the reactions of OH with haloalkanes, making use of thermochemical kinetic tools, which provided estimates of the Arrhenius preexponential factors.^{2,3} A few *ab initio* studies also have been carried out on the reactions of hydroxyl radicals with halogen-substituted methanes^{4–6} or ethanes.^{7–11} None of these, however, have included bromine-substituted methanes. In addition, there have been several *ab initio* studies on the reactions of fluorine and chlorine atoms with halogenated methanes^{12–14} and ethanes^{15,16} plus one on methyl radical reactions with halomethanes,¹⁷ and a theoretical study of the enthalpies of formation of fluoromethanes.¹⁸ Recently, two *ab initio* studies dealing with the structures, vibrational frequencies, thermodynamic properties, and bond dissociation energies of bromomethanes and bromomethyl radicals were published.^{19–21}

Table 1 summarizes the available results of the experimental studies of the reaction of OH with CH₂Br₂. The rate constant was measured by absolute techniques by Mellouki et al.²² and Zhang et al.²³ as well as by relative techniques by DeMore²⁴ and Orlando et al.²⁵ It was also measured recently in our laboratory at 298 K.²⁶ In general, all measurements agree with the value $k(298 \text{ K}) = 1.2 \times 10^{-13} \text{ cm}^3 \text{ molecule}^{-1} \text{ s}^{-1}$.

The kinetic parameters for the reaction of OH with CH₂Br₂ are consistent with a reaction that takes place by hydrogen abstraction. Recent work has demonstrated that the reaction of the hydroxyl radical with CF₃I proceeds rapidly by I atom abstraction.²⁸ The lack of reactivity of CF₃Br toward OH²⁷ however argues against any significant contribution of a bromine abstraction reaction pathway for OH + CH₂Br₂.

In this work, the energetics (heat of reactions and reaction barriers) as well reaction rate constants in the temperature range 250–400 K are computed at different levels of theory and basis sets. From the computed temperature dependence data, Arrhenius parameters (*A*-factor and activation energy) are obtained and the results compared to available experimental data.

* To whom Correspondence should be addressed. Fax: (301) 975–3672.
E-mail: (F.L.) flouis@nist.gov, (C.A.G.) carlos.gonzalez@nist.gov.

TABLE 1: Experimental Rate Parameters for the Reaction OH + CH₂Br₂ → H₂O + CHBr₂

<i>A</i> (cm ³ molecule ⁻¹ s ⁻¹)	<i>E_a</i> (kJ mol ⁻¹)	<i>T</i> (K)	<i>k</i> (298 K) (cm ³ molecule ⁻¹ s ⁻¹)	method	ref
1.9 × 10 ⁻¹²	7.0	244–370	1.1 × 10 ⁻¹³	FP/LIF ^a	22
1.9 × 10 ⁻¹²	7.0	293–375	1.1 × 10 ⁻¹³	RR ^b	24
3.2 × 10 ⁻¹²	7.5	293–375	1.5 × 10 ⁻¹³	RR ^b	24 ^c
		298	1.2 × 10 ⁻¹³	RR ^b	25
1.5 × 10 ⁻¹²	6.0	288–368	1.3 × 10 ⁻¹³	DF/RF ^c	23
		298	1.2 × 10 ⁻¹³	FP/RF ^d	26

^a FP/LIF = flash photolysis/laser-induced fluorescence. ^b RR = relative rate. ^c DF/RF = discharge flow/resonance fluorescence. ^d FP/RF = flash photolysis/resonance fluorescence. ^e Rate constants from ref 24 recalculated using the values of the rate constant for the reference reaction OH + CH₂Cl₂ reported in ref 27.

Computational Methods²⁹

All calculations described below were carried out with the Gaussian 94³⁰ suite of programs on a Cray C90/6256 supercomputer and a 32-processor Silicon Graphics Origin 2000 parallel computer. Fully optimized geometries, harmonic vibrational frequencies, and zero-point energy corrections (ZPE) of reactants, the transition structure, and products were calculated with the unrestricted second-order Møller–Plesset perturbation theory (UMP2) using the 6-311G(d,p) and 6-311G-(2d,2p) basis sets. Electron correlation was calculated with second- and fourth-order Møller–Plesset perturbation theory in the space of single, double, triple, and quadruple excitations with full annihilation of spin contamination³¹ as implemented in the Gaussian 94 package (noted in our results as PMP_{*n*}, with *n* = 2 or 4). These single-point calculations were carried out using basis sets ranging from 6-311G(2d,2p) to 6-311++G-(3df,3pd) and geometries previously optimized at the MP2/6-311G(2d,2p) level. All relative energies quoted and discussed in the present paper include zero-point energy corrections with unscaled vibrational frequencies. For comparison purposes, single-point energies at the MP2/6-311G(2d,2p)-optimized geometries were also computed with the highly correlated (and computationally more expensive) coupled cluster method including single and double electron excitations computed iteratively, and triple excitations computed in a noniteratively manner from the Hartree–Fock determinant, CCSD(T).³² The larger basis 6-311++G(3df,3pd) was used in these calculations.

Canonical transition-state theory³³ (TST) and tunneling corrections were used to predict the rate constant over the same range of temperatures as the available experimental measurements (250–400 K). Thus, rate constants, *k*(*T*), were computed with the following expression:

$$k(T) = \Gamma(T) \frac{k_B T}{h} \frac{Q^{\text{TS}}(T)}{Q^{\text{OH}}(T) Q^{\text{CH}_2\text{Br}_2}(T)} \exp\left(-\frac{\Delta E}{k_B T}\right) \quad (1)$$

where: $Q^{\text{TS}}(T)$, $Q^{\text{OH}}(T)$, and $Q^{\text{CH}_2\text{Br}_2}(T)$ are the total partition functions for the transition state, hydroxyl radical, and dibromomethane at temperature *T*, ΔE is the activation energy including thermal corrections to the internal energy and zero-point energy, k_B is Boltzmann's constant, and h is Planck's constant. $\Gamma(T)$ in eq 1 indicates the corresponding tunneling correction at temperature *T* (see the Results and Discussion).

Results and Discussion

1. Geometry Parameters and Vibrational Frequencies. 1.1.

Geometry Parameters. Reactants and Products. Table 2 lists the geometry parameters fully optimized at the MP2/6-311G-(d,p) and MP2/6-311G(2d,2p) levels of theory. In addition, the available experimental data characterizing the structures of these species are also shown for comparison purposes. As the results

TABLE 2: Optimized Geometry Parameters^a for Reactants and Products Involved in H Abstraction Reaction of CH₂Br₂ with Hydroxyl Radicals

		MP2 6-311G(d,p)	MP2 6-311G(2d,2p)	exptl
OH	<i>r</i> (OH)	0.967	0.965	0.971 ^b
CH ₂ Br ₂	<i>r</i> (CH)	1.086	1.078	1.097 ^c
	<i>r</i> (CBr)	1.929	1.933	1.925
	θ (HCH)	111.6	111.9	110.9
	θ (BrCH)	107.8	107.9	
	ϕ (BrCHH)	118.2	118.5	
H ₂ O	<i>r</i> (OH)	0.958	0.957	0.958 ^d
	θ (HOH)	102.4	103.3	104.5
CHBr ₂	<i>r</i> (CH)	1.082	1.074	
	<i>r</i> (CBr)	1.860	1.861	
	θ (BrCH)	116.0	116.1	
	ϕ (BrCHBr)	148.4	149.2	

^a Bond lengths are in angstroms; bond angles θ and dihedral angles ϕ are in degrees. ^b Reference 34. ^c Reference 40. ^d Reference 41.

show, the optimized geometries with both basis sets are in excellent agreement with the corresponding experimental values.

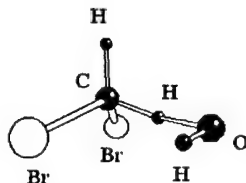
Transition-State Structure. The MP2-optimized parameters for the transition-state structure using the 6-311G(d,p) and 6-311G(2d,2p) basis sets are shown in Table 3 and Figure 1. Comparison of the results shows that, as in the case of reactants and products, the transition-state structures optimized with both basis sets are very similar. This agreement is further reflected in the transition-state parameter *L*, defined as the ratio of the increase in the length of the C–H bond being broken and the elongation of the O–H bond being formed, each with respect to its equilibrium value in the reactant (CH₂Br₂) and the product (H₂O).¹² This parameter characterizes the most important aspect of the geometric structure of the transition state. As the results in Table 3 show, addition of an extra set of d-orbital polarization functions on the heavy atoms (C and Br) and two p-orbital polarization functions on the H atoms leads to an *L* value very close to the one obtained at the MP2/6-311G(d,p) level (0.324 vs 0.314). Both values of the *L* parameter indicate a reactant-like character for the transition-state structure as expected for an exothermic reaction. The fact that the less computationally demanding MP2/6-311G(d,p) level of theory gives results for the geometry of the minima and transition state in excellent agreement with the ones computed with the larger basis 6-311G-(2d,2p) suggests that this level may be sufficient for treating systems similar to the one under study. More cases however must be studied before this level of theory can be recommended. In this work, we choose the MP2/6-311G(2d,2p)-optimized geometries for the single-point energy calculations.

1.2. Vibrational Frequencies. The vibrational frequencies, unscaled zero-point energies, and internal energy corrections at 298 K for reactants, the transition state, and products are given in Tables 4 and 5. For reactants and products, calculated vibrational frequencies at MP2/6-311G(d,p) and MP2/6-311G-(2d,2p) are about 7% greater than the experimental values. As

TABLE 3: Optimized Geometry Parameters^a for the Transition State Involved in H Atom Abstraction Reaction of CH₂Br₂ with Hydroxyl Radicals

	MP2 6-311G(d,p)	MP2 6-311G(2d,2p)	param ^a	MP2 6-311G(d,p)	MP2 6-311G(2d,2p)
<i>r</i> (C–H _R)	1.192	1.188	θ (Br _(b) CH _R)	108.0	107.8
<i>r</i> (CH)	1.087	1.078	θ (OH _R C)	166.2	165.3
<i>r</i> (CBr _(a))	1.910	1.911	θ (HOH _R)	97.1	97.2
<i>r</i> (CBr _(b))	1.917	1.919	ϕ (Br _(a) CH _R H)	117.8	118.1
<i>r</i> (OH _R)	1.296	1.296	ϕ (Br _(b) CH _R H)	–118.3	–118.4
<i>r</i> (HO)	0.968	0.967	ϕ (OH _R CH)	48.5	51.9
θ (HCH _R)	108.2	108.2	ϕ (HOH _R C)	50.7	51.5
θ (Br _(a) CH _R)	105.8	106.0	<i>L</i> ^b	0.314	0.324

^a Bond lengths are in angstroms; bond angles θ and dihedral angles ϕ are in degrees. The hydrogen atom involved in H atom abstraction is noted H_R. (a) refers to the in-plane bromine and (b) to the out-of-plane bromine. ^b The parameter *L* is the ratio between the elongation value of the C–H bond and the elongation of the O–H bond: $L = \delta r(\text{CH})/\delta r(\text{OH})$.

**Figure 1.** MP2/6-311G(2d,2p)-optimized geometry for the transition state involved in the OH + CH₂Br₂ reaction.**TABLE 4: Calculated^{a,b} Vibrational Frequencies (cm^{–1}) for the Reactants, Transition State, and Products Involved in H Atom Abstraction Reaction of CH₂Br₂ with Hydroxyl Radicals**

species	vibrational frequencies (cm ^{–1}) ^c
OH	(a) 3853 (b) 3833 3735 ^d
CH ₂ Br ₂	(a) 178, 604, 692, 835, 1150, 1265, 1459, 3169, 3254 (b) 175, 590, 672, 833, 1141, 1239, 1458, 3183, 3270 169, 588, 653, 812, 1095, 1195, 1382, 3009, 3073 ^e
TS	(a) 2075i, 70, 102, 155, 183, 473, 651, 713, 805, 959, 1210, 1319, 1405, 3211, 3840 (b) 2200i, 76, 109, 156, 182, 463, 640, 698, 803, 957, 1191, 1307, 1395, 3225, 3811
H ₂ O	(a) 1667, 3905, 4013 (b) 1685, 3875, 3989 1595, 3657, 3756 ^e
CHBr ₂	(a) 193, 492, 653, 805, 1241, 3267 (b) 189, 486, 644, 790, 1214, 3279 633, 778, 1164 ^f

^a MP2/6-311G(d,p). ^b MP2/6-311G(2d,2p). ^c The experimental values of the vibrational frequencies are in italics. ^d Reference 34. ^e Reference 42. ^f Reference 43.

TABLE 5: Calculated Zero-point Energy and Thermal Energy Corrections at 298 K for the Reactants, Transition State, and Products Involved in H Atom Abstraction Reaction of CH₂Br₂ with Hydroxyl Radicals

	zero-point Energy ^a	thermal energy ^a		zero-point energy ^a	thermal energy ^a
OH	23.1 ^b /22.9 ^c	6.2	CHBr ₂	39.8/39.5	10.2
CH ₂ Br ₂	75.4/75.1	10.1	TS	90.3/89.8	16.4
H ₂ O	57.3/57.1	7.5			

^a Units are kJ mol^{–1}. ^b Geometry optimization calculation at the MP2/6-311G(d,p) level of theory. ^c Geometry optimization calculation at the MP2/6-311G(2d,2p) level of theory.

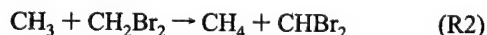
with the geometries, the vibrational frequencies computed with both basis sets are in excellent agreement. The eigenvector in the transition state corresponding to the imaginary frequency is primarily a motion of the reactive hydrogen atom being transferred between the C and the O centers. The calculated imaginary frequency is about 6% larger at the MP2/6-311G(2d,2p) level of theory than at the MP2/6-311G(d,p) level (2200

cm^{–1} vs 2075 cm^{–1}). A similar fact was observed previously in the series of H atom abstraction reactions F + CHCl_{3–x}F_x (*x* = 0, 1, 2, or 3).¹³

2. Reaction Enthalpies and Activation Energies. Table 6 lists reaction enthalpies ($\Delta_r H$), C–H bond strengths $D_{298}(\text{H–CHBr}_2)$, and activation energies (E_a), computed at different levels of theory and taking into account the zero-point energy differences and thermal energy corrections at 298 K (calculated using the vibrational frequencies given in Table 4) for the reaction OH + CH₂Br₂. Results obtained at the highly correlated level CCSD(T)/6-311++G(3df,3pd)/MP2/6-311G(2d,2p) are also listed for comparison purposes.

2.1. Reaction Enthalpies. Reaction enthalpies calculated at the PMP2/6-311G(d,p)/MP2/6-311G(d,p) and PMP2/6-311G(2d,2p)/MP2/6-311G(2d,2p) levels are very close to the literature values based on $\Delta_f H^\circ$ at 298 K for OH,³⁴ CH₂Br₂,³⁹ H₂O,³⁴ and CHBr₂,⁴⁰ especially if the experimental uncertainties for CH₂Br₂ (± 9 kJ mol^{–1}) and CHBr₂ (± 5 kJ mol^{–1}) are taken into consideration. Adding diffuse functions to the basis sets at the PMP2 level leads to reaction enthalpies significantly larger than the experimental value and outside the experimental uncertainties. A better agreement with experiment is obtained at the PMP4(SDTQ) level.

To improve on the agreement between *ab initio* and experimental values, especially in the case where basis sets have been expanded by including diffuse functions, reaction enthalpies for reaction R1 were also corrected by new values of $D_{298}(\text{H–CHBr}_2)$ computed at different levels of theory using the following isodesmic reaction:



The direct calculation of this bond dissociation energy from the reaction CH₂Br₂ → H + CHBr₂ is expected to be systematically in error due to insufficient treatment of electron correlation and incompleteness of the basis sets. The use of an isodesmic reaction, such as reaction R2, provides an indirect method that may lead to a more reliable value of the bond dissociation energy. In general, isodesmic reactions are characterized by having the same number and types of bonds on each side of the equation, so that the errors mentioned above are largely canceled when $D_{298}(\text{H–CHBr}_2)$ is calculated. The reaction enthalpy for reaction R2 was computed at the same levels of theory as that for reaction R1. Taking the experimental value of $D_{298}(\text{H–CH}_3) = 440$ kJ mol^{–1},⁴¹ we obtain calculated $D_{298}(\text{H–CHBr}_2)$ values at the various levels of theory used in this work (Table 6, column 3). These $D_{298}(\text{H–CHBr}_2)$ quantities were then used in the calculation of the reaction enthalpy for reaction R1 by means of the following relation:

$$\Delta_r H(\text{ISO}) = D_{298}(\text{H–CHBr}_2) - D_{298}(\text{H–OH}) \quad (2)$$

TABLE 6: Reaction Enthalpies $\Delta_r H$, Bond Strengths $D_{298}(\text{H}-\text{CHBr}_2)$, Reaction Enthalpies $\Delta_r H(\text{ISO})$ Calculated Using an Isodesmic Reaction, and Activation Energies E_a Calculated at 298 K for the Reaction $\text{OH} + \text{CH}_2\text{Br}_2 \rightarrow \text{H}_2\text{O} + \text{CHBr}_2$ at Various Levels of Theory

level of theory ^a	$\Delta_r H^{b,d}$	$D_{298}(\text{H}-\text{CHBr}_2)^d$	$\Delta_r H(\text{ISO})^{b,d}$	$E_a^{c,d}$
PMP2/6-311G(d,p)	-82.7	412.7	-86.1	20.3
PMP2/6-311G(2d,2p)	-86.0	415.1	-83.7	17.4
PMP2/6-311G(2df,2p)	-91.1	412.1	-86.7	13.9
PMP2/6-311G(3df,2p)	-92.4	411.3	-87.5	12.0
PMP4(SDTQ)/6-311G(3df,2p)	-79.1	409.3	-89.5	13.0
PMP2/6-311++G(3df,2p)	-100.4	413.3	-85.5	14.6
PMP4(SDTQ)/6-311++G(3df,2p)	-86.4	411.3	-87.5	15.1
PMP2/6-311++G(3df,3pd)	-102.3	414.9	-83.9	10.6
PMP4(SDTQ)/6-311++G(3df,3pd)	-88.7	413.1	-85.7	10.5
CCSD(T)/6-311++G(3df,3pd)	-86.9	410.3	-87.6	7.0
experimental	-81.6 ^e	417.1 ^e	-81.6 ^e	7.0 ^f

^a All the geometry optimization calculations were done with the MP2/6-311G(2d,2p) except the first with MP2/6-311G(d,p). ^b Including the sum of thermal energies ($\Delta\text{ZPE} + \text{thermal energy corrections}$). ^c Including the sum of thermal energies ($\Delta\text{ZPE} + \text{thermal energy corrections} + \text{RT}$). ^d In kJ mol⁻¹. ^e See the text. ^f From ref 22.

Table 6 (column 4) lists the $\Delta_r H(\text{ISO})$ values obtained by eq 2, which can be compared to the direct calculations (column 2) and to their experimental counterparts. The degree of improvement observed becomes more significant for basis sets with diffuse functions.

2.2. Activation Energies. The results reported in Table 6 indicate that PMP2/6-311G(d,p)/MP2/6-311G(d,p) calculations overestimate the experimental activation energy by about 13–14 kJ mol⁻¹. Adding an extra set of d and p functions to the basis sets decreases the activation energy by about 3.0 kJ mol⁻¹. Addition of more polarization and diffuse functions tends to improve the agreement with experiment. Thus, PMP4(SDTQ)/6-311++G(3df,3pd) and PMP2/6-311++G(3df,3pd) calculations lead to activation energies for the $\text{OH} + \text{CH}_2\text{Br}_2$ reaction that are 3.5 and 3.6 kJ mol⁻¹ higher than the experimental value, respectively. Similar calculations using the same basis sets with the highly correlated and more computationally demanding CCSD(T) level of theory predict an activation energy of 7.0 kJ mol⁻¹, in excellent agreement with the experimental value. This result clearly indicates that most of the error in the activation energies computed at PMP2 and PMP4 with the 6-311++G-(3df,3pd) basis can be attributed to the lack of correlation in such methods and not to an improper optimized geometry at the MP2/6-311G(2d,2p) level of theory. It is interesting to note that, at the PMP2 and PMP4 levels, a better agreement with experiment is achieved when the 6-311G(3df,2p) basis is used when compared to the larger 6-311++G(3df,2p) basis. This result is most probably a reflection of a better balance between basis set size and correlation in the case of the smaller basis. Similar results have been observed by Truong and Truhlar⁴⁴ in their *ab initio* transition-state theory calculations of the reaction rate for $\text{OH} + \text{CH}_4 \rightarrow \text{H}_2\text{O} + \text{CH}_3$.

The objective of the present work is to develop a method that can be applied to a range of reactants, typically much larger than CH_2Br_2 . Thus, although the CCSD(T) level of theory results in better values of the activation energy, it is too computationally intensive to be generally applicable at the present time. Therefore, in this work, we have chosen the energetics computed at PMP4(SDTQ)/6-311++G(3df,3pd)/MP2/6-311G(2d,2p) to calculate the reaction rate constants (see below). These rate constants are determined as a function of temperature and an activation energy calculated from this dependence.

3. Kinetic Parameters and Tunneling Effect. The calculation of the reaction rate constants using the TST formula given in eq 1 requires the proper computation of the partition functions of reactants and the transition state. In general, the total partition function $Q^X(T)$ of species X ($X = \text{CH}_2\text{Br}_2$, OH, or TS) can be

cast in terms of the translational (Q^X_{T}), rotational (Q^X_{R}), electronic (Q^X_{e}), and vibrational (Q^X_{v}) partition functions:

$$Q^X(T) = Q^X_{\text{T}}(T) Q^X_{\text{R}}(T) Q^X_{\text{e}}(T) Q^X_{\text{v}}(T) \quad (3)$$

In computing the electronic partition function for the OH radical, Q^{OH}_{e} , the multiplicity of the states $^2\Pi_{3/2}$ and $^2\Pi_{1/2}$ and the energy gap of 139.7 cm⁻¹ between the levels³⁴ have been taken into consideration.

3.1. Hindered Rotor Approximation. Direct inspection of the TS low-frequency modes (Table 4) indicates that the mode with a frequency of 109 cm⁻¹ consists of a hindered OH rotation about the nearly linear C–H–O axis with a rotational barrier of 5.5 kJ mol⁻¹. Consequently, this mode should be treated as a hindered rotor instead of a vibration.⁴³ Thus, this mode was removed from the vibrational partition function for the TS, and the corresponding hindered rotor partition function $Q_{\text{HR}}(T)$ was calculated, yielding the following expression for the total TS partition function:

$$Q^{\text{TS}} = Q^{\text{TS}}_{\text{T}}(T) Q^{\text{TS}}_{\text{R}}(T) Q^{\text{TS}}_{\text{e}}(T) Q^{\text{TS}}_{\text{v}}(T) Q_{\text{HR}}(T) \quad (4)$$

with $Q^{\text{TS}}_{\text{v}}(T)$ being the corrected vibrational partition function where the internal rotation mode has been removed.

In our calculations we have adopted the analytical approximation to $Q_{\text{HR}}(T)$ for a one-dimensional hindered internal rotation proposed by Ayala and Schlegel:⁴⁴

$$Q_{\text{HR}}(T) = \left(\frac{Q_i^{\text{h.o.q}}}{Q_i^{\text{h.o.cl}}} \right) Q_i^{\text{FR}} \frac{\left(1 + P_2 \exp \left[-\frac{V_0}{2k_{\text{B}}T} \right] \right)}{\left(1 + P_1 \exp \left[-\frac{V_0}{2k_{\text{B}}T} \right] \right)} \exp \left[-\frac{V_0}{2k_{\text{B}}T} \right] J_0 \left(\frac{iV_0}{2k_{\text{B}}T} \right) \quad (5)$$

where T is the temperature, k_{B} is Boltzmann's constant, V_0 is the internal rotational barrier, Q_i^{FR} is the free-rotor partition function, P_1 and P_2 are polynomial functions of $1/Q_i^{\text{FR}}$ and V_0/kT , J_0 is Bessel's function, and $Q_i^{\text{h.o.q}}$ and $Q_i^{\text{h.o.cl}}$ are the quantum and classical partition functions defined as

$$Q_i^{\text{h.o.q}} = \frac{e^{-u/2}}{1 - e^{-u}} \quad \text{and} \quad Q_i^{\text{h.o.cl}} = \frac{1}{u}, \quad u = \frac{\hbar \nu_i}{k_{\text{B}}T} \quad (6)$$

with ν_i being the vibrational frequency associated with the hindered rotation (109 cm⁻¹). Again following Ayala's and

Schlegel's recommendation,⁴⁴ we have used the following approximation for the free-rotor partition function:

$$Q_i^{\text{FR}}(T) = \left(\frac{8\pi^3 k_B}{h^2 \sigma^2} \right)^{1/2} (I_R T)^{1/2} \quad (7)$$

where I_R is the reduced moment of inertia for the internal rotation, σ is the periodicity of the internal rotation potential, and the rest of the symbols have the same meaning as in the previous equations. For the case of the OH + CH₂Br₂ transition-state structure, $\sigma = 1$, $V_0 = 5.5 \text{ kJ mol}^{-1}$, and $I_R = 1.52 \times 10^{-47} \text{ kg m}^2$ calculated at MP2/6-311G(2d,2p) were used to compute the free-rotor partition functions by means of eq 7.

3.2. Tunneling. Reactions involving hydrogen atom transfers are usually characterized by significant tunneling effects that must be accounted for when computing reaction rate constants. Tunneling is the result of quantum effects that couple the reaction path coordinate to the other degrees of freedom of the reacting system due to the curvature along the reaction path. In these cases, the separation of the reaction coordinate from the other degrees of freedom is no longer valid and tunneling can occur through a variety of paths involving all coordinates. Given that the quantum mechanical treatment of tunneling in a multidimensional potential energy surface is very complicated, the TST reaction rate constant is computed assuming the separability of the reaction path and further corrected by a tunneling correction factor $\Gamma(T)$ (see eq 1). In the present work, three expressions for tunneling corrections have been explored. The first consists of a closed form approximation for $\Gamma(T)$ obtained by Wigner⁴⁵ in 1932 using a method which is, to a first approximation, applicable to any shape of potential curve:

$$\Gamma(T) = 1 + \frac{1}{24} \left(\frac{\hbar \nu^\ddagger}{k_B T} \right)^2 \quad (8)$$

where ν^\ddagger is the imaginary frequency at the saddle point. In the second method, $\Gamma(T)$ is computed with the one-dimensional unsymmetrical potential developed by Eckart.^{33a,46}

$$V(s) = \frac{Ay}{(1+y)} + \frac{By}{(1+y)^2}, \quad y = \exp\left(\frac{2\pi s}{L}\right) \quad (9)$$

where s is the reaction coordinate, L is the barrier width, and the parameters A and B depend on the forward and reverse energy barriers, ΔV_1 and ΔV_2 . The parameters A , B , and L in eq 9 are related to ΔV_1 and ΔV_2 by

$$\begin{aligned} A &= \Delta V_2 - \Delta V_1 \\ B &= [\Delta V_1^{1/2} + \Delta V_2^{1/2}]^2 \\ L &= 2\pi \left(-\frac{2}{F^*} \right)^{1/2} \left[\frac{1}{\Delta V_1^{1/2}} + \frac{1}{\Delta V_2^{1/2}} \right]^{-1} \end{aligned} \quad (10)$$

with F^* equal to the force constant evaluated at the maximum of the potential. The third method is based on the symmetrical Eckart potential, which is obtained by making parameter A in eq 9 and 10 equal to zero. In this case, the following closed form for the tunneling correction is obtained:

$$\Gamma(T) = 1 + \frac{1}{24} \left(\frac{\hbar \nu^\ddagger}{k_B T} \right)^2 \left(1 + \frac{k_B T}{\Delta V_1} \right) \quad (11)$$

These three different expressions were then employed in two different approaches to the calculation of $\Gamma(T)$. In the first

approach, the unsymmetrical Eckart potential given by eqs 9 and 10 was fitted using the forward (ΔV_1) and reverse (ΔV_2) barriers obtained at the MP2/6-311G(2d,2p) level of theory, as well as the imaginary frequency computed at the same level of theory ($\nu^\ddagger \approx 2200 \text{ cm}^{-1}$). The resulting potential was finally used to compute $\Gamma(T)$ by numerical integration of the analytical Eckart transmission probability⁴⁶ using an efficient algorithm developed by Brown.⁴⁷ Wigner and symmetrical Eckart tunneling corrections were computed by eqs 8 and 11, respectively, using the MP2/6-311G(2d,2p) imaginary frequency.

In the second approach, the reaction path computed at the MP2/6-311G(2d,2p) level using Gonzalez and Schlegel's second-order IRC algorithm⁴⁸ with a step size of 0.05 bohr amu^{1/2} was fit to the following Eckart function:

$$V(s) = \sum_{i=1}^3 \left[\frac{A_i y_i}{(1+y_i)} + \frac{B_i y_i}{(1+y_i)^2} \right] \quad (12)$$

where $y_i = \exp[c_i(s - s_0)]$ and A_i , B_i , c_i , and s_0 are constants. In the fitting procedure, an RMS of $4 \times 10^{-2} \text{ kJ mol}^{-1}$ was obtained. The fitted parameters together with eq 12 were then used to interpolate the necessary IRC points to fit the Eckart potential given by eqs 9 and 10 in the vicinity of the transition state ($-0.3 \text{ bohr amu}^{1/2} \leq s \leq +0.3 \text{ bohr amu}^{1/2}$) with the constraint that the difference between the forward and reverse barriers is equal to the heat of reaction computed at the MP2/6-311G(2d,2p) level ($\Delta V_1 - \Delta V_2 = \Delta H_{\text{rxn}} = -82.68 \text{ kJ mol}^{-1}$). In this step, the imaginary frequency was not fixed to the MP2 value, and it was considered as another fitting parameter. This procedure gave an r^2 approximately equal to 0.97 and a standard deviation of 0.30. An imaginary frequency significantly lower than the one obtained at the MP2/6-311G(2d,2p) level was found (1245 cm^{-1} vs 2200 cm^{-1}). The parameters generated by this second fitting were used together with the Eckart potential (eqs 9 and 10) to compute the corresponding unsymmetrical Eckart tunneling correction using the same integration scheme described in the previous approach. In addition, the imaginary frequency obtained from this fitting (1245 cm^{-1}) was used to compute the Wigner (eq 8) and symmetrical Eckart (eq 11) tunneling corrections. In this work we refer to the Wigner, symmetrical and unsymmetrical Eckart tunneling corrections computed by these two approaches as W-I, SE-I, UE-I, W-II, SE-II, and UE-II, respectively. In both UE-I and UE-II the fitting of eqs 9 and 10 was carried out with the constraint that the heat of reaction was given by the difference between the forward and reverse barriers ($\Delta H_{\text{rxn}} = \Delta V_1 - \Delta V_2$). The significantly small value of the imaginary frequency obtained by the UE-II method when compared to the value obtained at the MP2 level indicates that UE-I tunneling corrections are expected to be larger than the corresponding UE-II values.

It is important to note that the tunneling corrections obtained by either Wigner's formalism or the symmetrical and unsymmetrical Eckart potentials are just approximations based on a one-dimensional representation of the surface and, as in the case of the Eckart potentials, on an *a priori* assumption of the shape of the barrier. More sophisticated and computationally demanding algorithms such as the ones developed by Truhlar⁴⁹ and Miller⁵⁰ should be used if more accurate results are necessary. In these methods, detailed knowledge of the reaction path is needed, making the computation of tunneling corrections of relatively large electronic structure systems such as the ones containing bromine atoms very time-consuming. Given that the purpose of the proposed screening tools (see the Introduction) is to develop a set of inexpensive methodologies leading to a

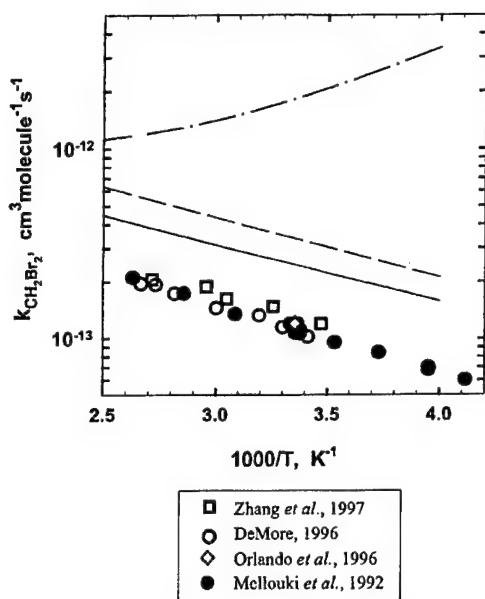


Figure 2. Temperature dependence of the rate constants for the reaction of CH_2Br_2 with OH computed at PMP4(SDTQ)/6-311++G(3df,3pd)//MP2/6-311G(2d,2p) using the imaginary frequency computed at the MP2/6-311G(2d,2p) level. Solid line: Wigner tunneling correction W-I. Short dashed line: symmetrical Eckart tunneling correction SE-I. Dashed-dotted line: unsymmetrical Eckart tunneling correction UE-I. UE-I tunneling correction was computed after fitting expression 9 to the forward and reverse barrier, using the MP2/6-311G(2d,2p) imaginary frequency.

semiquantitative description of the kinetics of hydrogen abstraction reactions of haloalkanes by OH radicals, the use of approximated methods such as Wigner and Eckart tunneling corrections are adequate for the purpose of this work.

The results of the calculations of the rate constants at the PMP4/6-311++G(3d,3pd)//MP2/6-311G(2d,2p) level of theory using tunneling corrections previously discussed are shown in Figures 2 and 3. As Figure 2 shows, the rate constants computed with the unsymmetrical Eckart tunneling correction UE-I are significantly larger than the experimental values. In addition, it is observed that UE-I predicts the wrong shape of the Arrhenius plot. Similar results have been reported⁵¹ in the case of reactions between OH and CHF_3 , CH_2F_2 , CH_3F , CHF_3 , and CH_4 . Wigner and symmetrical Eckart tunneling corrections computed by methods W-I and SE-I predict reaction rate constants that are consistently larger than the experimental values over the whole temperature range. These methods, however, reproduce the shape of the experimental curve, contrary to the unsymmetrical Eckart potential. In addition, the theoretical results computed with W-I are in better agreement with the experimental rate constants than the results obtained with symmetrical Eckart tunneling, SE-I.

In all of the calculations with approach II, a better agreement with the experimental values is observed than with approach I, in particular in the case of W-II, where the predicted rate constants are in excellent agreement with the experimental values over the whole temperature range. Despite the better behavior in the temperature range 380–400 K, the unsymmetrical Eckart method UE-II still overestimates the rate constants, producing a curved Arrhenius plot unlike the experimental data (see Figure 3). As in the previous case, symmetrical Eckart and Wigner corrections SE-II and W-II reproduce the shape of the experimental curve. The failure of unsymmetrical Eckart to reproduce the right shape of the

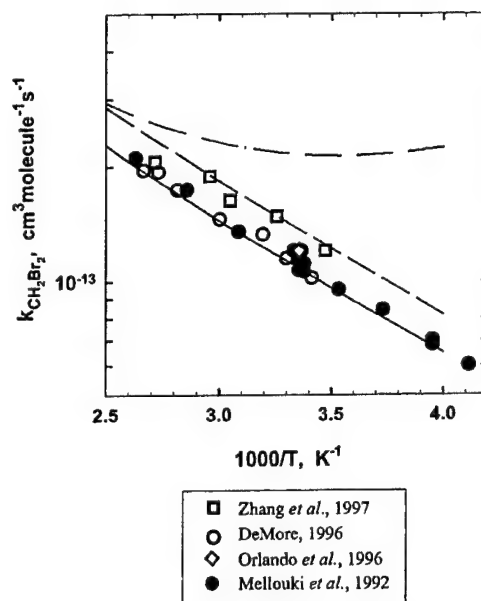


Figure 3. Temperature dependence of the rate constants for the reaction of CH_2Br_2 with OH computed at PMP4(SDTQ)/6-311++G(3df,3pd)//MP2/6-311G(2d,2p). Solid line: Wigner tunneling correction W-II. Short dashed line: symmetrical Eckart tunneling correction SE-II. Dashed-dotted line: unsymmetrical Eckart tunneling correction UE-II. In all cases, the imaginary frequency was obtained by the fitting of the Eckart function 8 to the results of the MP2/6-311G(2d,2p) IRC as described in the text.

Arrhenius plot can probably be attributed to the prediction of a too thin and sharp potential barrier, which results in the overestimation of tunneling, especially at low temperatures. This is not surprising given that the shape of the barrier predicted by unsymmetrical Eckart is more representative of large tunneling processes such as heavy-light-heavy abstractions. These conclusions seem to be supported by the fact that Wigner and symmetrical Eckart tunneling corrections predict the right shape of the Arrhenius plot. It is well known that these tunneling corrections work well in cases where the potential barriers are broad and tunneling is not so large. In addition, the improvement observed in the results of UE-II relative to UE-I is an indication of how the fit of the unsymmetrical Eckart potential to the IRC in the vicinity of the transition state provides a better description of the shape of the potential at the top of the barrier. An in-depth study of the applicability and limitations of unsymmetrical Eckart tunneling corrections in hydrogen abstractions is beyond the goal of this work. A more systematic study of this and related issues concerning tunneling will be addressed in a future publication.

The Arrhenius expression $k(T) = A \exp(-E_a/RT)$ fitted to the rate constants computed with the Wigner tunneling correction in the temperature range 250–400 K gives the Arrhenius parameters $A = 2.5 \times 10^{-12} \text{ cm}^3 \text{ molecule}^{-1} \text{ s}^{-1}$ and $E_a/R = 690 \text{ K}$ computed with the W-I method and $A = 1.8 \times 10^{-12} \text{ cm}^3 \text{ molecule}^{-1} \text{ s}^{-1}$ and $E_a/R = 835 \text{ K}$ computed with the more expensive method W-II. Both results are in good agreement with the experimental values:²⁷ $A = 2.4 \times 10^{-12} \text{ cm}^3 \text{ molecule}^{-1} \text{ s}^{-1}$ and $E_a/R = 900 \text{ K}$ and result in rate constants within a factor of 2 of the experimental values over the range of atmospheric interest. Since the W-I method does not require a detailed knowledge of the reaction path, it is concluded that it may be the method of choice for the screening tool proposed in this work. Table 7 lists the reaction rate constants computed at 250, 298, and 400 K using the Arrhenius expression obtained with

TABLE 7: Summary of Rate Constants ($\text{cm}^3\text{molecule}^{-1}\text{s}^{-1}$) Calculated at PMP4(SDTQ)/6-311++G(3df,3pd)/UMP2/6-311G(2d,2p) Including the Wigner Tunneling Correction

	250 K	298 K	400 K
$k(\text{theory, this work})^a$	1.6×10^{-13}	2.5×10^{-13}	4.5×10^{-13}
$k(\text{experimental, JPL 1997})$	0.7×10^{-13}	1.2×10^{-13}	2.5×10^{-13}
$k(\text{theory})/k(\text{experimental})$	2.3	2.1	1.8

^a Computed using the following Arrhenius expression: $k(T) = 2.5 \times 10^{-12} \exp(-690/T)$ fitted to the theoretical results obtained in this work in the temperature range 250–400 K.

the W-I method as well as the corresponding experimental values.

The results shown in Figures 2 and 3 as well as Table 7 seem to indicate that at least in the temperature range under study (250–400 K), rate constants computed at the PMP4/6-311++G(3df,3pd)/MP2/6-311G(2d,2p) level using Wigner tunneling corrections provide a viable methodology for the implementation of the proposed screening tool in the case of hydrogen abstractions from haloalkanes by OH radicals. Preliminary studies⁵² on several different hydrogen abstraction reactions involving OH and a series of halogenated substituted methanes $\text{CX}_n\text{Y}_m\text{H}_{4-n-m}$ ($X = \text{Cl, F, Br}$) support this conclusion. More cases should be included in this systematic study however before a final recommendation can be made.

Conclusion

Ab initio calculations were performed at different levels of theory for the H atom abstraction reaction between dibromomethane and the hydroxyl radical. The geometry parameters for the reactants, products, and transition state were fully optimized at the MP2 level of theory with the 6-311G(d,p) and 6-311G(2d,2p) basis sets. The transition structure parameter L , defined as the ratio between the increase in length of the C–H bond being broken and the elongation of the O–H bond being formed, changes only slightly with the basis sets. The calculation of the energetics of the reaction proved to be more dependent on the level of theory, and on the nature and extent of the basis set. A reaction barrier of 7.0 kJ mol^{-1} is obtained at the highly correlated level CCSD(T)/6-311++G(3df,3pd)/MP2/6-311G(2d,2p), in excellent agreement with the experimental value. Among the lower levels of theory explored in this study, the best agreement with these values was obtained at the PMP4-(SDTQ)/6-311++G(3df,3pd)/MP2/6-311G(2d,2p) level. The calculation of reaction rate constants over the temperature range 250–400 K using Wigner tunneling corrections reproduces the shape of the experimental Arrhenius plot. It is found that the use of the unsymmetrical Eckart potential in the calculation of tunneling corrections gives reaction rate constants significantly higher than the experimental values. In addition, the predicted Arrhenius plot has the wrong shape. Even though tunneling corrections computed using the symmetrical Eckart potential leads to an Arrhenius plot with the right shape, it consistently predicts rate constants in poorer agreement with experiment than the ones obtained with the Wigner tunneling corrections. These results seem to suggest that PMP4(SDTQ)/6-311++G(3df,3pd)/MP2/6-311G(2d,2p) calculations combined with Wigner tunneling corrections might be a viable methodology for the semiquantitative study of hydrogen abstraction reactions of other haloalkanes by OH radicals. It is important to note that the reasonable success of the Wigner tunneling corrections in these types of reactions should not be used to generalize the superiority of this method over more sophisticated techniques. Rather, these results should be critically analyzed in the context

of the creation of a very computationally inexpensive screening tool that will allow the prediction of the atmosphere lifetimes of new chemical species.

Acknowledgment. This work was supported by the Upper Atmosphere Research Program of the National Aeronautics and Space Administration and by the Next Generation Fire Suppression Technology Program, funded by the Department of Defense Strategic Environmental Research and Development Program under MIPR Number W74RDV73243630. We are grateful to D. Burgess, V. Orkin, and Tom Allison (NIST) for helpful discussions, and to the anonymous reviewers for their useful comments.

References and Notes

- (1) Noto, T.; Babushok, V.; Burgess, D. R.; Hamins, A.; Tsang, W.; Miziolek, A. *Twenty-Sixth Symp. (Int.) Comb.* **1996**, 1377.
- (2) Jeong, K. M.; Kaufman, F. J. *Phys. Chem.* **1982**, *86*, 1816.
- (3) Cohen, N.; Benson, S. W. *J. Phys. Chem.* **1987**, *91*, 162.
- (4) Bottoni, A.; Poggi, G.; Emmi, S. S. *J. Mol. Struct.: THEOCHEM* **1993**, *279*, 299.
- (5) Fu, Y.; Lewis-Bevan, W.; Tyrell, J. J. *Phys. Chem.* **1995**, *99*, 630.
- (6) Schwartz, M.; Marshall, P.; Berry, R. J.; Ehlers, C. J.; Petersson, G. A. *J. Phys. Chem. A* **1998**, *102*, 10074.
- (7) Martell, J. M.; Boyd, R. J. *J. Phys. Chem.* **1995**, *99*, 13402.
- (8) Sekusak, S.; Gusten, H.; Sabljic, A. *J. Chem. Phys.* **1995**, *102*, 7504.
- (9) Sekusak, S.; Gusten, H.; Sabljic, A. *J. Phys. Chem.* **1996**, *100*, 6212.
- (10) Sekusak, S.; Sabljic, A. *Chem. Phys. Lett.* **1997**, *272*, 353.
- (11) Sekusak, S.; Liedl, K. R.; Rode, B. M.; Sabljic, A. *J. Phys. Chem. A* **1997**, *101*, 4245.
- (12) Rayez, M.-T.; Rayez, J.-C.; Sawersyn, J.-P. *J. Phys. Chem.* **1994**, *98*, 11342.
- (13) Louis, F. Ph.D. Thesis University of Lille: Lille, France, 1997.
- (14) Louis, F.; Rayez, M.-T.; Rayez, J.-C.; Sawersyn, J.-P. *Phys. Chem. Chem. Phys.* **1999**, *3*, 383.
- (15) Talhaoui, A.; Louis, F.; Devolder, P.; Meriaux, B.; Sawersyn, J.-P.; Rayez, M.-T.; Rayez, J.-C. *J. Phys. Chem.* **1996**, *100*, 13531.
- (16) Louis, F.; Talhaoui, A.; Sawersyn, J.-P.; Rayez, M.-T.; Rayez, J.-C. *J. Phys. Chem. A* **1997**, *101*, 8503.
- (17) Bernardi, F.; Bottoni, A. *J. Phys. Chem. A* **1997**, *101*, 1912.
- (18) Berry, R. J.; Burgess, D. R. F.; Nyden, M. R.; Zachariah, M. R. *J. Phys. Chem.* **1995**, *99*, 17145.
- (19) Paddison, S. J.; Tschuikow-Roux, E. *J. Phys. Chem.* **1998**, *102*, 6191.
- (20) Paddison, S. J.; Tschuikow-Roux, E. *Int. J. Thermophys.* **1998**, *19*, 719.
- (21) Kambanis, K. G.; Lazarou, Y. G.; Papagiannakopoulos, P. *J. Phys. Chem. A* **1997**, *101*, 8496.
- (22) Mellouki, A.; Talukdar, R. K.; Schmoltner, A. M.; Gierczak, T.; Mills, M. J.; Solomon, S.; Ravishankara, A. R. *Geophys. Res. Lett.* **1992**, *19*, 2059.
- (23) Zhang, D. Q.; Zhong, J. X.; Qiu, L. X. *J. Atmos. Chem.* **1997**, *27*, 209.
- (24) DeMore, W. B. *J. Phys. Chem.* **1996**, *100*, 5813.
- (25) Orlando, J. J.; Tyndall, G. S.; Wallington, T. J.; Dill, M. *Int. J. Chem. Kinet.* **1996**, *28*, 433.
- (26) Orkin, V.; Huie, R. E.; Kurylo, M. J. Unpublished work.
- (27) DeMore, W. B.; Sander, S. P.; Golden, D. M.; Hampson, R. F.; Kurylo, M. J.; Howard, C. J.; Ravishankara, A. R.; Kolb, C. E.; Molina, M. J. *JPL Publication 97-4*; 1997, *Evaluation 12*.
- (28) Berry, R. J.; Yuan, J.; Misra, A.; Marshall, P. *J. Phys. Chem. A* **1998**, *102*, 5182.
- (29) The identification of commercial equipment or materials does not imply recognition or endorsement by the National Institute of Standards and Technology, nor does it imply that the material or equipment identified are necessarily the best available for the purpose.
- (30) Frisch, M. J.; Trucks, G. W.; Schlegel, H. B.; Gill, P. M. W.; Johnson, B. G.; Robb, M. A.; Cheeseman, J. R.; Keith, T.; Petersson, G. A.; Montgomery, J. A.; Raghavachari, K.; Al-Laham, M. A.; Zakrzewski, V. G.; Ortiz, J. V.; Foresman, J. B.; Cioslowski, J.; Stefanov, B. B.; Nanayakkara, A.; M. Challacombe; Peng, C. Y.; Ayala, P. Y.; Chen, W.; Wong, M. W.; Andres, J. L.; Replogle, E. S.; Gomperts, R.; Martin, R. L.; Fox, D. J.; Binkley, J. S.; Defrees, D. J.; Baker, J.; Stewart, J. P.; Head-Gordon, M.; Gonzalez, C.; Pople, J. A. *GAUSSIAN 94*, Revision D.4 ed.; Gaussian, Inc: Pittsburgh, PA, 1995.
- (31) (a) Schlegel, H. B. *J. Chem. Phys.* **1986**, *84*, 4530. (b) Schlegel, H. B. *J. Phys. Chem.* **1988**, *92*, 3075. (c) Sosa, C.; Schlegel, H. B. *Int. J. Quantum Chem.* **1986**, *29*, 1001. (d) Sosa, C.; Schlegel, H. B. *Int. J. Quantum Chem.* **1987**, *30*, 155.

- (32) (a) Bartlett, R. J.; Purvis, G. D. *Int. J. Quantum Chem.* **1978**, *14*, 516. (b) Cizek, J. *Adv. Chem. Phys.* **1969**, *14*, 35. (c) Purvis, G. D.; Bartlett, R. J. *J. Phys. Chem.* **1982**, *76*, 1910. (d) Scuseria, G. E.; Janssen, C. L.; Schaefer, H. F., III. *J. Chem. Phys.* **1988**, *89*, 7382. (e) Scuseria, G. E.; Schaefer, H. F., III. *J. Chem. Phys.* **1989**, *90*, 3700. (f) Pople, J. A.; Head-Gordon, M.; Raghavachari, K. *J. Chem. Phys.* **1987**, *87*, 5968.
- (33) (a) Johnston, H. S. *Gas-Phase Reaction Rate Theory*; The Roland Press Company: New York, 1966. (b) Laidler, K. J. *Theories of Chemical Reaction Rates*; McGraw-Hill: New York, 1969. (c) Weston, R. E.; Schwartz, H. A. *Chemical Kinetics*; Prentice Hall: New York, 1972. (d) Rapp, D. *Statistical Mechanics*; Holt, Reinhard, and Winston: New York, 1972. (e) Nikitin, E. E. *Theory of Elementary Atomic and Molecular Processes in Gases*; Clarendon Press: Oxford, 1974. (f) Smith, I. W. M. *Kinetics and Dynamics of Elementary Gas Reactions*; Butterworth: London, 1980. (g) Steinfield, J. I.; Francisco, J. S.; Hase, W. L. *Chemical Kinetics and Dynamics*; Prentice Hall: Englewood Cliffs, New Jersey, 1989. (h) Rate constants calculated with the Turbo-Rate module in the β version of the TURBO-OPT geometry optimization package, developed by C. Gonzalez. National Institute of Standards and Technology, Gaithersburg, MD.
- (34) Chase, M. W. *J. Phys. Chem. Ref. Data* **1998**, *Monograph 9*.
- (35) Bickerton, J.; Minas da Piedade, M. E.; Pilcher, G. *J. Chem. Thermodyn.* **1984**, *16*, 661.
- (36) Tschuikow-Roux, E.; Paddison, S. *Int. J. Chem. Kinet.* **1987**, *19*, 15.
- (37) Tsang, W. In *Heats of formation of organic free radicals by kinetic methods*; Tsang, W., Ed.; Blackie Academic & Professional: London, 1996; p 22.
- (38) Wigner, E. P. *Z. Phys. Chem.* **1932**, *B19*, 203.
- (39) Skodje, R. T.; Truhlar, D. G.; Garret, B. C. *J. Chem. Phys.* **1982**, *77*, 5955.
- (40) Kudchadker, S. A.; Kudchadker, A. P. *J. Phys. Chem. Ref. Data* **1975**, *4*, 457.
- (41) Lide, D. R. In *Handbook of Chemistry and Physics*; Lide, D. R., Ed.; CRC Press: Boca raton, FL, 1990.
- (42) Shimanouchi, T. *NSRDS-NBS* **1972**, *39*.
- (43) Jacox, M. E. In *Vibrational and Electronic Energy Levels of Polyatomic Transient Molecules*; Jacox, M. E., Ed.; National Institute of Standards and Technology; Gaithersburg, MD, 1998; Vol. 69, p 945.
- (44) Truong, T. N.; Truhlar, D. G. *J. Chem. Phys.* **1990**, *93*, 1761.
- (45) (a) Pitzer, K. S.; Gwinn, W. D. *J. Chem. Phys.* **1942**, *10*, 428. (b) Pitzer, K. S. *J. Chem. Phys.* **1946**, *14*, 239. (c) Kilpatrick, J. E.; Pitzer, K. S. *J. Chem. Phys.* **1949**, *11*, 1064. (d) Li, J. C. M.; Pitzer, K. S. *J. Phys. Chem.* **1956**, *60*, 466.
- (46) (a) Eckart, C. *Phys. Rev.* **1930**, *35*, 1303. (b) Bell, R. P. *The Tunnel Effect in Chemistry*; Chapman and Hall: New York, 1980.
- (47) Brown, R. L. *J. Res. Natl. Bur. Stand. (U.S.)* **1981**, *86*, 357.
- (48) (a) Gonzalez, C.; Schlegel, H. B. *J. Chem. Phys.* **1989**, *90*, 2154. (b) Gonzalez, C.; Schlegel, H. B. *J. Phys. Chem.* **1990**, *94*, 5523.
- (49) (a) Garret, B. C.; Truhlar, D. G. *J. Phys. Chem.* **1979**, *83*, 2921. (b) Garret, B. C.; Truhlar, D. G. *J. Chem. Phys.* **1984**, *81*, 309. (c) Skodje, R. T.; Garret, B. C.; Truhlar, D. G. *J. Phys. Chem.* **1981**, *85*, 3019. (d) Skodje, R. T.; Garret, B. C.; Truhlar, D. G. *J. Chem. Phys.* **1982**, *77*, 5955. (e) Garret, B. C.; Truhlar, D. G.; Grev, R. S. *Magnuson, A. W. J. Chem. Phys.* **1980**, *84*, 1730. (f) Garret, B. C.; Truhlar, D. G.; Grev, R. S. *Magnuson, A. W. J. Chem. Phys.* **1983**, *87*, 4554.
- (50) (a) Miller, W. H.; Shi, S.-h. *J. Chem. Phys.* **1981**, *75*, 2258. (b) Miller, W. H.; Smith, F. T. *Phys. Rev.* **1978**, *A 17*, 939.
- (51) Reference 6 and references therein.
- (52) The results of these studies will be reported elsewhere.

An ab Initio Study of the Kinetics of the Reactions of Halomethanes with the Hydroxyl Radical. 2. A Comparison between Theoretical and Experimental Values of the Kinetic Parameters for 12 Partially Halogenated Methanes

Florent Louis,* Carlos A. Gonzalez,* Robert E. Huie, and Michael J. Kurylo

Physical and Chemical Properties Division, National Institute of Standards and Technology,
Gaithersburg, Maryland 20899

Received: March 30, 2000; In Final Form: July 10, 2000

Ab initio calculations have been performed for the H-atom abstraction reactions from a series of 12 halogenated methanes by the hydroxyl radical. Geometry optimization and vibrational frequency calculations were performed for reactants, transition states, and products at the MP2/6-311G(2d,2p) level of theory. Single-point energy calculations were carried out at the PMP4(SDTQ) level with both 6-311G(3df,2p) and 6-311++G(3df,3pd) basis sets. Canonical transition state theory with Wigner's tunneling correction was used to predict the rate constants as function of the temperature (250–400 K). It is found that the treatment of the kinetics of these reactions with the lower level of theory, PMP4(SDTQ)/6-311G(3df,2p)/MP2/6-311G(2d,2p), leads to results in good agreement with experimental values and suggests the possibility of using this methodology in the implementation of a theoretical tool that properly describes the kinetics of reactions such as hydrogen abstractions by OH radicals from partially halogenated organic compounds.

Introduction

In the first paper of this series¹ (herein referred to as paper I), we initiated an investigation regarding the feasibility of applying relatively inexpensive ab initio electronic structure calculations together with canonical transition state theory, TST, leading to the generation of efficient and reliable computational tools that properly describe the kinetics of processes such as hydrogen-atom abstraction reactions by the hydroxyl radical from partially halogenated organic compounds. These reactions are of particular importance in the determination of the atmospheric lifetimes of compounds suggested as replacements for fully halogenated alkanes, widely used in industry. In light of the very large number of potential replacement compounds, and the need to select a few for more thorough evaluation, efficient computational screening methods are needed to help in establishing their environmental acceptability, along with other physical and chemical properties. Presently, there exists a wealth of reliable kinetic data on the reactions of OH with small haloalkanes.² These data can be very valuable in the validation of computationally efficient theoretical tools for predicting the reactivity of larger haloalkanes and as a starting point for calculations on halogenated compounds containing additional functional groups. In this work, we extend our previous study of the reaction of OH with CH₂Br₂ to the set of monohalomethanes (CH₃F, CH₃Cl, and CH₃Br), dihalomethanes (CH₂F₂, CH₂Cl₂, and CH₂Br₂), and trihalomethanes (CHF₃, CHF₂Cl, CHF₂Br, CHFCl₂, and CHCl₃). Although a few ab initio studies of the reactivity of OH toward some fluorochloro-substituted methanes have been previously performed at various levels of theory,^{3–6} we decided also to include these reactions in our study in order to provide additional insight into the search for the minimum level of theory required for a reliable

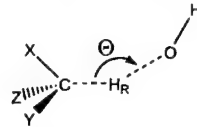
and efficient computational tool able to properly describe the kinetics of these and similar reactions.

In our investigation of the reaction of OH with CH₂Br₂, we demonstrated that full optimization of the geometric parameters for all stationary points at the second-order Møller–Plesset perturbation theory level, MP2, with the 6-311G(2d,2p) basis set was sufficient to provide reasonable values. Furthermore, in the calculation of the energetics of the reaction and the subsequent kinetic parameters, the best agreement with the experimental data was obtained by single-point calculations performed with the 6-311++G(3df,3pd) basis set employing unrestricted spin-projected second-order Møller–Plesset perturbation theory, PMP2/6-311++G(3df,3pd)/MP2/6-311G(2d,2p), and fourth-order Møller–Plesset perturbation theory, in the space of single, double, triple, and quadruple excitations, PMP4-(SDTQ)/6-311++G(3df,3pd)/MP2/6-311G(2d,2p). In addition, a quite reasonable agreement for the value of the activation energy was obtained with the far less computationally intensive level of theory PMP4(SDTQ)/6-311G(3df,2p)/MP2/6-311G(2d,2p). Even though these results are encouraging, it is clear that a more extensive study including more reactions is needed in order to assess the possibility of computing the kinetic parameters for H-atom abstraction by OH radicals with this relatively inexpensive level of theory. In this study, we compare the use of both PMP4(SDTQ)/6-311G(3df,2p)/MP2/6-311G(2d,2p) and PMP4(SDTQ)/6-311++G(3df,3pd)/MP2/6-311G(2d,2p) levels of theory in the calculation of kinetic parameters for a set of mono-, di-, and tri-halomethanes, and the results are compared with the experimental kinetic data available in the literature.²

Computational Methods⁷

All calculations described below were carried out with the Gaussian 94⁸ suite of programs on a CRAYC90/6256 supercomputer and a 32-processor Silicon Graphics Origin 2000

* To whom correspondence should be addressed. Fax: (301) 975-3672.
E-mail: flouis@nist.gov (F.L.), carlos.gonzalez@nist.gov (C.A.G.).

TABLE 1: Essential Structural Parameters,^a Imaginary Vibrational Frequencies for the Transition States of Each Reaction, and Internal Rotation Barrier of the -OH Group at the MP2/6-311G(2d,2p) Level of Theory


	$r(\text{C}-\text{H}_R)$	$r(\text{O}-\text{H}_R)$	$\Theta(\text{OH}_R\text{C})$	L^b	ν^\ddagger (cm ⁻¹)	V_0 (kJ mol ⁻¹)	treatment of $\nu_{\text{ROT}}(\text{HO}\cdots\text{H}\cdots\text{C})^c$
CH ₃ F	1.194	1.303	162.5	0.315	2094i	11.5	harmonic
CH ₃ Cl	1.194	1.291	170.5	0.338	2182i	6.9	hindered rotor
CH ₃ Br	1.195	1.288	171.4	0.347	2194i	6.7	hindered rotor
CH ₂ F ₂	1.195	1.294	164.6	0.329	2236i	8.3	hindered rotor
CH ₂ FCI	1.191	1.294	162.1	0.326	2203i	8.5	hindered rotor
CH ₂ Cl ₂	1.188	1.294	168.0	0.326	2219i	4.4	hindered rotor
CH ₂ ClBr	1.188	1.294	167.9	0.326	2224i	4.6	hindered rotor
CH ₂ Br ₂	1.188	1.296	165.3	0.324	2200i	5.5	hindered rotor
CHF ₃	1.215	1.246	166.9	0.460	2560i	4.9	hindered rotor
CHF ₂ Cl	1.200	1.271	164.6	0.376	2376i	6.6	hindered rotor
CHF ₂ Br	1.195	1.281	162.8	0.352	2302i	7.1	hindered rotor
CHFCI ₂	1.191	1.285	163.7	0.317	2262i	7.3	hindered rotor
CHCl ₃	1.184	1.295	172.7	0.317	2236i	2.6	hindered rotor

^a Bond lengths r are in angstroms, bond angles θ in degrees; the hydrogen atom involved in H-atom abstraction is noted H_R. ^b The parameter L is the ratio between the elongation value of the C-H bond and the elongation value of the O-H bond in the transition state: $L = \delta r(\text{C}-\text{H})/\delta r(\text{O}-\text{H})$. ^c Low-frequency mode associated with the -OH rotation around the axis along the C-H bond being broken.

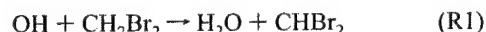
parallel computer, as discussed in our previous publication.¹ Fully optimized geometries, harmonic frequencies, and zero-point energy corrections (ZPE) of reactants, transition structures, and products were calculated with the second-order Møller-Plesset perturbation theory (UMP2) using the 6-311G(2d,2p) basis set. Electron correlation was calculated with fourth-order Møller-Plesset perturbation theory in the space of single, double, triple, and quadruple excitations with full annihilation of spin contamination⁹ as implemented in the Gaussian 94 package (noted in our results as PMP4). These single-point energy calculations were carried out with the 6-311G(3df,2p) and 6-311++G(3df,3pd) basis sets using geometries previously optimized at the MP2/6-311G(2d,2p) level. All relative energies quoted and discussed in this paper include zero-point energy corrections with unscaled frequencies obtained at the MP2/6-311G(2d,2p) level.

As in paper I,¹ canonical transition state theory¹⁰ (TST) and tunneling corrections were used to predict the rate constants over the same range of temperatures as the experimental measurements (250–400 K). Accordingly, the rate constants, $k(T)$, were computed using the following expression:

$$k(T) = \Gamma(T) \frac{k_B T}{h} \frac{Q^{\text{TS}}(T)}{Q^{\text{OH}}(T) Q^{\text{CHXYZ}}(T)} \exp\left(-\frac{\Delta E}{k_B T}\right) \quad (1)$$

where $Q^{\text{OH}}(T)$, $Q^{\text{CHXYZ}}(T)$, and $Q^{\text{TS}}(T)$, are the total partition functions for the hydroxyl radical, halomethane of type CHXYZ, and transition state respectively, at temperature T ; ΔE is the activation energy including zero-point energy and thermal corrections to the internal energy; k_B is Boltzman's constant, and h is Planck's constant. The total partition function of all species can be cast in terms of the translational (Q^{T}), rotational (Q^{R}), electronic (Q^{e}), and vibrational (Q^{v}) partition functions. In computing the electronic partition function for the OH radical, Q^{OH} , the multiplicity of the states $^2\Pi_{3/2}$ and $^2\Pi_{1/2}$, and the energy gap of 139.7 cm⁻¹ between the levels,¹¹ have been taken into consideration. $\Gamma(T)$ in eq 1 indicates the corresponding tunneling correction at temperature T . Given the demonstrated success of the Wigner's tunneling correction in the case of the

reaction:



we decided to adopt such methodology in the calculation of all tunneling corrections for the reactions reported in this work. As described in paper I,¹ the expression for Wigner's tunneling correction is given by

$$\Gamma(T) = 1 + \frac{1}{24} \left(\frac{h\nu^\ddagger}{k_B T} \right)^2 \quad (2)$$

where ν^\ddagger is the imaginary frequency at the saddle point and the other terms have the same meaning as in eq 1. The rate constant calculations over the temperature range 250–400 K were carried out using the TURBO-RATE program.¹²

Results and Discussion

1. Geometry Parameters and Vibrational Frequencies.

Table 1 lists the essential structural parameters calculated at the UMP2/6-311G(2d,2p) level of theory for the transition states corresponding to the 12 reactions under study. All other structural parameters as well as those for halomethanes, and halomethyl radicals, are reported in the supplementary Tables 1S–8S of the Supporting Information. For the species containing fluorine atoms, the observed trends suggest that the transition state becomes increasingly product-like as the number of F atoms increases. These results are reflected by the systematic increase of the parameter L , which is defined as the ratio between the increase in length of the C-H bond being broken and the elongation of the O-H bond being formed, each with respect to its equilibrium value in the reactants and the products. This parameter characterizes the most important aspect of the geometric structure of the transition state. Values for this parameter are included in Table 1. By contrast, the opposite trend is observed in the case of Cl and Br substitution, where the L parameter decreases with the degree of halogen substitution. For the 12 transition states, the eigenvector corresponding to the imaginary frequency was observed to be primarily a

TABLE 2: Calculated Reaction Enthalpies $\Delta_r H$, $\Delta_r H(\text{ISO})$, and Vibrationally Adiabatic Barriers at PMP4(SDTQ)/6-311G(3df,2p)//MP2/6-311G(2d,2p) and PMP4(SDTQ)/6-311++G(3df,3pd)//MP2/6-311G(2d,2p) Levels of Theory

		$\Delta_r H^{a,b}$	$\Delta_r H(\text{ISO})^{a,b}$	vibrationally adiabatic barrier ^c
OH + CH ₃ F	PMP4(SDTQ)/6-311G(3df,2p)	-64.8	-75.8	16.1
	PMP4(SDTQ)/6-311++G(3df,3pd)	-74.0	-71.6	14.0
	literature ^c	-75.2	-75.2	12.5
OH + CH ₃ Cl	PMP4(SDTQ)/6-311G(3df,2p)	-69.5	-80.5	14.7
	PMP4(SDTQ)/6-311++G(3df,3pd)	-81.3	-78.9	10.7
	literature ^c	-81.5	-81.5	11.6
OH + CH ₃ Br	PMP4(SDTQ)/6-311G(3df,2p)	-64.9	-75.9	15.5
	PMP4(SDTQ)/6-311++G(3df,3pd)	-76.3	-73.9	12.0
	literature ^c	-74.5	-74.5	12.2
OH + CH ₂ F ₂	PMP4(SDTQ)/6-311G(3df,2p)	-63.2	-74.2	15.5
	PMP4(SDTQ)/6-311++G(3df,3pd)	-70.4	-68.0	14.9
	literature ^c	-67.5	-67.5	14.8
OH + CH ₂ FCI	PMP4(SDTQ)/6-311G(3df,2p)	-72.0	-83.1	13.1
	PMP4(SDTQ)/6-311++G(3df,3pd)	-80.7	-78.3	11.0
	literature ^c	-78.2	-78.2	11.6
OH + CH ₂ Cl ₂	PMP4(SDTQ)/6-311G(3df,2p)	-82.9	-93.9	10.0
	PMP4(SDTQ)/6-311++G(3df,3pd)	-92.5	-90.1	6.7
	literature ^c	-96.8	-96.8	8.7
OH + CH ₂ ClBr	PMP4(SDTQ)/6-311G(3df,2p)	-81.0	-92.0	10.3
	PMP4(SDTQ)/6-311++G(3df,3pd)	-90.7	-88.3	7.3
	literature ^c	-89.3	-89.3	7.7
OH + CH ₂ Br ₂	PMP4(SDTQ)/6-311G(3df,2p)	-79.1	-90.1	10.5
	PMP4(SDTQ)/6-311++G(3df,3pd)	-88.7	-86.3	7.9
	literature ^c	-81.6	-81.6	7.5
OH + CHF ₃	PMP4(SDTQ)/6-311G(3df,2p)	-41.5	-52.5	25.2
	PMP4(SDTQ)/6-311++G(3df,3pd)	-48.7	-46.3	24.3
	literature ^c	-54.0	-54.0	20.3
OH + CHF ₂ Cl	PMP4(SDTQ)/6-311G(3df,2p)	-61.0	-72.0	16.2
	PMP4(SDTQ)/6-311++G(3df,3pd)	-68.7	-66.3	14.5
	literature ^c	-76.6	-76.6	13.3
OH + CHF ₂ Br	PMP4(SDTQ)/6-311G(3df,2p)	-66.0	-76.9	13.9
	PMP4(SDTQ)/6-311++G(3df,3pd)	-73.4	-71.0	12.8
	literature ^c			11.6
OH + CHFCI ₂	PMP4(SDTQ)/6-311G(3df,2p)	-77.3	-88.3	10.1
	PMP4(SDTQ)/6-311++G(3df,3pd)	-85.1	-82.7	7.7
	literature ^c	-85.3	-85.3	10.4
OH + CHCl ₃	PMP4(SDTQ)/6-311G(3df,2p)	-93.7	-104.7	4.7
	PMP4(SDTQ)/6-311++G(3df,3pd)	-101.0	-98.7	1.9
	literature ^c	-107.1	-107.1	7.5

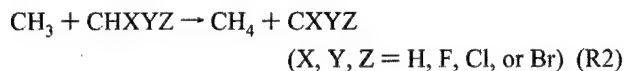
^a Units are kJ.mol⁻¹. ^b Including the sum of thermal energies (ΔZPE + thermal energy corrections). ^c Literature values based on the $\Delta_r H^\circ$ at 298 K for reactants and products taken from supplementary Table 9S of the Supporting Information. Experimental activation energies taken from ref 2, and ref 14 for the activation energy of the reaction OH + CH₂ClBr.

motion of the reactive hydrogen atom that is being transferred. The absolute values of the vibrational frequencies corresponding to these transition vectors are also reported in Table 1.

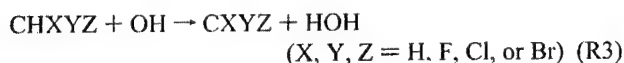
Direct inspection of the TS low-frequency modes (given in Table 8S of the Supporting Information) indicates that in all cases there are low-frequency modes consisting of an internal OH rotation about the nearly linear C-H-O axis. Given that, with the exception of the reaction of OH with CH₃F, the barriers for these rotations were sufficiently small (Table 1), these modes were treated as hindered rotors instead of a vibration. As explained in our first paper,¹ these modes were removed from the vibrational partition function for the TS, and the corresponding hindered rotor partition function $Q_{\text{HR}}(T)$ calculated by the method devised by Ayala and Schlegel¹³ was included in the expression for the rate constant.¹ In the case of the reaction of OH with CH₃F, the rotational barrier was found to be large enough (11.5 kJ mol⁻¹ in Table 1) so the internal rotational mode was treated by the harmonic approximation.

2. Reaction Enthalpies. Table 2 summarizes the results for reaction enthalpies ($\Delta_r H$) at 298 K calculated directly using the difference between the electronic energy of products and reactants computed at the PMP4(SDTQ)/6-311G(3df,2p)//MP2/6-311G(2d,2p) and PMP4(SDTQ)/6-311++G(3df,3pd)//MP2/6-311G(2d,2p) levels of theory for the series of reactions OH

+ CHXYZ (X, Y, Z = H, F, Cl, or Br). With the exception of the reaction OH + CHF₂Br, the corresponding literature values are also listed for comparison purposes. Following a similar procedure to the one adopted in our earlier publication,¹ reaction enthalpies for the 12 reactions were also corrected by new values of $D_{298}(\text{H}-\text{CXYZ})$ computed at the both levels of theory proposed in this work, utilizing the following isodesmic reactions:



The use of an isodesmic reaction, such as reaction R2, provides an indirect method that may lead to a more reliable value of the bond dissociation energy, mainly due to systematic cancellation of errors arising from insufficient treatment of electron correlation and incompleteness of the basis sets. In general, isodesmic reactions are characterized by having the same number and types of bonds on each side of the equation, so that the errors mentioned above are largely canceled when $D_{298}(\text{H}-\text{CHXYZ})$ is calculated. The reaction enthalpy for reaction R2 was computed at the same levels of theory as that for the abstraction reactions under study:



Taking the experimental value of $D_{298}(\text{H}-\text{CH}_3) = 440 \text{ kJ mol}^{-1}$,¹⁵ we obtain calculated $D_{298}(\text{H}-\text{CXYZ})$ values at the various levels of theory used in this work. These $D_{298}(\text{H}-\text{CXYZ})$ quantities were then used in the calculation of the reaction enthalpy for reactions R3 by means of the following relation:

$$\Delta_r H(\text{ISO}) = D_{298}(\text{H}-\text{CXYZ}) - D_{298}(\text{H}-\text{OH}) \quad (3)$$

Table 2 lists the different values of $\Delta_r H(\text{ISO})$ for all the reactions under study. In general, PMP4(SDTQ)/6-311G(3df,2p)/MP2/6-311G(2d,2p) underestimates the experimental values of the heats of reactions by up to 15 kJ mol⁻¹ when computed by direct subtraction of the energies between products and reactants. A better agreement is obtained at the PMP4(SDTQ)/6-311++G-(3df,3pd)/MP2/6-311G(2d,2p) level of theory, where errors no larger than 7 kJ mol⁻¹ are observed. As observed in our previous work,¹ an excellent agreement with the results reported in the literature is obtained in the case of the heats of reactions computed using the isodesmic reactions shown in (R2).

The results of Table 2 indicate an increase in the endothermicity of the reaction with the progressive substitution of H atoms by fluorine while the substitution by chlorine atoms leads to increased exothermicities. These trends can be explained by the relatively large σ acceptor and π donor characters of fluorine when compared to chlorine and bromine. Thus, the interaction between two or more adjacent fluorine atoms stabilizes the fluoromethane, while similar interactions between chlorine atoms as well as between bromine atoms have a negligible stabilizing effect. In addition, geminal interactions between fluorine and second and/or third row halogen atoms (Cl and Br) on the same halomethane lead to a weak stabilization.¹⁶

3. Reaction Barriers. Table 2 shows the computed vibrationally adiabatic barriers, VAB, for the 12 reactions under study. The following relation defines these barriers:

$$\text{VAB} = E_{\text{TS}} - E_{\text{R}} + \text{ZPE}_{\text{TS}} - \text{ZPE}_{\text{R}} \quad (4)$$

where E_{TS} and E_{R} are the ab initio energies of the transition state and reactants, while ZPE_{TS} and ZPE_{R} are their corresponding zero-point energy corrections. The experimental activation energies, E_a , as reported in the literature are also listed in Table 2 for comparison purposes. Overall, the agreement between the barriers computed at the PMP4(SDTQ)/6-311++G-(3df,3pd)/MP2/6-311G(2d,2p) and the recommended activation energies is reasonably good, with errors that range from 0.2 to 6 kJ mol⁻¹. It is interesting to notice that the errors obtained at the lower level PMP4(SDTQ)/6-311G(3df,2p)/MP2/6-311G(2d,2p) range from 0.3 to 4.0 kJ mol⁻¹. These results are encouraging in view of the fact of the considerable savings in computational expense when using the lower level. The results depicted in Table 2 indicate that the VAB's increase with fluorine substitution while the corresponding heats of reaction decrease. The opposite trend is observed in the case of chlorine and bromine substitution.

4. Kinetic Parameters. Table 3 lists the Arrhenius A factor and E_a/R values obtained from fitting of the rate constants computed over the temperature range 250–400 K. Table 3 also shows the rate constants at 298 K, computed at the PMP4-(SDTQ)/6-311G(3df,2p)/MP2/6-311G(2d,2p) and PMP4(SDTQ)/6-311++G-(3df,3pd)/MP2/6-311G(2d,2p) levels of theory. The experimental values recommended in the literature are shown in the same table. The ratios between the theoretical and the

experimental rate constants at 298 K are also reported in Table 3. With the exception of the reaction of OH with trichloromethane (CHCl_3), a reasonable agreement is observed between the theoretical and experimental values. The A factors computed at both levels of theory are very close, and they are found to be within a factor of 1.0–2.5 of the values reported in the literature. It is interesting to notice that the values of E_a/R computed with the smaller basis set are closer to the experimental values (maximum deviation = 15.6%, average deviation = 9.4%) when compared to the corresponding E_a/R 's computed with the larger basis sets (maximum deviation = 51.4%, average deviation = 19.4%). The same trends are observed in the case of the reaction rate constants, where better agreements with the experimental values are obtained when using the smaller basis sets (see Table 3). Even though not shown, it was found that the TST treatment of the 12 reactions under study, together with Wigner's tunneling correction, gives linear Arrhenius plots similar to the ones derived from experimental data over the same temperature range (250–400 K). Overall, these results are in good agreement with the findings reported in our previous paper¹ and suggest that PMP4(SDTQ)/6-311G(3df,2p)/MP2/6-311G(2d,2p) is a good compromise between accuracy and computational expense in the theoretical treatment of hydrogen abstraction reactions between OH radicals and halomethanes. Consequently, this seems to be the method of choice for computing rate constants within a factor of 2–3 with respect to the experimental values over the temperature range 250–400 K.

The case of the abstraction reaction $\text{OH} + \text{CHCl}_3$ requires special attention. Even though the kinetic parameters computed with the smaller basis sets are closer to the experimental values, larger deviations from the experimental values are observed compared to the results obtained for the other 11 reactions. This can be attributed to the fact that a relatively small activation barrier characterizes this reaction, and canonical transition state theory, TST, might not be entirely adequate. As indicated in Table 2, the activation energy is underestimated at both levels of theory used in this work. This amplifies the overestimation of the reaction rate constants by TST. This conclusion is confirmed by the fact that a significantly better agreement is obtained if the rate constant is computed without including tunneling corrections (see Table 3). In such cases, Variational transition state theory¹⁷ and more sophisticated models for tunneling corrections such as the ones developed by Truhlar's¹⁸ and Miller's groups¹⁹ seem to be the methodologies of choice. The results shown in Table 2 clearly indicate that these problems are more significant in the case of the chlorinated methanes CH_3Cl , CH_2Cl_2 , and CHCl_3 , where the vibrationally adiabatic barriers are considerably low, in contrast to the corresponding values of their fluorinated counterparts (CH_3F , CH_2F_2 , and CHF_3). In addition to these very important issues, it is also possible that the existence of the complex formed in the entrance channel (not discussed in this work) could affect the energetics and kinetics of the reaction. Moreover, the optimized structures obtained at MP2/6-311G(2d,2p) can be considerably different from the geometries of the corresponding stationary points (reactants, complexes, and transition states) in the PMP4(SDTQ) surfaces computed with the 6-311G(3df,2p) and 6-311++G-(3df,3pd) basis sets. This could explain why a decrease in the barriers is observed when chlorine substitution increases, in contrast to the trend found in the case of the fluorinated species. However, careful examination of the hydrogen-atom abstraction reactions under study (results not shown) indicates that similar trends in the energetics are observed at the UMP2/6-311G(2d,2p) and PMP4/6-311G(3df,2p)/UMP2/6-311G(2d,2p) levels of

TABLE 3: Summary of Kinetic Parameters Calculated at PMP4(SDTQ)/6-311G(3df,2p)/MP2/6-311G(2d,2p) and PMP4(SDTQ)/6-311++G(3df,3pd)/MP2/6-311G(2d,2p) Levels of Theory Including Wigner Tunneling Correction

		E_a/R (K)	A , 10^{-12} a	$k(\text{theory}, 298 \text{ K})$, 10^{-15} a	$\{k(\text{theory})/$ $k(\text{exptl})\}$ (298 K)
OH + CH ₃ F	PMP4(SDTQ)/6-311G(3df,2p)	1585	1.9	9.3	0.5
	PMP4(SDTQ)/6-311++G(3df,3pd)	1340	1.9	21	1.1
	literature ^b	1500	3.0	20	
OH + CH ₃ Cl	PMP4(SDTQ)/6-311G(3df,2p)	1500	5.7	37	1.0
	PMP4(SDTQ)/6-311++G(3df,3pd)	1015	5.7	189	5.3
	literature ^b	1400	4.0	36	
OH + CH ₃ Br	PMP4(SDTQ)/6-311G(3df,2p)	1610	5.4	24	0.8
	PMP4(SDTQ)/6-311++G(3df,3pd)	1190	5.4	100	3.4
	literature ^b	1470	4.0	29	
OH + CH ₂ F ₂	PMP4(SDTQ)/6-311G(3df,2p)	1680	4.8	17	1.7
	PMP4(SDTQ)/6-311++G(3df,3pd)	1595	4.8	23	2.3
	literature ^b	1550	1.9	10	
OH + CH ₂ FCI	PMP4(SDTQ)/6-311G(3df,2p)	1415	3.9	34	0.9
	PMP4(SDTQ)/6-311++G(3df,3pd)	1160	3.9	80	2.1
	literature ^b	1270	2.8	39	
OH + CH ₂ Cl ₂	PMP4(SDTQ)/6-311G(3df,2p)	905	2.4	115	1.0
	PMP4(SDTQ)/6-311++G(3df,3pd)	510	2.4	433	3.9
	literature ^b	1050	3.8	110	
OH + CH ₂ ClBr	PMP4(SDTQ)/6-311G(3df,2p)	945	2.2	92	0.9
	PMP4(SDTQ)/6-311++G(3df,3pd)	590	2.2	304	3.0
	literature ^b	930	2.3	100	
OH + CH ₂ Br ₂	PMP4(SDTQ)/6-311G(3df,2p)	995	2.5	89	0.75
	PMP4(SDTQ)/6-311++G(3df,3pd)	690	2.5	247	2.1
	literature ^b	900	2.4	120	
OH + CHF ₃	PMP4(SDTQ)/6-311G(3df,2p)	2745	2.0	0.20	0.7
	PMP4(SDTQ)/6-311++G(3df,3pd)	2640	2.0	0.28	1.0
	literature ^b	2440	1.0	0.28	
OH + CHF ₂ Cl	PMP4(SDTQ)/6-311G(3df,2p)	1740	1.6	4.7	1.0
	PMP4(SDTQ)/6-311++G(3df,3pd)	1540	1.6	9.1	1.9
	literature ^b	1600	1.0	4.7	
OH + CHF ₂ Br	PMP4(SDTQ)/6-311G(3df,2p)	1505	1.5	10	1.0
	PMP4(SDTQ)/6-311++G(3df,3pd)	1375	1.5	15	1.5
	literature ^b	1400	1.1	10	
OH + CHFCl ₂	PMP4(SDTQ)/6-311G(3df,2p)	1055	1.5	44	1.7
	PMP4(SDTQ)/6-311++G(3df,3pd)	765	1.5	115	4.4
	literature ^b	1250	1.7	26	
OH + CHCl ₃	PMP4(SDTQ)/6-311G(3df,2p)	345 (855)	0.9 (0.9)	283 (51)	2.9 (0.5)
	PMP4(SDTQ)/6-311++G(3df,3pd)	10 (515)	0.9 (0.9)	870 (160)	8.9 (1.6)
	literature ^b	900	2.0	98	

^a Units are cm³·molecule⁻¹·s⁻¹. ^b Literature values are taken from ref 2 and ref 14 for the reaction OH + CH₂ClBr. Values in parentheses correspond to the kinetic parameters without tunneling correction.

theory. The decrease in the barrier height with chlorine substitution has also been observed by Rayez et al. in an ab initio study of the H-atom abstraction of a series of halomethanes by chlorine atoms.²⁰

Regardless of these problems, the use of PMP4(SDTQ)/6-311G(3df,2p)/MP2/6-311G(2d,2p) in the case of OH + CHCl₃ provides a rate constant that is approximately 3 times the experimental value, which may be adequate for lifetime estimations suitable for use in screening environmental acceptability of proposed industrial compounds.

Conclusions

In this study, we have confirmed our previous observation that calculations at the UMP2 level of theory with the 6-311G(2d,2p) basis set provide reliable values of the geometric parameters in the case of hydrogen-atom abstraction reactions of halomethanes by OH radicals. Calculated reaction enthalpies, as before, depend on the level of theory, but were all within 0.2–15 kJ mol⁻¹ when computed by direct subtraction of the energies between products and reactants, and 0.1–10 kJ mol⁻¹ when isodesmic corrections were applied. The calculated kinetics of the reactions, which depend strongly on the calculated energetics, also differed for the two levels of theory tested. Surprisingly, the calculations at the lower level of theory, the

PMP4(SDTQ) method with a 6-311G(3df,2p) basis set, appear to produce kinetic results which are in better agreement with experiment as those derived from calculations at the more computationally intensive PMP4(SDTQ) method with the 6-311++G(3df,3pd) basis set. Indeed, for this limited reaction set the calculated activation energies appear to be somewhat better for the lower level of theory. It would appear that the lower level provides a fortuitous but systematic cancellation of errors (probably resulting from a balance between basis set size and perturbation theory) that leads to better kinetic parameters in the case of hydrogen-atom abstraction reactions between OH radicals and halomethanes. This is a quite encouraging result, since it suggests that this less computationally intensive approach may be adequate in the creation of a screening tool for the environmental acceptability of new chemical compounds.

It is important to point out that in this project we are not developing new theory; nor are we attempting to adjust the theory to fit experimental data. We are applying conventional theoretical methodologies in order to build a screening tool, which will allow the estimation of the reactivity of new molecules toward the hydroxyl radical, leading to the systematic estimation of the atmospheric effects of these molecules. Further refinements in theoretical methods leading to faster and accurate calculations should allow additional improvement in this tool.

In particular, better approximations which lead to the efficient calculation of accurate tunneling correction factors as well as the efficient use of variational transition state theory in reactions characterized by low barriers seems to be of critical importance.

Acknowledgment. This work was supported by the Upper Atmosphere Research Program of the National Aeronautics and Space Administration and by the Next Generation Fire Suppression Technology Program, funded by the Department of Defense Strategic Environmental Research and Development Program under MIPR no. W74RDV73243630.

Supporting Information Available: Tables of (i) the optimized geometry parameters of the halomethanes, halomethyl radicals, and transition states (Tables 1S–5S), (ii) their vibrational frequencies (Tables 6S–8S), and (iii) the literature enthalpy values used for the calculation of the “experimental” reaction enthalpy (Table 9S). This material is available free of charge via the Internet at <http://pubs.acs.org>.

References and Notes

- (1) Louis, F.; Gonzalez, C. A.; Huie, R. E.; Kurylo, M. J. *J. Phys. Chem. A* **2000**, *104*, 2931.
- (2) DeMore, W. B.; Sander, S. P.; Golden, D. M.; Hampson, R. F.; Kurylo, M. J.; Howard, C. J.; Ravishankara, A. R.; Kolb, C. E.; Molina, M. J. *JPL Publication 97-4* **1997**, Evaluation 12.
- (3) Bottoni, A.; Poggi, G.; Emmi, S. S. *J. Mol. Struct.: THEOCHEM* **1993**, *279*, 299.
- (4) Fu, Y.; Lewis-Bevan, W.; Tyrell, J. J. *J. Phys. Chem.* **1995**, *99*, 630.
- (5) Schwartz, M.; Marshall, P.; Berry, R. J.; Ehlers, C. J.; Petersson, G. A. *J. Phys. Chem. A* **1998**, *102*, 10074.
- (6) Korchowiec, J.; Kawahara, S.; Matsumura, K.; Uchimaru, T.; Sugie, M. *J. Phys. Chem. A* **1999**, *103*, 3548.
- (7) The identification of commercial equipment or materials does not imply recognition or endorsement by the National Institute of Standards and Technology, nor does it imply that the material or equipment identified is necessarily the best available for the purpose.
- (8) Frisch, M. J.; Trucks, G. W.; Schlegel, H. B.; Gill, P. M. W.; Johnson, B. G.; Robb, M. A.; Cheeseman, J. R.; Keith, T.; Petersson, G. A.; Montgomery, J. A.; Raghavachari, K.; Al-Laham, M. A.; Zakrzewski, V. G.; Ortiz, J. V.; Foresman, J. B.; Cioslowski, J.; Stefanov, B. B.; Nanayakkara, A.; M. Challacombe; Peng, C. Y.; Ayala, P. Y.; Chen, W.; Wong, M. W.; Andres, J. L.; Replogle, E. S.; Gomperts, R.; Martin, R. L.; Fox, D. J.; Binkley, J. S.; Defrees, D. J.; Baker, J.; Stewart, J. P.; Head-Gordon, M.; Gonzalez, C.; Pople, J. A. *GAUSSIAN 94*. Revision D.4; Gaussian, Inc.: Pittsburgh, PA, 1995.
- (9) (a) Schlegel, H. B. *J. Chem. Phys.* **1986**, *84*, 4530. (b) Schlegel, H. B. *J. Phys. Chem.* **1988**, *92*, 3075. (c) Sosa, C.; Schlegel, H. B. *Int. J. Quantum Chem.* **1986**, *29*, 1001. (d) Sosa, C.; Schlegel, H. B. *Int. J. Quantum Chem.* **1987**, *30*, 155.
- (10) (a) Johnston, H. S. *Gas-Phase Reaction Rate Theory*; The Roland Press Co.: New York, 1966. (b) Laidler, K. J. *Theories of Chemical Reaction Rates*; McGraw-Hill: New York, 1969. (c) Weston, R. E.; Schwartz, H. A. *Chemical Kinetics*; Prentice Hall: New York, 1972. (d) Rapp, D. *Statistical Mechanics*; Holt, Reinhard, and Winston: New York, 1972. (e) Nikitin, E. E. *Theory of Elementary Atomic and Molecular Processes in Gases*; Clarendon Press: Oxford, UK, 1974. (f) Smith, I. W. M. *Kinetics and Dynamics of Elementary Gas Reactions*; Butterworths: London, 1980. (g) Steinfeld, J. I.; Francisco, J. S.; Hase, W. L. *Chemical Kinetics and Dynamics*; Prentice Hall: New Jersey, 1989.
- (11) Chase, M. W. *J. Phys. Chem. Ref. Data* **1998**, Monograph 9.
- (12) Rate constants calculated with the Turbo-Rate module in the beta version of the TURBO-OPT geometry optimization package, developed by C. Gonzalez, National Institute of Standards and Technology, Gaithersburg, MD.
- (13) Ayala, P. Y.; Schlegel, H. B. *J. Chem. Phys.* **1998**, *108*, 2314.
- (14) Orkin, V. L.; Khamaganov, V. G.; Guschin, A. G.; Huie, R. E.; Kurylo, M. J. *J. Phys. Chem.* **1997**, *101*, 174.
- (15) Tsang, W. In *Heats of formation of organic free radicals by kinetic methods*; Tsang, W., Ed.; Blackie Academic & Professional: London, 1996; p 22.
- (16) (a) Rodriguez, C. F.; Sirois, S.; Hopkinson, A. C. *J. Org. Chem.* **1992**, *57*, 4869. (b) *Organofluorine Chemistry: Principles and Commercial Applications*; Banks, R. E., Smart, B. E., Tatlow, J. C., Eds.; Plenum Press: New York, 1994.
- (17) (a) Truhlar, D. G.; Isaacson, A. D.; Garret, B. C. In *Theory of Chemical Reaction Dynamics*; Baer, M., Ed.; CRC Press: Boca Raton, FL, 1985; p 65. (b) Truhlar, D. G. *J. Chem. Phys.* **1970**, *53*, 2041. (c) Garret, B. C.; Truhlar, D. G. *J. Phys. Chem.* **1979**, *83*, 1052. (d) Garret, B. C.; Truhlar, D. G. *J. Phys. Chem.* **1979**, *83*, 1079. (e) Garret, B. C.; Truhlar, D. G. *J. Am. Chem. Soc.* **1979**, *101*, 4534. (f) Garret, B. C.; Truhlar, D. G. *J. Am. Chem. Soc.* **1980**, *2*, 2559. (g) Kreevoy, M. M.; Truhlar, D. G. In *Investigation of Rates and Mechanisms of Reactions*; Bernasconi, C. F., Ed.; John Wiley & Sons: New York, 1986; Part 1, p 13.
- (18) (a) Garret, B. C.; Truhlar, D. G. *J. Phys. Chem.* **1979**, *83*, 2921. (b) Garret, B. C.; Truhlar, D. G. *J. Chem. Phys.* **1984**, *81*, 309. (c) Skodke, R. T.; Garret, B. C.; Truhlar, D. G. *J. Phys. Chem.* **1981**, *85*, 3019. (d) Skodje, R. T.; Garret, B. C.; Truhlar, D. G. *J. Chem. Phys.* **1982**, *77*, 5955. (e) Garret, B. C.; Truhlar, D. G.; Grev, R. S.; Magnuson, A. W. *J. Chem. Phys.* **1980**, *84*, 1730. (f) Garret, B. C.; Truhlar, D. G.; Grev, R. S.; Magnuson, A. W. *J. Chem. Phys.* **1983**, *87*, 4554.
- (19) (a) Miller, W. H.; Shi, S.-h. *J. Chem. Phys.* **1981**, *75*, 2258. (b) Miller, W. H.; Smith, F. T. *Phys. Rev.* **1978**, *A 17*, 939.
- (20) Rayez, M.-T.; Rayez, J.-C.; Sawersyn, J.-P. *J. Phys. Chem.* **1994**, *98*, 11342.

SUPPORTING INFORMATION

Table 1S: MP2/6-311G(2d,2p) optimized geometry parameters for halomethanes

Species	Parameter a)
CH ₃ F	r _{CH} = 1.085, r _{CF} = 1.384, θ(HCH) = 109.8, θ(FCH) = 109.2, φ(HCHF) = 119.6
CH ₃ Cl	r _{CH} = 1.081, r _{CCl} = 1.793, θ(HCH) = 110.4, θ(ClCH) = 108.5, φ(HCHCl) = 118.8
CH ₃ Br	r _{CH} = 1.080, r _{CBr} = 1.941, θ(HCH) = 110.8, θ(BrCH) = 108.1, φ(HCHBr) = 118.3
CH ₂ F ₂	r _{CH} = 1.084, r _{CF} = 1.358, θ(HCH) = 113.1, θ(FCH) = 108.7, φ(FCHH) = 120.8
CH ₂ FCI	r _{CH} = 1.081, r _{CF} = 1.361, r _{CCl} = 1.784, θ(HCH) = 112.5, θ(FCH) = 109.3, θ(ClCH) = 107.6, φ(FCHH) = -121.7, φ(ClCHH) = 118.3
CH ₂ Cl ₂	r _{CH} = 1.078, r _{CCl} = 1.778, θ(HCH) = 111.6, θ(ClCH) = 108.1, φ(ClCHH) = 118.8
CH ₂ CIBr	r _{CH} = 1.078, r _{CCl} = 1.777, r _{CBr} = 1.935, θ(HCH) = 111.8, θ(ClCH) = 108.5, θ(BrCH) = 107.5, φ(ClCHH) = 119.6, φ(BrCHH) = -117.8
CHF ₃	r _{CH} = 1.082, r _{CF} = 1.336, θ(FCH) = 110.3, φ(FCHF) = 120.0
CHF ₂ Cl	r _{CH} = 1.080, r _{CF} = 1.339, r _{CCl} = 1.777, θ(FCH) = 110.1, θ(ClCH) = 108.9, φ(FCHCl) = 120.3
CHF ₂ Br	r _{CH} = 1.081, r _{CF} = 1.340, r _{CBr} = 1.938, θ(FCH) = 110.1, θ(BrCH) = 108.6, φ(FCHBr) = 120.2
CHFCl ₂	r _{CH} = 1.078, r _{CF} = 1.346, r _{CCl} = 1.773, θ(FCH) = 109.7, θ(ClCH) = 108.3, φ(ClCHF) = 119.5
CHCl ₃	r _{CH} = 1.077, r _{CCl} = 1.774, θ(ClCH) = 107.7, φ(ClCHCl) = 120.0

a) Bond lengths are in Angstroms, bond angles θ and dihedral angles φ are in degrees.

RECEIVED

JUL 10 2000

JOURNAL OF PHYSICAL
CHEMISTRY

REVISED

Table 2S: MP2/6-311G(2d,2p) optimized geometry parameters for halomethyl radicals

Species	Parameter a)
CH₂F	$r_{CH} = 1.075$, $r_{CF} = 1.342$, $\theta(HCF) = 114.4$, $\phi(HCFH) = 149.7$
CH₂Cl	$r_{CH} = 1.071$, $r_{CCl} = 1.711$, $\theta(HCCl) = 117.2$, $\phi(HCClH) = 166.4$
CH₂Br	$r_{CH} = 1.071$, $r_{CBr} = 1.855$, $\theta(HCBr) = 117.5$, $\phi(HCBrH) = 167.0$
CHF₂	$r_{CH} = 1.082$, $r_{CF} = 1.329$, $\theta(FCH) = 113.7$, $\phi(FCHF) = 129.0$
CHFCI	$r_{CH} = 1.078$, $r_{CF} = 1.331$, $r_{CCl} = 1.723$, $\theta(FCH) = 114.1$, $\theta(ClCH) = 116.1$, $\phi(FCHCl) = 136.7$
CHCl₂	$r_{CH} = 1.073$, $r_{CCl} = 1.712$, $\theta(ClCH) = 116.5$, $\phi(ClCHCl) = 148.2$
CHClBr	$r_{CH} = 1.074$, $r_{CCl} = 1.711$, $r_{CBr} = 1.862$, $\theta(ClCH) = 116.2$, $\theta(BrCH) = 116.5$, $\phi(BrCHCl) = 148.8$
CF₃	$r_{CF} = 1.319$, $\theta(FCF) = 111.3$, $\phi(FCFF) = 124.9$
CF₂Cl	$r_{CF} = 1.320$, $r_{CCl} = 1.743$, $\theta(FCCl) = 113.8$, $\phi(FCClF) = 128.0$
CF₂Br	$r_{CF} = 1.319$, $r_{CBr} = 1.907$, $\theta(FCBr) = 114.1$, $\phi(FCBrF) = 128.1$
CFCl₂	$r_{CF} = 1.324$, $r_{CCl} = 1.730$, $\theta(ClCF) = 113.2$, $\phi(ClCFCl) = 136.4$
CCl₃	$r_{CCl} = 1.720$, $\theta(ClCCl) = 116.7$, $\phi(ClCClCl) = 144.4$

a) Bond lengths are in Angstroms, bond angles θ and dihedral angles ϕ are in degrees.

Table 3S: MP2/6-311G(2d,2p) optimized geometry parameters for the transition states in the series of reactions OH with monohalomethanes of type CH₃X (X = F, Cl or Br)

Parameter ^{a)}	OH + CH ₃ F	OH + CH ₃ Cl	OH + CH ₃ Br
r (C-H _R)	1.194	1.194	1.195
r (C-H)	1.083	1.080	1.080
r (C-X)	1.369	1.768	1.916
r (O-H _R)	1.303	1.291	1.288
r (H-O)	0.966	0.966	0.966
θ (HCH)	106.8	106.5	106.7
θ (XCH)	107.9	109.0	108.8
θ (OH _R C)	162.5	170.5	171.4
θ (HOH _R)	95.7	95.9	95.7
φ (HCHX)	119.0	119.2	119.1
φ (OH _R CH)	0.0	0.2	0.2
φ (HOH _R C)	0.0	-0.1	-0.1

^{a)} Bond lengths are in Angstroms, bond angles θ and dihedral φ are in degrees; the hydrogen atom involved in H-atom abstraction is noted H_R

Table 4S: MP2/6-311G(2d,2p) optimized geometry parameters for the transition states in the series of reactions OH with dihalomethanes of type CH₂XY (X, Y = F, Cl or Br)

Parameter ^{a)}	OH + CH ₂ F ₂	OH + CH ₂ Cl ₂	OH + CH ₂ ClBr
r (C-H _R)	1.195	1.188	1.188
r (C-H)	1.085	1.079	1.079
r (C-X)	1.341	1.764	1.755
r (C-Y)	1.348	1.756	1.920
r (O-H _R)	1.294	1.294	1.294
r (H-O)	0.966	0.967	0.967
θ (HCH)	109.6	107.6	107.7
θ (XCH)	108.5	108.1	106.8
θ (YCH)	107.7	106.6	107.5
θ (OH _R C)	164.6	162.1	167.9
θ (HOH _R)	96.6	97.1	96.8
φ (XCHH)	121.2	118.5	118.9
φ (YCHH)	-120.2	-118.5	-117.8
φ (OH _R CH)	110.2	264.2	59.9
φ (HOH _R C)	22.0	-31.0	50.1

^{a)} Bond lengths are in Angstroms, bond angles θ and dihedral φ are in degrees; the hydrogen atom involved in H-atom abstraction is noted H_R

Table 5S: MP2/6-311G(2d,2p) optimized geometry parameters for the transition states in the series of reactions OH with trihalomethanes of type CHXYZ (X, Y, Z = F, Cl or Br)

Parameter ^{a)}	OH + CHF ₃	OH + CHF ₂ Cl	OH + CHF ₂ Br	OH + CHFCl ₂	OH + CHCl ₃
r (C-H _R)	1.215	1.200	1.195	1.191	1.184
r (C-X)	1.325	1.760	1.923	1.344	1.758
r (C-Y)	1.325	1.329	1.329	1.755	1.762
r (C-Z)	1.332	1.336	1.336	1.755	1.762
r (O-H _R)	1.246	1.271	1.281	1.285	1.295
r (H-O)	0.966	0.966	0.966	0.967	0.967
θ (XCH)	109.3	107.6	107.1	107.9	105.0
θ (YCH)	109.3	109.1	109.3	107.2	107.1
θ (ZCH)	108.9	108.5	108.7	107.2	107.1
θ (OH _R C)	166.9	164.6	162.8	163.7	172.7
θ (HOH _R)	98.3	98.5	98.7	98.6	98.4
φ (YCHX)	120.4	121.0	120.9	118.9	119.4
φ (ZCHX)	-119.8	-120.4	-120.3	-118.9	-119.7
φ (OH _R CX)	119.8	151.6	158.7	0.0	179.9
φ (HOH _R C)	0.0	-18.0	-22.2	0.0	0.0

^{a)} Bond lengths are in Angstroms, bond angles θ and dihedral φ are in degrees; the hydrogen atom involved in H-atom abstraction is noted H_R

Table 6S: Calculated MP2/6-311G(2d,2p) vibrational frequencies (in cm^{-1}) for halomethanes

Species	Vibrational frequencies (cm^{-1})
CH₃F	1090, 1223, 1223, 1531, 1535, 1535, 3099, 3192, 3192 <i>1049, 1182, 1182, 1464, 1467, 1467, 2965, 3006, 3006 a)</i>
CH₃Cl	751, 1048, 1048, 1411, 1513, 1513, 3132, 3240, 3240 <i>732, 1017, 1017, 1355, 1455, 1455, 2968, 3054, 3054 a)</i>
CH₃Br	631, 986, 986, 1365, 1507, 1507, 3135, 3248, 3248 <i>611, 955, 955, 1306, 1443, 1443, 2935, 3056, 3056 b)</i>
CH₂F₂	538, 1147, 1149, 1215, 1316, 1524, 1571, 3125, 3208 <i>530, 1090, 1116, 1176, 1262, 1435, 1508, 2949, 3013 a)</i>
CH₂FCI	387, 767, 1024, 1108, 1283, 1407, 1536, 3159, 3244 <i>385, 760, 1004, 1068, 1236, 1351, 1470, 2993, 3048 a)</i>
CH₂Cl₂	289, 723, 780, 916, 1198, 1310, 1485, 3180, 3262 <i>282, 717, 758, 898, 1153, 1268, 1467, 2999, 3040 a)</i>
CH₂CIBr	231, 625, 758, 871, 1173, 1274, 1472, 3181, 3268 <i>229, 614, 744, 852, 1128, 1231, 1482, 3003, 3066 b)</i>
CHF₃	511, 511, 703, 1158, 1189, 1189, 1440, 1440, 3222 <i>508, 508, 700, 1137, 1152, 1152, 1376, 1376, 3035 a)</i>
CHF₂Cl	370, 414, 600, 814, 1135, 1167, 1357, 1408, 3217 <i>400, 417, 598, 812, 836, 1108, 1312, 1350, 3024 a)</i>
CHF₂Br	319, 325, 583, 725, 1129, 1163, 1332, 1403, 3212
CHFCI₂	281, 371, 460, 742, 814, 1119, 1276, 1359, 3221 <i>270, 368, 455, 741, 806, 1079, 1242, 1313, 3023 a)</i>
CHCl₃	265, 265, 372, 675, 782, 782, 1252, 1252, 3233 <i>261, 261, 363, 680, 774, 774, 1220, 1220, 3034 a)</i>

The experimental values of the vibrational frequencies are in italics. These values are taken from ^{a)} ref. 1S, ^{b)} ref. 2S

Table 7S: Calculated MP2/6-311G(2d,2p) vibrational frequencies (in cm^{-1}) for halomethyl radicals

Species	Vibrational frequencies (cm^{-1})
CH₂F	693, 1192, 1210, 1518, 3196, 3356 <i>1163, 1170 a)</i>
CH₂Cl	272, 843, 1028, 1460, 3240, 3347 <i>827, 1391 a)</i>
CH₂Br	246, 717, 954, 1431, 3239, 3395 <i>368, 693, 953, 1356 a)</i>
CHF₂	553, 1072, 1191, 1210, 1385, 3201 <i>1164, 1173, 1317 a)</i>
CHFCI	412, 770, 881, 1191, 1339, 3242 <i>757, 1151, 1283 a)</i>
CHCl₂	311, 546, 773, 898, 1273, 3285 <i>902, 1226 a)</i>
CHClBr	250, 513, 690, 864, 1245, 3281 <i>866, 1196 a)</i>
CF₃	434, 434, 611, 955, 1114, 1114 <i>500, 500, 701, 1090, 1259, 1259 b)</i>
CF₂Cl	370, 426, 608, 779, 1181, 1251 <i>599, 761, 1148, 1208 a)</i>
CF₂Br	316, 333, 591, 696, 1176, 1240 <i>684, 1138, 1198 a)</i>
CFCl₂	288, 386, 477, 619, 918, 1194 <i>747, 919, 1143 a)</i>
CCl₃	254, 254, 360, 469, 827, 827 <i>240, 240, 450, 460, 898, 898 b)</i>

The experimental values of the vibrational frequencies are in italics. These values are taken from ^{a)} ref. 3S, ^{b)} ref. 1S

Table 8S: Calculated MP2/6-311G(2d,2p) vibrational frequencies (in cm^{-1}) for transition states

Species	Vibrational frequencies (cm^{-1})
OH + CH ₃ F	2094i, 126, 177, 263, 728, 900, 1118, 1187, 1281, 1310, 1514, 1574, 3135, 3235, 3817
OH + CH ₃ Cl	2182i, 44, 117, 261, 707, 757, 853, 1026, 1150, 1260, 1454, 1481, 3167, 3267, 3814
OH + CH ₃ Br	2194i, 12, 104, 263, 641, 696, 832, 968, 1118, 1245, 1421, 1468, 3171, 3271, 3813
OH + CH ₂ F ₂	2236i, 98, 143, 165, 527, 655, 877, 1150, 1156, 1173, 1324, 1419, 1571, 3171, 3817
OH + CH ₂ FCl	2203i, 94, 132, 169, 391, 584, 824, 859, 1036, 1126, 1324, 1335, 1552, 3198, 3814
OH + CH ₂ Cl ₂	2219i, 77, 95, 164, 290, 554, 734, 790, 841, 977, 1245, 1302, 1434, 3219, 3812
OH + CH ₂ ClBr	2224i, 83, 92, 161, 233, 522, 649, 775, 816, 967, 1218, 1305, 1403, 3221, 3810
OH + CHF ₃	2560i, 81, 124, 126, 441, 512, 522, 750, 886, 1141, 1159, 1250, 1274, 1552, 3816
OH + CHF ₂ Cl	2376i, 78, 90, 131, 366, 388, 454, 627, 876, 920, 1147, 1166, 1223, 1527, 3815
OH + CHF ₂ Br	2302i, 76, 82, 132, 317, 325, 397, 597, 869, 885, 1145, 1165, 1223, 1525, 3814
OH + CHFCl ₂	2262i, 78, 109, 116, 276, 376, 385, 509, 850, 855, 892, 1112, 1127, 1531, 3813
OH + CHCl ₃	2236i, 15, 91, 100, 269, 269, 326, 481, 727, 815, 827, 880, 1091, 1405, 3811

Vibrational frequencies indicated in italics correspond to the hindered rotation of the -OH group

Table 9S: Literature enthalpy values used

Compound	$\Delta_f H^\circ(298K)$, kJ mol ⁻¹	Reference
OH	39.349 ± 0.210	4S
H ₂ O	-241.826 ± 0.040	5S
CH ₃	147.0 ± 1.0	6S
CH ₄	-74.48 ± 0.41	7S
CH ₂ F	-32.0 ± 8.0	8S
CH ₃ F	-238.0 ± 8.0	9S, estimated
CH ₂ Cl	117.3 ± 3.1	10S
CH ₃ Cl	-82.38 ± 0.67	9S, estimated
CH ₂ Br	169.0 ± 4.0	11S
CH ₃ Br	-37.7 ± 1.5	12S
CHF ₂	-239.0 ± 4.0	8S
CH ₂ F ₂	-452.7 ± 0.8	9S
CHFCI	-61.0 ± 10.0	11S
CH ₂ FCI	-264.0 ± 8.0	13S, estimated
CHCl ₂	89.0 ± 3.0	10S
CH ₂ Cl ₂	-95.4 ± 0.8	9S
CHClBr	146.9 ± 6.3	15S, estimated
CH ₂ ClBr	-45.0 ± 8.0	14S, estimated
CF ₃	-465.7 ± 2.1	16S
CHF ₃	-692.9 ± 2.1	16S
CF ₂ Cl	-279.0 ± 8.0	17S
CHF ₂ Cl	-484.8	13S, estimated
CF ₂ Br		No Data Available
CHF ₂ Br	-425.3 ± 0.9	18S
CFCl ₂	-89.1 ± 10.0	11S
CHFCI ₂	-285.0 ± 9.0	13S, estimated
CCl ₃	71.1 ± 2.5	19S
CHCl ₃	-102.9 ± 0.8	9S

REFERENCES FOR SUPPORTING INFORMATION:

- 1S) NIST-JANAF, Thermochemical Tables, Fourth Edition, *J.Phys.Chem.Ref.Data*, 1998, Monograph N°9, Malcolm W.Chase Jr.
- 2S) Shimanouchi, T. *Tables of Molecular Vibrational Frequencies Consolidated Volume I*, Nat.Stand.Ref.Data.Ser., NBS, 1972, 39, 164 pages.
- 3S) Jacox, M.E. *Vibrational and Electronic Energy Levels of Polyatomic Transient Molecules*, *J.Phys.Chem.Ref.Data*, 1994, Monograph N°3.
- 4S) Gurvich, L.V.; Veyts, I.V.; Alcock, C.B. *Thermodynamic Properties of Individual Substances*; Fourth Edition; Hemisphere Publishing Corp.: New-York, 1991; Vol.2.
- 5S) Cox, J.D.; Wagman, D.D.; Medvedev, V.A. *CODATA Key Values for Thermodynamics*; Hemisphere Publishing Corp.: New-York, 1989.
- 6S) Tsang, W. *Heats of formation of organic free radicals by kinetic methods*; in **Energetics of Organic Free Radicals**, J.A.M. Simoes, A. Greenberg, J.F. Liebman, Ed.; Blackie Academic & Professional: London, 1996, pp22.
- 7S) Pittam, D.A.; Pilcher, G. *J.Chem.Soc.Faraday.Trans.1*, 1972, 68, 2224.
- 8S) Pickard, J.M.; Rodgers, A.S. *Int.J.Chem.Kinet.*, 1983, 15, 569.
- 9S) Rodgers, A.S.; Chao, J.; Wilhoit, R.C.; Zwolinski, B.J. *J.Phys.Chem.Ref.Data*, 1974, 3, 117.
- 10S) Seetula, J.A. *J.Chem.Soc.Faraday.Trans.*, 1996, 92, 3069.
- 11S) Tschuikow-Roux, E.; Paddison, S. *Int.J.Chem.Kinet.*, 1987, 19, 15.
- 12S) Kudchadker, S.A.; Kudchadker, A.P. *J.Phys.Chem.Ref.Data*, 1975, 4, 457.
- 13S) Chen, S.S.; Wilhoit, R.C.; Zwolinski, B.J. *J.Phys.Chem.Ref.Data*, 1976, 5, 571.
- 14S) Kudchadker, S.A.; Kudchadker, A.P. *J.Phys.Chem.Ref.Data*, 1978, 7, 1285.
- 15S) Espinosa-Garcia, J.; Dobe, S. *J.Phys.Chem.A*, 1999, 103, 6387.
- 16S) Ruscic, B.; Michael, J.V.; Redfern, L.A.; Curtiss, L.A.; Raghavachari, K. *J.Phys.Chem.A*, 1998, 102, 10889
- 17S) Miyokawa, K; Tschuikow-Roux, E. *J.Phys.Chem.*, 1992, 96, 7328

18S) Okafo, E.N.; Whittle, E. *Trans. Faraday Soc.*, **1974**, *17*, 1366-1375.

19S) Hudgens, J.W.; Johnson, R.D.; Timonen, R.S.; Seetula, J.A.; Gutman, D. *J.Phys.Chem.*, **1991**, *95*, 4400

An *Ab initio*-Based Screening Tool for the Atmospheric Lifetimes of Halon Replacements

Robert E. Huie, Florent Louis, Carlos A. Gonzalez, and Michael J. Kurylo

*Physical and Chemical Properties Division,
National Institute of Standards and Technology
Gaithersburg, Maryland 20899-8381
301-975-2559 robert.huie@nist.gov
301-975-4423 florent.louis@nist.gov
301-975-4063 carlos.gonzalez@nist.gov
301-975-2567 michael.kurylo@nist.gov*

INTRODUCTION

The decision to phase out the use of halons due to their role in stratospheric ozone loss has led to accelerated efforts to find "environmentally friendly" replacements. Thus, the need has arisen for an efficient means to evaluate the large suite of proposed alternatives for environmental acceptability. In particular, this means obtaining one of the most important pieces of information relating to the atmospheric fate of volatile species: the reactivity towards the hydroxyl radical. The reaction with tropospheric OH typically controls the atmospheric lifetime of many substances and is thus a starting point in the evaluation of its acceptability. Carrying out laboratory measurements on all the proposed replacements is an expensive proposition, made worse by the fact that many of the compounds would have to be synthesized and provided in sufficient purity for kinetic measurements. Clearly, the development of screening tools capable of predicting the properties important in assessing environmental persistence would be beneficial to this process.

STATEMENT OF THE PROBLEM

Over the years, various structure-activity relationships have been used to estimate rate constants for chemical reactions, including those of the hydroxyl radical. These usually require a substantial amount of data on a suite of chemicals in order to provide reliable predictions for similar compounds. The magnitude and difficulty of this task is illustrated by the results of studies on hydrofluoroethers. Normally, it has been assumed that the presence of an ether linkage decreases the bond strength of adjacent C-H bonds and, thus, increases their reactivity. In comparing fluoroalkanes and the corresponding fluoroethers, however, both activation and deactivation are observed (Figure 1). [1] An analysis of these results has not revealed any consistent pattern, suggesting that experimental kinetic studies for many more fluoroethers would need to be conducted.

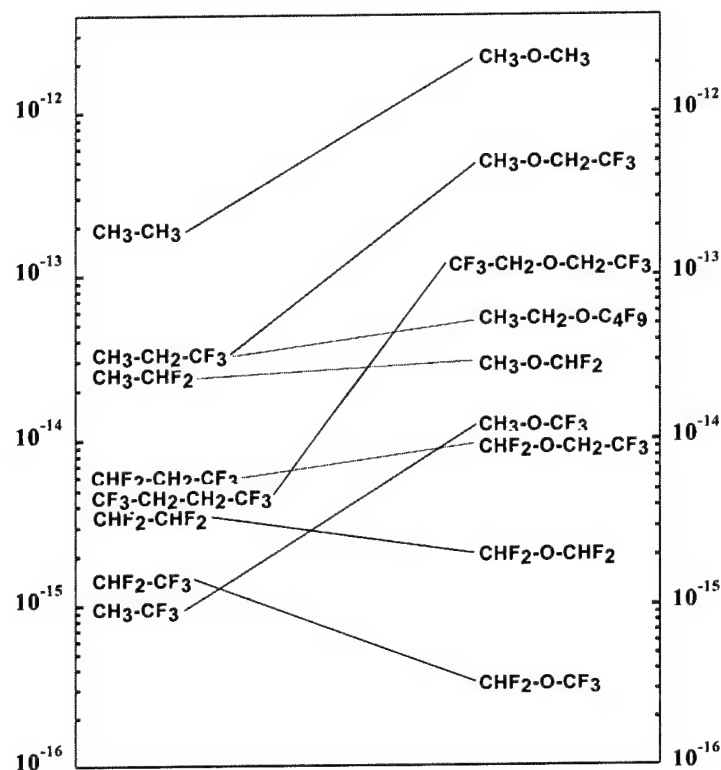
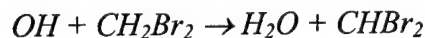


Figure 1. Graph of the relationship between the reactivity of OH towards fluoroalkanes and fluoroethers. [1]

Rather than taking this brute force approach, we have decided to explore the possibility of applying fundamental theory to the problem of predicting reactivity. We initiated a systematic study of the application of *ab initio* electronic structure calculations combined with transition state theory to the kinetics of hydrogen-atom abstractions by hydroxyl radicals. The objective was to develop efficient and reliable computational chemistry "screening tools" useful in predicting the fate of halon replacements once they are released into the atmosphere.

DEVELOPMENT OF METHODOLOGY

The initial study [2] focused on the reaction:



Dibromomethane was chosen both because there are reliable experimental kinetic data available and because bromine is an important element in fire suppression. Further, the relatively large electronic system associated with the bromine atom makes this a stringent test of the proposed quantum chemical methodologies.

Ab initio calculations were carried out with Møller-Plesset second and fourth order perturbation theory (MP2 and MP4), and the coupled cluster method, in the space of singles, doubles and triple electronic excitations, CCSD(T). Full geometry optimization and vibrational frequency calculations at the MP2 level were performed on reactants, products and the transition state using the 6-311G(d,p) and 6-311G(2d,2p) basis sets. The geometry parameters optimized at the MP2/6-311G(2d,2p) level of theory were used in single-point energy calculations with increasing basis set sizes, from 6-311G(2d,2p) to 6-311++G(3df,3pd) at both the MP2 and MP4(SDTQ) levels of theory. Canonical transition state theory was used to predict the rate constants as a function of the temperature (250-400 K) making use of the expression:

$$k(T) = \Gamma(T) \times \frac{k_B T}{h} \times \frac{Q^{TS}(T)}{Q^{OH}(T)Q^{alk}(T)} \times \exp\left(-\frac{\Delta E}{k_B T}\right)$$

where: $Q^{TS}(T)$, $Q^{OH}(T)$ and $Q^{alk}(T)$ are the total partition functions for the transition state, hydroxyl radical, and the haloalkane at temperature T ; ΔE is the activation energy including thermal corrections to the internal energy and zero-point energy; k_B is Boltzman's constant; and h is Planck's constant. $\Gamma(T)$ in the equation indicates the corresponding tunneling correction at temperature T .

Three different expressions were tested for the tunneling correction: the closed-form approximation by Wigner; and calculations based on the symmetrical and unsymmetrical Eckart potentials. These three expressions were then applied in two different ways to obtain $\Gamma(T)$. The first approach is the normal way in which these corrections are calculated, making use of the imaginary frequency, ν^* , calculated at the same level of theory as the forward and reverse reaction barriers. In the second approach, the reaction path was calculated by the intrinsic reaction coordinate (IRC) algorithm and fit to the Eckart potential in the region of the transition state. In this case, ν^* was an adjustable parameter in the fit.

The results of these fits for the reaction of OH with CH_2Br_2 are shown in Figures 2 and 3.

It is clear that calculations with the unsymmetrical Eckart treatment for tunneling not only do not reproduce the magnitude of the rate constants well, they do not even reproduce the shape of the Arrhenius plot. Interestingly, the best fits are obtained when the Wigner correction is utilized. Although excellent agreement with experiment is obtained when the imaginary frequency was derived from a fit to the IRC, reasonable agreement, within a factor of two, was obtained when ν^* was obtained directly from the transition state calculations. This is a considerably less expensive approach and will be employed in the subsequent calculations.

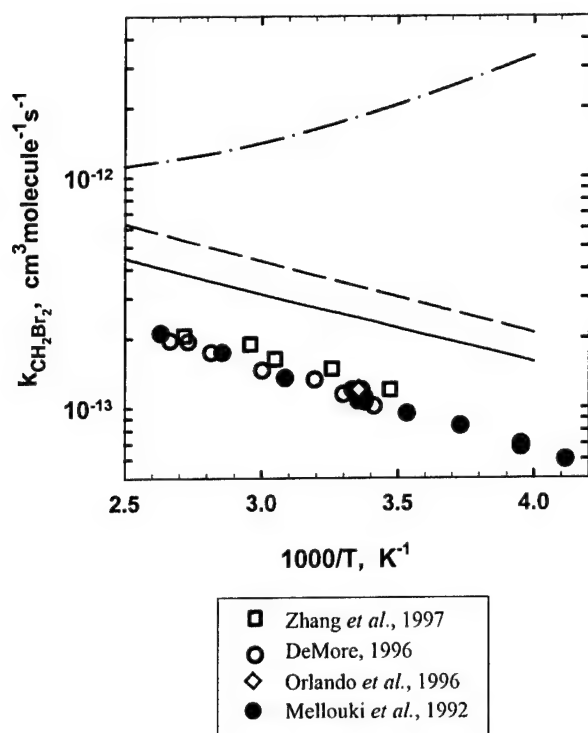


Figure 2: Temperature dependence of the rate constants for the reaction of CH_2Br_2 with OH computed at PMP4 (SDTQ)/6-311++G(3df,3pd)//MP2/6-311G(2d,2p) using the imaginary frequency computed at the MP2/6-311G(2d,2p) level. Solid line: Wigner tunneling correction; short dashed line: symmetrical Eckart tunneling correction; and dash-dotted line: unsymmetrical Eckart tunneling correction. [2]

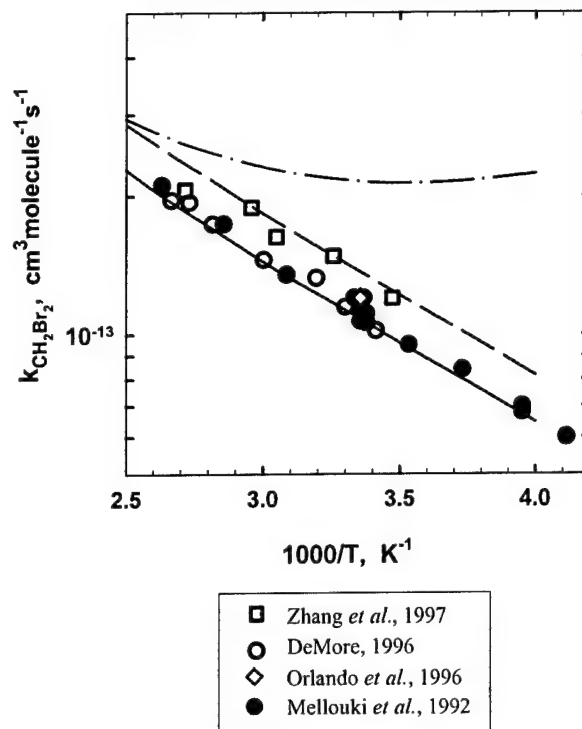


Figure 3: Temperature dependence of the rate constants for the reaction of CH_2Br_2 with OH computed at PMP4 (SDTQ)/6-311++G(3df,3pd)//MP2/6-311G(2d,2p). Solid line: Wigner tunneling correction; short dashed line: symmetrical Eckart tunneling correction; and dash-dotted line: unsymmetrical Eckart tunneling correction. In all cases, the imaginary frequency was obtained by the fitting of the Eckart function to the results of the MP2/6-311G(2d,2p) IRC. [2]

In the second phase of the project, kinetic parameters were calculated for a series of twelve partially halogenated methanes for which reliable experimental data exist. [3] Following the results for dibromomethane, geometry optimization and vibrational frequency calculations were performed for reactants, transition states and products at the MP2/6-311G(2d,2p) level of theory. Single-point energy calculations were carried out at the PMP4(SDTQ) level with both 6-311G(3df,2p), and 6-311++G(3df,3pd) basis sets. Then, canonical transition state theory with Wigner's tunneling correction was used to predict the rate constants as function of temperature. The results of these calculations at 298K are presented in Figure 4.

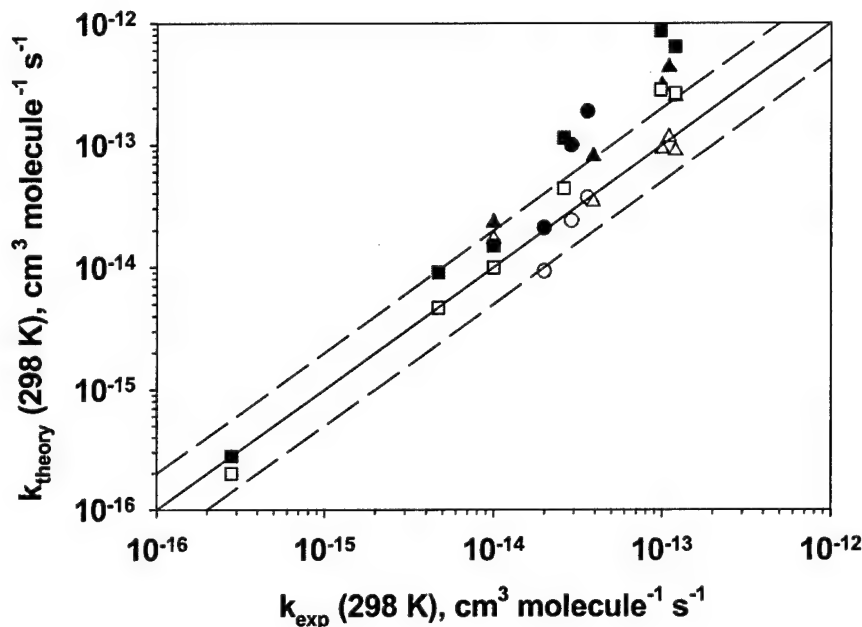


Figure 4. Comparison of experimental and calculated rate constants. Open symbols, PMP4(SDTQ)/6-311G(3df,2p); closed symbols, PMP4(SDTQ)/6-311++G(3df,3pd). Circles, monosubstituted; triangles, disubstituted; squares, trisubstituted.

Interestingly, the rate constants calculated with the smaller basis set were found to be in better agreement with experiment than those calculated with the larger basis set. The A-factors computed at both levels of theory are very close, and they are found to be within a factor of 1.0 - 2.5 of the values reported in the literature. As with the rate constants at 298K, the values of E_a/R computed with the smaller basis set are closer to the experimental values (max. deviation = 15.6 %, average deviation of 9.4%) when compared to the corresponding E_a/R 's computed with the larger basis sets (max. deviation = 51.4%, average deviation = 19.4%). Overall, these results suggest that PMP4(SDTQ)/6-311G(3df,2p)/MP2/6-311G(2d,2p) is a good compromise between accuracy and computational expense in the theoretical treatment of hydrogen abstraction reactions between OH radicals and halomethanes, possibly as a result of a systematic cancellation of errors between the convergence rate of the perturbation theory and the size of the basis sets used.

APPLICATION OF METHODOLOGY

In the third phase of the project, we have calculated rate constants for a series of bromine-containing halomethanes for which experimental data do not exist. [4] These calculations have resulted in the following rate constants at 298K:

Bromoalkane	$k \times 10^{14} \text{ cm}^3 \text{ s}^{-1}$
CH_2FBr	3.0
CHFBr_2	10.0
CHFCIBr	6.8
CHCl_2Br	26
CHClBr_2	35

In general, we consider these rate constants to be accurate to within a factor of two to three, although it was apparent from the set of 12 halomethanes originally tested that the level of agreement with measurements worsened with increasing reactivity. From the point of view of a screening tool, this is not a problem since these reactions are already quite fast and hence environmental persistence is diminished.

Finally, the reason we started this project was the difficulty in rationalizing the behavior of the hydrofluoroethers by simple structure-activity concepts. Therefore, we have carried out some preliminary calculations on the reactions of three selected ethers and their corresponding alkanes. These calculations are not yet complete in that we have not yet applied hindered rotor corrections to the transition state partition functions, nor have we taken into account all possible rotational conformers. Yet the calculations are sufficient to ascertain if this level of theory will correctly predict the observed reactivity patterns. Below we present the ratio of the rate constants for the alkane relative to those of the ethers at 298K:

Ethane/Ether	Theory	Experiment
$\text{CH}_3\text{CF}_3 / \text{CH}_3\text{OCF}_3$	14.3	10.0
$\text{CHF}_2\text{CF}_3 / \text{CHF}_2\text{OCF}_3$	0.3	0.2
$\text{CHF}_2\text{CHF}_2 / \text{CHF}_2\text{OCHF}_2$	0.2	0.4

These results demonstrate that this basic approach is a viable method of predicting the reactivity of new functional groups towards the hydroxyl radical and thus can form a component of a screening tool for the environmental acceptability of proposed fire suppressants.

CONCLUSIONS

These studies have been quite successful and we have been able to demonstrate that a relatively reasonable level of theory is sufficient to predict rate constants to a degree of accuracy sufficient for a screening tool. These full transition state calculations are still difficult, however, for larger systems. Therefore, we have been exploring additional strategies for the prediction of rate constants. Since the thermodynamics are far easier to calculate than reaction kinetics, we have begun looking into applying the simple relationship between rate constant and reaction enthalpy and the rate constant embodied in the Evans-Polanyi equation. We have found that there is a simple quadratic relationship between the logarithm of the rate constant and the calculated reaction

enthalpy for the halomethanes. It remains to be seen if we can make this concept work beyond a simple homologous series.

Acknowledgement

We thank Drs. Marc Nyden and Vladimir Orkin of NIST for helpful conversations. This work was supported by the Upper Atmosphere Research Program of the National Aeronautics and Space Administration and by the Next Generation Fire Suppression Technology Program, funded by the Department of Defense Strategic Environmental Research and Development Program under MIPR number W74RDV73243630.

REFERENCES

- (1) Orkin, V. L., Villenave, E., Huie, R. E., and Kurylo, M. J., "Atmospheric Lifetimes and Global Warming Potentials of Hydrofluoroethers: Reactivity Toward OH, UV Spectra, and IR Absorption Cross Sections", *J. Phys. Chem. A* **103**, 9770-9779 (1999)
- (2) Louis, F., Gonzalez, C., Huie, R. E., and Kurylo, M. J., "An *ab Initio* Study of the Reaction of Halomethanes with the Hydroxyl Radical. Part 1: CH₂Br₂", *J. Phys Chem. A* **104**, 2931-2938 (2000)
- (3) Louis, F., Gonzalez, C., Huie, R. E., and Kurylo, M. J., "An *Ab Initio* Study of the Kinetics of the Reactions of Halomethanes with the Hydroxyl Radical. Part 2: A Comparison between Theoretical and Experimental Values of the Kinetic Parameters for 12 Partially Halogenated Substituted Methanes.", *J. Phys Chem. A*, submitted.
- (4) Louis, F., Gonzalez, C., Huie, R. E., and Kurylo, M. J., "An *Ab Initio* Study of the Kinetics of the Reactions of Halomethanes with the Hydroxyl Radical. Part 3. Reactivity Trends and Kinetics Parameter Predictions for the Potential Halon Replacements CH₂FBr, CHFBr₂, CHFClBr, CHCl₂Br, and CHClBr₂", in preparation.

An ab Initio Study of the Kinetics of the Reactions of Halomethanes with the Hydroxyl Radical. 3. Kinetic Parameters Predictions for the Potential Halon Replacements CH₂FBr, CH₂Br₂, CHFClBr, CHCl₂Br, and CHClBr₂[†]

Florent Louis,^{*,‡} Carlos A. Gonzalez,^{*,§} Robert E. Huie, and Michael J. Kurylo

Physical and Chemical Properties Division, National Institute of Standards and Technology, Gaithersburg, Maryland 20899

Received: May 24, 2000; In Final Form: October 24, 2000

Ab initio PMP4(SDTQ)/6-311G(3df,2p)/MP2/6-311G(2d,2p) calculations, together with canonical transition state theory, were used in order to compute the energetics and predict the kinetics (in the temperature range 250–400 K) of the H atom abstraction reaction between the hydroxyl radical and the five halomethanes: CH₂FBr, CH₂Br₂, CHFClBr, CHCl₂Br, and CHClBr₂. The procedure adopted in this study has been discussed and validated in our previous two publications (Louis, F.; Gonzalez, C. A.; Huie, R. E.; Kurylo, M. J. *J. Phys. Chem. A* 2000, 104, 2931. Louis, F.; Gonzalez, C. A.; Huie, R. E.; Kurylo, M. J. *J. Phys. Chem. A* 2000, 104, 8773.). In the present work, this computational procedure is extended to develop relations of the Evans–Polanyi type, which provide an alternate method to predict rate constants for other reactions where computational expense becomes a limiting factor. In addition, rate constants computed at 277 K were used in the estimation of the atmospheric lifetimes for the five halomethanes. The validity of these results is also discussed.

Introduction

In the first two papers^{1,2} of this series (herein referred to as Paper I¹ and Paper II²), we presented an exhaustive and systematic study regarding the feasibility of applying relatively inexpensive ab initio electronic structure calculations together with canonical transition state theory, TST, leading to the generation of efficient and reliable computational tools that properly describe the kinetics of hydrogen-atom abstraction reactions by the hydroxyl radical from partially halogenated organic compounds. As explained in our previous work,^{1,2} these reactions are of particular importance in the determination of the atmospheric lifetimes of compounds suggested as replacements for fully halogenated alkanes, widely used in industry.

By using a validation set of 13 hydrogen-atom abstraction reactions between the hydroxyl radical and a series of halomethanes of type CHXYZ, (X = F, Cl, or Br), we found that the relatively inexpensive level of theory PMP4(SDTQ)/6-311G(3df,2p)/MP2/6-311G(2d,2p) combined with TST and the simple Wigner's tunneling correction formalism predicts kinetic parameters in quite reasonable agreement with the experimental data.² This can be appreciated by inspecting the results presented in Figure 1, where the temperature dependence of the ratio $k_{\text{theory}}/k_{\text{experiment}}$ in the range 250–400 K is shown for the thirteen reactions included in the validation set of Paper II.² As can be seen in this plot, even at low temperatures, most of the computed rate constants deviate from the corresponding experimental values by no more than a factor of 2. The only exception is the reaction OH + CHCl₃, where the predicted rate constants lie within a factor of 2 at 400 K and 4 at 250 K with respect to the experimental results. As discussed in Paper II,² this is not

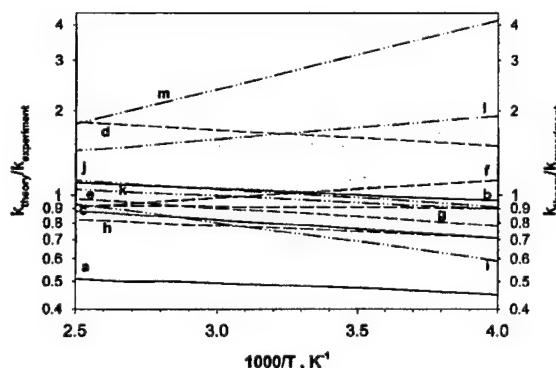


Figure 1. Evolution of the ratio $k_{\text{theory}}/k_{\text{experiment}}$ over the temperature range 250–400 K for the validation set of thirteen H atom abstraction reactions: a: CH₃F. b: CH₃Cl. c: CH₃Br. d: CH₂F₂. e: CH₂FCF₃. f: CH₂Cl₂. g: CH₂ClBr. h: CH₂Br₂. i: CHF₃. j: CHF₂Cl. k: CHF₂Br. l: CHFCl₂. m: CHCl₃.

surprising, given the low barrier this reaction exhibits, making the assumptions used by the canonical transition state theory questionable. The previously observed^{1,2} reliability of the theoretical procedure used in this work can be attributed to a fortuitous but systematic cancellation of errors between the Møller–Plesset perturbation theory and the truncated basis sets employed. In Papers I and II, it was also shown that Wigner tunneling corrections predict Arrhenius plots in better agreement with experiment in the case of H atom abstractions from halocarbons by OH radicals, while an unsymmetrical Eckart correction leads to Arrhenius plots with the wrong shape. As explained in Paper I, these results can be explained by the significantly wide barriers exhibited by this class of reactions, for which the Wigner tunneling formulation seems to be a better model compared with Eckart's treatment. On the basis of these very encouraging results, we have recommended this methodology as a de facto computational procedure for a "screening tool"

[†] Part of the special issue "Harold Johnston Festschrift".

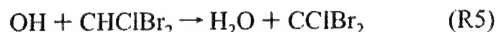
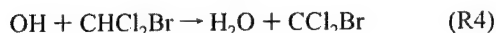
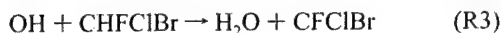
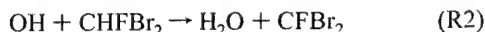
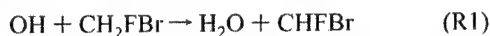
^{*} To whom correspondence should be addressed. Fax: (301) 975-3672.

[‡] E-mail: flouis@nist.gov.

[§] E-mail: carlos.gonzalez@nist.gov.

that can be used to help in establishing the environmental acceptability of partially halogenated organic compounds.

In this work, we apply the same methodology recommended in Paper II to compute the energetics and kinetic parameters of the following five H atom abstraction reactions:



The main goal of this study is to utilize our theoretical procedure to provide Arrhenius parameters for these reactions. This is particularly relevant in view of the lack of experimental data available for these reactions, with the exception of $\text{OH} + \text{CHCl}_2\text{Br}$ for which the rate constant has been only measured at 298 K.³ These reactants all contain bromine, which is a chemically active fire suppressant agent⁴ and are thus potential halon replacements (ref 1 from Paper I). To our knowledge, no theoretical calculations dealing with the thermochemistry and kinetics of these reactions have been reported previously.

In this study we are also extending our computational approach to the problem of estimating these rate constants to include computationally less expensive methods. Specifically, we have explored predictive schemes, based on the enthalpies of the reactions, calculated at the same level of theory we have applied to the kinetics. Enthalpy calculations are much easier to carry out and lower levels of theory may possibly be adequate. We explore this approach now in anticipation of the difficulties we may face in calculating rate constants for larger molecules.

Computational Methods^{5a}

All calculations described below were carried out with the Gaussian 94^{5b} suite of programs on a Cray C90/6256 supercomputer and a 32-processor Silicon Graphics Origin 2000 parallel computer. Details with the methodology used in the present calculations have been discussed elsewhere.^{1,2} Briefly, fully optimized geometries, harmonic frequencies, and zero-point energy corrections, ZPE, of reactants, transition structures, and products were computed with the second-order Møller–Plesset perturbation theory, UMP2, using the 6-311G(2d,2p) basis set. Electron correlation was calculated with the fourth-order Møller–Plesset perturbation theory in the space of single, double, triple, and quadruple excitations with full annihilation of spin contamination,⁶ PMP4(SDTQ). These single-point energy calculations were carried out with the 6-311G(3df,2p) basis set using the geometries previously optimized at the MP2/6-311G(2d,2p) level. All relative energies quoted and discussed in this paper include zero-point energy corrections with unscaled frequencies obtained at the MP2/6-311G(2d,2p) level.

Rate constants, $k(T)$, were computed using the following transition state theory expression:⁷

$$k(T) = \Gamma(T) \frac{k_B T}{h} \frac{Q^{\text{TS}}(T)}{Q^{\text{OH}}(T) Q^{\text{CHXYZ}}(T)} \exp\left(-\frac{\Delta E}{k_B T}\right) \quad (1)$$

where $Q^{\text{OH}}(T)$, $Q^{\text{CHXYZ}}(T)$, and $Q^{\text{TS}}(T)$ are the total partition functions for the hydroxyl radical, halomethane of type CHXYZ, and transition state respectively at temperature T ; ΔE is the activation energy including zero-point energy corrections; k_B

is Boltzman's constant, and h is Planck's constant. For all species, the total partition function can be cast in terms of the translational (Q^{X}_{T}), rotational (Q^{X}_{R}), electronic (Q^{X}_{e}), and vibrational (Q^{X}_{v}) partition functions. In computing the electronic partition function for the OH radical Q^{OH}_{e} , the multiplicity of the states $^2\Pi_{3/2}$ and $^2\Pi_{1/2}$ and the energy gap of 139.7 cm^{-1} between the low-lying electronic states⁸ have been taken into consideration. As in our previous work,² the tunneling correction $\Gamma(T)$ in eq 1 is computed by the simple Wigner's formalism:⁹

$$\Gamma(T) = 1 + \frac{1}{24} \left(\frac{h\nu^{\ddagger}}{k_B T} \right)^2 \quad (2)$$

where ν^{\ddagger} is the imaginary frequency at the saddle point and the other terms have the same meaning as in eq 1. The rate constant calculations over the temperature range 250–400 K were carried out using the TURBO-RATE program.¹⁰

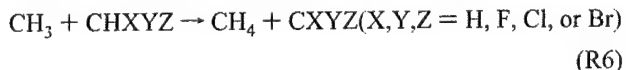
Results and Discussion

Transition Structures and Vibrational Frequencies. Table 1 lists all essential structural parameters as well as the imaginary frequencies computed at the UMP2/6-311G(2d,2p) level of theory for the transition structures corresponding to the five reactions (R1–R5). A complete list of all optimized geometrical parameters and vibrational frequencies corresponding to all reactants, transition structures, and products is shown in Tables 1S–5S provided in the Supporting Information.

The results shown in Table 1 indicate that, for all five transition states, the C–H bond being broken is elongated by approximately 10% while the H–O bond being formed is elongated by approximately 35% when compared to their equilibrium values. This is a clear indication of the “reactant-like” nature of these stationary points. These results seem to indicate relatively large exothermicities and low reaction barriers (see below), in keeping with Hammond's postulate.¹¹

Direct inspection of the transition state low-frequency modes reported in Table 5S indicates that, in all cases, there is one mode consisting of an internal –OH rotation about the nearly linear C–H–O axis. Given that the barriers for these rotations were sufficiently small (Table 1), these modes were treated as hindered rotors instead of a vibration. As explained in our previous papers,^{1,2} these modes were removed from the vibrational partition function for the transition state and the corresponding hindered rotor partition function $Q_{\text{HR}}(T)$, calculated by the method devised by Ayala and Schlegel,¹² was included in the expression for the rate constant.¹

Reaction Enthalpies and Barriers. Table 2 summarizes the results for reaction enthalpies $\Delta_r H(\text{ISO})$ calculated at 298 K by a procedure similar to the one adopted in our earlier publications,^{1–2} where the reaction enthalpies for the five reactions computed by direct subtraction of electronic energies between products and reactants are corrected by values of $D_{298}(\text{H–CXYZ})$ utilizing the following isodesmic reactions:



First, the reaction enthalpies of these reactions (R6) are computed at the same level of theory as that for the five abstraction reactions under study. These enthalpies are then used, in conjunction with the experimental value of $D_{298}(\text{H–CH}_3) = 440 \text{ kJ mol}^{-1}$,¹³ to calculate the corresponding $D_{298}(\text{H–CXYZ})$ values. Finally, these $D_{298}(\text{H–CXYZ})$ quantities are used in the calculation of the reaction enthalpy for reactions R1–R5 by

TABLE 1: Essential Structural Parameters,^a Imaginary Vibrational Frequencies for the Transition States of Each Reaction, and Internal Rotation Barrier of the -OH Group at the MP2/6-311G(2d,2p) Level of Theory

	<i>r</i> (C-H _R)	<i>r</i> (O-H _R)	θ (OH _R C)	<i>ν</i> ^{cm⁻¹}	<i>V</i> ₀ kJ mol ⁻¹	treatment of <i>ν</i> _{ROT} (HO...H...C) ^b
CH ₂ FBr	1.190	1.296	160.3	2184i	8.7	hindered rotor
CH ₂ Br ₂	1.186	1.296	162.0	2183i	7.8	hindered rotor
CHFCIBr	1.189	1.291	162.7	2220i	7.3	hindered rotor
CHCl ₂ Br	1.183	1.299	170.8	2174i	3.4	hindered rotor
CHClBr ₂	1.182	1.300	171.3	2173i	3.3	hindered rotor

^a Bond lengths *r* are in angstroms, bond angles θ in degrees; the hydrogen atom involved in H atom abstraction is noted H_R. ^b Low-frequency mode associated with the -OH rotation around the axis along the C-H bond being broken.

TABLE 2: Calculated Reaction Enthalpies Δ_rH(ISO) and Vibrationally Adiabatic Barriers at PMP4(SDTQ)/6-311G(3df,2p)/MP2/6-311G(2d,2p) Level of Theory

	Δ _r H(ISO) ^a (kJ mol ⁻¹)	<i>V</i> _a ^G (kJ mol ⁻¹) ^b
OH + CH ₂ FBr	-81.9	13.1
OH + CH ₂ Br ₂	-92.5	7.7
OH + CHFCIBr	-90.7	8.9
OH + CHCl ₂ Br	-105.3	4.5
OH + CHClBr ₂	-105.7	3.8

^a Including the sum of thermal energies (ΔZPE + thermal energy corrections at 298 K). ^b Including the ΔZPE correction.

TABLE 3: Summary of Kinetic Parameters Calculated at PMP4(SDTQ)/6-311G(3df,2p)/MP2/6-311G(2d,2p) Level of Theory Including Wigner's Tunneling Correction

	<i>E</i> ₀ / <i>R</i> (K)	<i>A</i> , 10 ⁻¹² ^a	<i>k</i> (theory, 298 K), 10 ⁻¹⁴ ^a
OH + CH ₂ FBr	1440	3.8	3.0
OH + CH ₂ Br ₂	825	1.6	10.0
OH + CHFCIBr	920	1.5	6.8
OH + CHCl ₂ Br	330	0.8	26.4
			12.0 ^b
OH + CHClBr ₂	250	0.8	34.6

^a Units are cm³ molecule⁻¹ s⁻¹. ^b Experimental value measured by Bilde et al.³

means of the following relation:

$$\Delta_r H(\text{ISO}) = D_{298}(\text{H-CXYZ}) - D_{298}(\text{H-OH}) \quad (3)$$

As observed in Table 2, the five reactions are significantly exothermic with values of the reaction enthalpies varying from -81.9 to -105.7 kJ mol⁻¹.

Table 2 also lists the vibrationally adiabatic barriers *V*_a^G for the five reactions under study. The values of *V*_a^G are computed by the following relation:

$$V_a^G = E_{\text{TS}} - E_{\text{R}} + \text{ZPE}_{\text{TS}} - \text{ZPE}_{\text{R}} \quad (4)$$

where *E*_{TS} and *E*_R are the computed ab initio total energies for the transition state and reactants, while ZPE_{TS} and ZPE_R are the corresponding zero-point energy corrections.

The results in Table 2 indicate that the substitution in the halomethane's structure of F atom by Cl or Br tends to decrease the barrier, but the substitution of Cl by Br does not seem to have a significant impact in the barrier height. Overall, reactions R1-R5 are characterized by large heats of reaction and relatively low barrier heights (3.8 to 13.1 kJ mol⁻¹), in keeping with the "reactant-like" nature of their corresponding transition states.

Kinetic Parameters. Table 3 shows the Arrhenius parameters obtained from a fit of the equation

$$k(T) = A \exp(-E_a/RT) \quad (5)$$

to the reaction rate constants computed in the temperature range 250-400 K. In addition, the rate constants computed at 298 K

are also shown. For the first three compounds, CH₂FBr, CH₂Br₂, and CHFCIBr, the *A*-factors per C-H bond, are the same. The *A*-factors for the compounds CHCl₂Br, and CHClBr₂ are about a factor of 2 lower. These latter compounds also have lower computed activation energies and higher rate constants at 298 K. Given the low barrier heights for these reactions, it is possible that canonical transition state theory might not be entirely appropriate and that the predicted rate constants might be just an upper bound to the real results. In these cases, more computationally expensive methodologies, such as the variational transition state theory formalism, VTST,¹⁴ should be used in order to compute rate constants with a higher accuracy. On the basis of our previous results on the reaction between OH + CHCl₃,² however, we believe that the TST results are accurate within a factor of 2-4 in the case of these two reactions. This is further confirmed by the computed *k*(298 K) for the reaction OH + CHCl₂Br (Table 3), which is approximately 2.2 times higher than the value measured by Bilde et al.³

Evans-Polanyi Relations. Despite the success of the methodology used in this work in predicting kinetic parameters in reasonable agreement with experimental results for H atom abstraction reactions between OH radicals and halogenated methanes,^{1,2} it is clear that the treatment of larger systems might be prohibitively expensive from a computational point of view. This is particularly true in the case of halogenated organic compounds with more than three carbon atoms, where the number of possible transition states could increase significantly. This situation gets worse in cases where a sizable number of halogens such as bromine are also present, given that the full ab initio treatment of the electronic structure problem could become unfeasible.

Given that the ab initio computation of heats of reaction are far less expensive (and less laborious) than the theoretical prediction of the kinetics, it would seem logical to look for other less expensive alternatives that involve only the treatment of the thermochemistry. In this work, we have adopted relations of the Evans-Polanyi type where properties such as vibrationally adiabatic barriers and/or reaction rate constants are related to the corresponding heats of reaction.

As a first approach, we have plotted the natural logarithm of the rate constant obtained experimentally at 298 K, ln *k*_{exp}(298 K), as a function of the calculated Δ_rH(ISO) at the same temperature for the 13 H atom abstraction reactions included in the validation set used in Paper II.² The resulting Evans-Polanyi plot is shown in Figure 2. A least-squares polynomial fit of the data leads to the following quadratic relation:

$$\ln k_{\text{exp}}(298 \text{ K}) = -2.003 \times 10^{-3} \Delta_r H(\text{ISO})^2 - 0.435 \Delta_r H(\text{ISO}) - 53.29 \quad (6)$$

This relation can now be used together with the calculated reaction enthalpies for the five reactions presented in this study in order to predict their corresponding ln *k*_{exp}(298 K) values. The predicted results using this approach are also depicted in

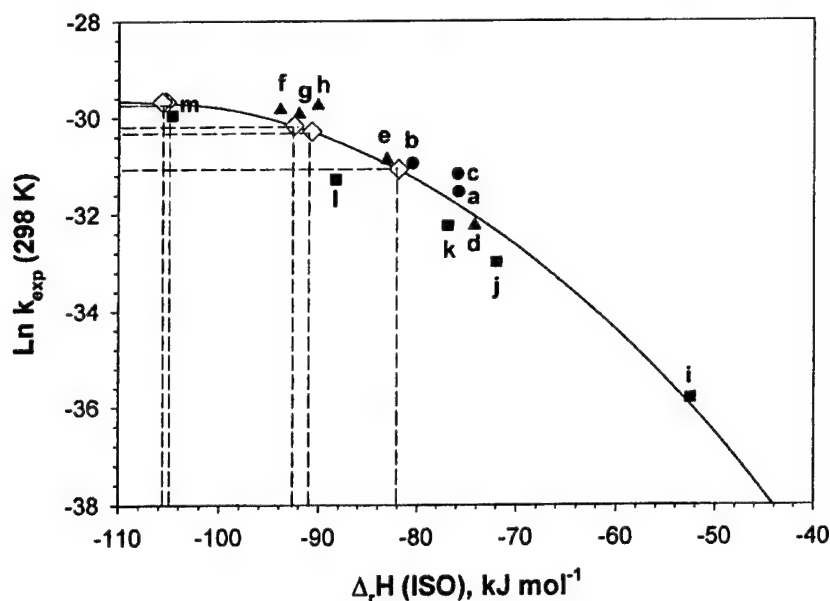


Figure 2. Quadratic variation of the $\ln k_{\text{exp}}(298 \text{ K})$ versus $\Delta_r H(\text{ISO})$ in kJ mol^{-1} . a: CH_3F . b: CH_3Cl . c: CH_3Br . d: CH_2F_2 . e: CH_2FCl . f: CH_2Cl_2 . g: CH_2ClBr . h: CH_2Br_2 . i: CHF_3 . j: CHF_2Cl . k: CHF_2Br . l: CHFCl_2 . m: CHCl_3 .

TABLE 4: Vibrational Adiabatic Barriers V_a^G in kJ mol^{-1} and Rate Constants at 298 K in $\text{cm}^3 \text{ molecule}^{-1} \text{ s}^{-1}$

compound	V_a^G (theory) ^a	$V_a^G(E-P)^b$	$k_{E-P}^{\text{theory}} \times 10^{13}$	$k_{E-P}^{\text{exp}} \times 10^{13}$	$k_{\text{ab initio}} \times 10^{13}$
CH_2FBr	13.1	13.2	0.29	0.32	0.30
CH_2FBr_2	7.7	9.5	1.00	0.79	1.00
CH_2FClBr	8.9	10.1	0.83	0.70	0.68
$\text{CH}_2\text{Cl}_2\text{Br}$	4.5	5.3	2.90	1.30	2.60
CH_2ClBr_2	3.8	5.1	3.00	1.30	3.50

^a Computed with the full ab initio treatment. ^b Predicted from the Evans–Polanyi eq 8. ^c Predicted from the Evans–Polanyi eq 7. ^d Predicted from the Evans–Polanyi eq 6. ^e Computed with the full ab initio treatment.

Figure 2. In addition, the results in Table 4 show that the predicted $k(298)$'s are in reasonable good agreement with the computed values obtained by the full ab initio treatment previously discussed.

Although the previous approach seems to work very well, it is rather limited in scope since it requires the knowledge of the experimental rate constants for a suitable validation set of reactions. This information might not be available, especially in instances where proposed partially halogenated organic compounds are being screened as potential replacements for their fully halogenated counterparts. In these cases, the prediction of the reaction rate constants based on purely theoretical calculations might be the best course of action. Figure 3 shows an Evans–Polanyi plot (using the same validation set) where the natural logarithm of the rate constant calculated at 298 K, $\ln k_{\text{theory}}(298 \text{ K})$, is plotted vs the corresponding calculated $\Delta_r H(\text{ISO})$ values. As with the previous approach, a quadratic relation is obtained:

$$\ln k_{\text{theory}}(298 \text{ K}) = -1.368 \times 10^{-3} \Delta_r H(\text{ISO})^2 - 0.354 \Delta_r H(\text{ISO}) - 50.96 \quad (7)$$

Again, the results for the five reactions discussed in this work (see Table 4) show an excellent agreement between the predicted values using eq 7 and the $k(298)$'s computed by the full ab initio treatment. The Evans–Polanyi relations discussed above are general and can be applied to temperatures other than 298 K.

Sometimes, information regarding the adiabatic vibrational barrier for a particular reaction is needed. Figure 4 shows the plot of V_a^G vs $\Delta_r H(\text{ISO})$ for the validation set of reactions. As

in the previous two approaches, a polynomial fit of the data gives the following Evans–Polanyi relation for V_a^G (in kJ mol^{-1}):

$$V_a^G = 1.025 \times 10^{-3} \Delta_r H(\text{ISO})^2 + 0.533 \Delta_r H(\text{ISO}) + 49.98 \quad (8)$$

As can be observed in Table 4, the five V_a^G 's predicted by eq 8 are in excellent agreement with the corresponding values computed by the full ab initio formalism.

Atmospheric Lifetimes. Reactions with hydroxyl radicals in the troposphere constitute the main removal pathways of hydrogen-containing compounds. Following Prather and Spivakovsky,¹⁵ we can estimate the atmospheric lifetime of a halomethane of the type CHXYZ due to reactions with hydroxyl radicals in the troposphere as

$$\tau_{\text{CHXYZ}}^{\text{OH}} = \frac{k_{\text{CH}_3\text{CCl}_3}^{\text{OH}}(277 \text{ K})}{k_{\text{CHXYZ}}^{\text{OH}}(277 \text{ K})} \tau_{\text{CH}_3\text{CCl}_3}^{\text{OH}} \quad (9)$$

Where $\tau_{\text{CHXYZ}}^{\text{OH}}$ and $\tau_{\text{CH}_3\text{CCl}_3}^{\text{OH}}$ are the atmospheric lifetimes of the halomethane CHXYZ and methyl chloroform (CH_3CCl_3), respectively, due to reactions with hydroxyl radicals in the troposphere only. In eq 9, $k_{\text{CHXYZ}}^{\text{OH}}(277 \text{ K})$ and $k_{\text{CH}_3\text{CCl}_3}^{\text{OH}}(277 \text{ K}) = 6.69 \times 10^{-15} \text{ cm}^3 \text{ molecule}^{-1} \text{ s}^{-1}$ ¹⁶ are the rate constants for the reactions of OH with these compounds at $T = 277 \text{ K}$. A value of $\tau_{\text{CH}_3\text{CCl}_3}^{\text{OH}}$ equal to 5.9 years was used, which was obtained following the procedure used by Prinn et al.¹⁷ from the measured lifetime of CH_3CCl_3 , $\tau_{\text{CH}_3\text{CCl}_3} = 4.8$ years, taking

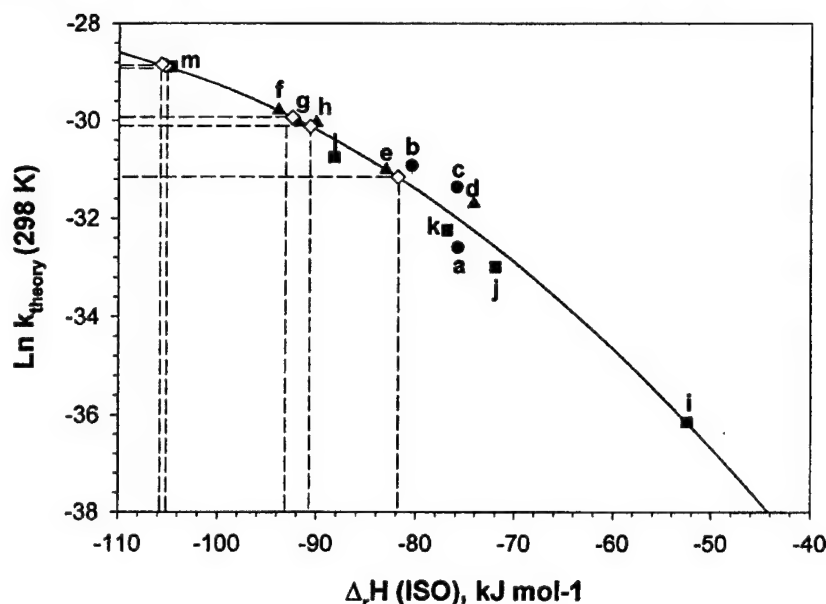


Figure 3. Quadratic variation of the $\text{Ln } k_{\text{theory}}(298 \text{ K})$ versus $\Delta_r H(\text{ISO})$ in kJ mol^{-1} . a: CH_3F . b: CH_3Cl . c: CH_3Br . d: CH_2F_2 . e: CH_2FCl . f: CH_2Cl_2 . g: CH_2ClBr . h: CH_2Br_2 . i: CHF_3 . j: CHF_2Cl . k: CHF_2Br . l: CHFCl_2 . m: CHCl_3 .

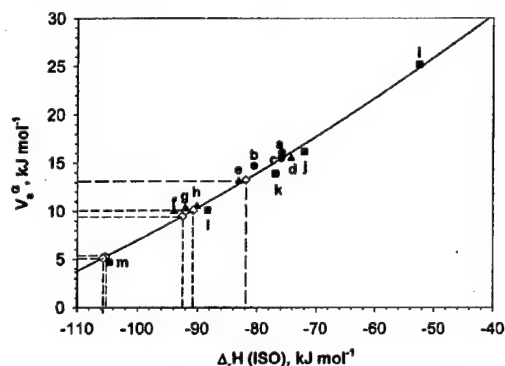


Figure 4. Quadratic variation of the vibrationally adiabatic barriers V_a^{\ddagger} versus $\Delta_r H(\text{ISO})$ in kJ mol^{-1} . a: CH_3F . b: CH_3Cl . c: CH_3Br . d: CH_2F_2 . e: CH_2FCl . f: CH_2Cl_2 . g: CH_2ClBr . h: CH_2Br_2 . i: CHF_3 . j: CHF_2Cl . k: CHF_2Br . l: CHFCl_2 . m: CHCl_3 .

into account partial lifetimes due to ocean loss of 85 years and to stratospheric loss of 37 years.

Table 5 shows the results of these predictions as well as the results obtained using the experimental rate constants for the validation set of thirteen H atom abstraction reactions discussed in Paper II.² The atmospheric lifetimes estimated by these calculations are in quite reasonable agreement with those estimated by the experimental data. As can be seen in Table 5, the theoretical atmospheric lifetimes deviate from their experimental counterparts by no more than a factor of 2, except in the case of the reaction of OH with chloroform (CHCl_3) for which a factor of 3.4 is obtained.

For the reactions of OH with CH_2FBr , CHFBr_2 , and CHFClBr , we estimate the atmospheric lifetimes to be 1.88, 0.49, and 0.73 years, respectively. On the basis of the agreement between the rate constants calculated for the validation set and the measurements, we estimate an uncertainty of less than a factor of 2 in the rate constants from which these are derived. For the bromochloromethanes CHCl_2Br and CHClBr_2 , the corresponding atmospheric lifetimes estimated by our calculations are 58 and 43 days. We estimate an uncertainty of no more than a factor of 4 for the rate constants from which these

TABLE 5: Atmospheric Lifetimes in Years for a Series of Halomethanes of Type CHXYZ

compound	$\tau_{\text{CHXYZ}}^{\text{OH}}(\text{theory})^a$	$\tau_{\text{CHXYZ}}^{\text{OH}}(\text{experiment})^b$
CH_3F	6.37	2.92
CH_3Cl	1.55	1.55
CH_3Br	2.47	1.97
CH_2F_2	3.59	5.60
CH_2FCl	1.68	1.38
CH_2Cl_2	0.43	0.46
CH_2ClBr	0.54	0.49
CH_2Br_2	0.57	0.42
CHF_3	397	263
CHF_2Cl	13.16	12.73
CHF_2Br	6.03	5.64
CHFCl_2	1.18	2.13
CHCl_3	0.15	0.51
CH_2FBr	1.88	unknown
CHFBr_2	0.49	unknown
CHFClBr	0.73	unknown
CHCl_2Br	0.16	unknown
CHClBr_2	0.12	unknown

^a Computed with the full ab initio treatment. ^b Experimental values of the rate constant at 277 K are calculated from the Arrhenius expressions reported in ref 16, and in ref 18 for the reaction $\text{OH} + \text{CH}_2\text{ClBr}$.

are derived. The rate constants for their reaction with OH are indeed likely to be very similar to that of CHCl_3 and CHBr_3 .

Note that the estimates of the lifetimes of these compounds do not include loss mechanisms due to photolysis or to hydrolysis. Any contribution from these sources will lead to a lower actual lifetime. In addition, the above estimates assume a uniform distribution of the gas throughout the troposphere. This assumption is probably reasonable for longer-lived compounds such as CH_2FBr , somewhat questionable for CHFBr_2 and CHFClBr , and is probably not valid for the short-lived compounds CHCl_2Br and CHClBr_2 , which are not likely to have a uniform distribution over the troposphere. Atmospheric modeling calculations are probably required to obtain more valid estimates. Nevertheless, from the point of view of a screening tool, the important information is that these compounds are predicted to be short-lived and are thus potentially suitable replacement compounds.

Conclusions

PMP4(SDTQ)/6-311G(3df,2p)/MP2/6-311G(2d,2p) molecular orbital calculations combined with transition state theory have been used in order to study the kinetics of the H atom abstraction reactions between the radical OH and a series of five bromine-containing halomethanes for which no experimental data are available. Given the previous success of this methodology² in predicting rate constants within a factor of 2 for similar reactions, we believe the kinetic parameters for the five reactions in this study are predicted with similar accuracy. The results presented in this work also show the feasibility of using relationships of the Evans–Polanyi type in order to predict the kinetics of other H atom abstraction reactions by OH radicals using only theoretical calculations of the reaction thermodynamics. These Evans–Polanyi relations provide a powerful addition to the computational “screening tool” proposed in our previous publications^{1,2} aimed at the implementation of inexpensive semiquantitative methodologies that could aid scientists in the understanding of the kinetics processes similar to the ones discussed in this work. Finally, rate constants computed at 277 K were used in order to provide estimates of the atmospheric lifetimes for the five halomethanes: CH₂FBr, CHFBr₂, CHFClBr, CHCl₂Br, and CHClBr₂. It is observed that the species CH₂FBr, CHFBr₂, and CHFClBr exhibit considerably larger atmospheric lifetimes (from 0.5 to 1.9 years) when compared to the bromochloromethanes CHCl₂Br, and CHClBr₂ (in the order of days). As explained in the Discussion section, these numbers should be used only as a semiquantitative guide given that more sophisticated models are needed in order to get accurate atmospheric lifetimes.

Acknowledgment. This work was supported by the Upper Atmosphere Research Program of the National Aeronautics and Space Administration and by the Next Generation Fire Suppression Technology Program, funded by the Department of Defense Strategic Environmental Research and Development Program under MIPR number W74RDV73243630.

Supporting Information Available: Tables of (i) the optimized geometry parameters of the halomethanes, halomethyl radicals, and transition states (Tables 1S–3S), and (ii) their vibrational frequencies (Tables 4S and 5S).

References and Notes

- (1) Louis, F.; Gonzalez, C. A.; Huie, R. E.; Kurylo, M. J. *J. Phys. Chem. A* **2000**, *104*, 2931.
- (2) Louis, F.; Gonzalez, C. A.; Huie, R. E.; Kurylo, M. J. *J. Phys. Chem. A* **2000**, *104*, 8773.
- (3) Bilde, M.; Wallington, T. J.; Ferronato, C.; Orlando, J. J.; Tyndall, G. S.; Estupiñan, E.; Haberkorn, S. *J. Phys. Chem. A* **1998**, *102*, 1976.
- (4) Noto, T.; Babushok, V.; Burgess, D. R.; Hamins, A.; Tsang, W.; Miziolek, A. *26th Symp. (Int.) Combust.* **1996**, 1377.
- (5) (a) The identification of commercial equipment or materials does not imply recognition or endorsement by the National Institute of Standards and Technology, nor does it imply that the material or equipment identified are necessarily the best available for the purpose. (b) Frisch, M. J.; Trucks, G. W.; Schlegel, H. B.; Gill, P. M. W.; Johnson, B. G.; Robb, M. A.; Cheeseman, J. R.; Keith, T.; Petersson, G. A.; Montgomery, J. A.; Raghavachari, K.; Al-Laham, M. A.; Zakrzewski, V. G.; Ortiz, J. V.; Foresman, J. B.; Cioslowski, J.; Stefanov, B. B.; Nanayakkara, A.; M. Challacombe; Peng, C. Y.; Ayala, P. Y.; Chen, W.; Wong, M. W.; Andres, J. L.; Replogle, E. S.; Gomperts, R.; Martin, R. L.; Fox, D. J.; Binkley, J. S.; Defrees, D. J.; Baker, J.; Stewart, J. P.; Head-Gordon, M.; Gonzalez, C.; Pople, J. A. *Gaussian 94*, Revision D.4; Gaussian, Inc.: Pittsburgh, PA, 1995.
- (6) (a) Schlegel, H. B. *J. Chem. Phys.* **1986**, *84*, 4530. (b) Schlegel, H. B. *J. Phys. Chem.* **1988**, *92*, 3075. (c) Sosa, C.; Schlegel, H. B. *Int. J. Quantum Chem.* **1986**, *29*, 1001. (d) Sosa, C.; Schlegel, H. B. *Int. J. Quantum Chem.* **1987**, *30*, 155.
- (7) (a) Johnston, H. S. *Gas-Phase Reaction Rate Theory*; The Roland Press Company: New York, 1966. (b) Laidler, K. J. *Theories of Chemical Reaction Rates*; McGraw-Hill: New York, 1969. (c) Weston, R. E.; Schwartz, H. A. *Chemical Kinetics*; Prentice Hall: New York, 1972. (d) Rapp, D. *Statistical Mechanics*; Holt, Reinhard, and Winston: New York, 1972. (e) Nikitin, E. E. *Theory of Elementary Atomic and Molecular Processes in Gases*; Clarendon Press: Oxford, 1974. (f) Smith, I. W. M. *Kinetics and Dynamics of Elementary Gas Reactions*; Butterworth: London, 1980. (g) Steinfeld, J. I.; Francisco, J. S.; Hase, W. L. *Chemical Kinetics and Dynamics*; Prentice Hall: New Jersey, 1989.
- (8) Chase, M. W. *J. Phys. Chem. Ref. Data* **1998**, *Monograph 9*.
- (9) Wigner, E. P. *Z. Phys. Chem.* **1932**, *B19*, 203.
- (10) Rate constants calculated with the Turbo-Rate module in the beta version of the TURBO–OPT geometry optimization package, developed by C. Gonzalez and Tom Allison, National Institute of Standards and Technology, Gaithersburg, MD.
- (11) Hammond, G. S. *J. Am. Chem. Soc.* **1955**, *77*, 334.
- (12) Ayala, P. Y.; Schlegel, H. B. *J. Chem. Phys.* **1998**, *108*, 2314.
- (13) Tsang, W. *Heats of Formation of Organic Free Radicals by Kinetic Methods*; Tsang, W., Ed.; Blackie Academic & Professional: London, 1996; p 22.
- (14) (a) Truhlar, D. G.; Isaacson, A. D.; Garret, B. C. In *Theory of Chemical Reaction Dynamics*; Baer, M. Ed.; CRC Press: Boca Raton, FL, **1985**, p 65. (b) Truhlar, D. G. *J. Chem. Phys.* **1970**, *53*, 2041. (c) Garret, B. C.; Truhlar, D. G. *J. Phys. Chem.* **1979**, *83*, 1052. (d) Garret, B. C.; Truhlar, D. G. *J. Phys. Chem.* **1979**, *83*, 1079. (e) Garret, B. C.; Truhlar, D. G. *J. Am. Chem. Soc.* **1979**, *101*, 4534. (f) Garret, B. C.; Truhlar, D. G. *J. Am. Chem. Soc.* **1980**, *2*, 2559. (g) Kreevoy, M. M.; Truhlar, D. G. In *Investigation of Rates and Mechanisms of Reactions*; Bernasconi, C. F., Ed.; John Wiley & Sons: New York, 1986; Part 1, p 13.
- (15) Prather, M.; Spivakovsky, C. M. *J. Geophys. Res.* **1990**, *95*, 18723.
- (16) DeMore, W. B.; Sander, S. P.; Golden, D. M.; Hampson, R. F.; Kurylo, M. J.; Howard, C. J.; Ravishankara, A. R.; Kolb, C. E.; Molina, M. J. *JPL Publication 97-4*; Jet Propulsion Laboratory, California Institute of Technology: Pasadena, CA, 1997.
- (17) Prinn, R. G.; Weiss, R. F.; Miller, B. R.; Huang, A.; Alyea, F. N.; Cunnold, D. M.; Fraser, P. J.; Hartley, D. E.; Simmonds, P. G. *Science* **1995**, *269*, 187.
- (18) Orkin, V. L.; Khamaganov, V. G.; Guschin, A. G.; Huie, R. E.; Kurylo, M. J. *J. Phys. Chem. A* **1997**, *101*, 174.

SUPPORTING INFORMATION

Table 1S: MP2/6-311G(2d,2p) optimized geometry parameters for halomethanes

Species	Parameter ^{a)}
CH ₃ FBr	r _{CH} = 1.080, r _{CF} = 1.361, r _{CBr} = 1.940, θ(HCH) = 112.6, θ(FCH) = 109.6, θ(BrCH) = 107.2, φ(FCHH) = 122.3, φ(BrCHH) = -117.6
CHFBr ₂	r _{CH} = 1.079, r _{CF} = 1.349, r _{CBr} = 1.933, θ(FCH) = 109.9, θ(BrCH) = 107.8, φ(BrCHF) = 119.3
CHFClBr	r _{CH} = 1.079, r _{CF} = 1.347, r _{CCl} = 1.772, r _{CBr} = 1.935, θ(FCH) = 109.8, θ(ClCH) = 108.4, θ(BrCH) = 107.7, φ(ClCHF) = 119.7, φ(BrCHF) = -119.1
CHCl ₂ Br	r _{CH} = 1.077, r _{CCl} = 1.772, r _{CBr} = 1.938, θ(ClCH) = 108.0, θ(BrCH) = 106.7, φ(ClCHBr) = 119.7
CHClBr ₂	r _{CH} = 1.077, r _{CCl} = 1.770, r _{CBr} = 1.937, θ(ClCH) = 108.2, θ(BrCH) = 107.0, φ(ClCHBr) = 120.3

^{a)} Bond lengths are in Angstroms, bond angles θ and dihedral angles φ are in degrees.

Table 2S: MP2/6-311G(2d,2p) optimized geometry parameters for halomethyl radicals

Species	Parameter ^{a)}
CHFBr	r _{CH} = 1.078, r _{CF} = 1.331, r _{CBr} = 1.876, θ(FCH) = 113.9, θ(BrCH) = 116.1, φ(BrCHF) = 137.1
CFBr ₂	r _{CF} = 1.325, r _{CBr} = 1.889, θ(BrCF) = 113.2, φ(BrCFBr) = 137.7
CFCBr	r _{CF} = 1.325, r _{CCl} = 1.728, r _{CBr} = 1.889, θ(ClCF) = 113.0, θ(BrCF) = 113.4, φ(BrCFCl) = 137.0
CCl ₂ Br	r _{CCl} = 1.719, r _{CBr} = 1.877, θ(ClCBr) = 117.0, φ(ClCBrCl) = 145.0
CClBr ₂	r _{CCl} = 1.718, r _{CBr} = 1.877, θ(BrCCl) = 116.8, φ(BrCClBr) = 145.9

^{a)} Bond lengths are in Angstroms, bond angles θ and dihedral angles φ are in degrees.

jp001923

Table 3S: MP2/6-311G(2d,2p) optimized geometry parameters for the transition states in the series of reactions OH with CH₃FBBr, CHFBr₂, CHFClBr, CHCl₂Br and CHClBr₂

Parameter ^{a)}	OH + CH ₃ FBBr	OH + CHFBr ₂	OH + CHFClBr	OH + CHCl ₂ Br	OH + CHClBr ₂
r (C-H _R)	1.190	1.186	1.189	1.183	1.182
r (C-X)	1.081	1.346	1.345	1.922	1.757
r (C-Y)	1.355	1.918	1.755	1.761	1.921
r (C-Z)	1.914	1.918	1.919	1.761	1.927
r (O-H _R)	1.296	1.296	1.291	1.299	1.300
r (H-O)	0.966	0.967	0.967	0.967	0.967
θ (XCH)	109.1	108.2	108.1	104.1	107.4
θ (YCH)	108.2	106.7	107.5	107.4	104.3
θ (ZCH)	106.6	106.7	106.4	107.4	106.5
θ (OH _R C)	160.3	162.0	162.7	170.8	171.3
θ (HOH _R)	97.1	98.7	98.6	98.6	98.3
φ (YCHX)	120.4	118.9	119.2	119.5	119.9
φ (ZCHX)	-119.2	-118.9	-118.6	-119.5	-120.7
φ (OH _R CX)	272.2	0.0	-9.9	180.0	67.0
φ (HOH _R C)	-35.6	0.0	4.0	-0.1	11.0

^{a)} Bond lengths are in Angstroms, bond angles θ and dihedral φ are in degrees; the hydrogen atom involved in H-atom abstraction is noted H_R

Table 4S: Calculated MP2/6-311G(2d,2p) vibrational frequencies (in cm^{-1}) for halomethanes and halomethyl radicals

Species	Vibrational frequencies (cm^{-1})
CH_2FBr	316, 660, 961, 1104, 1276, 1372, 1529, 3160, 3248
CHFBr_2	174, 301, 361, 628, 719, 1106, 1213, 1340, 3218
CHFCIBr	228, 318, 426, 667, 787, 1112, 1244, 1351, 3220
CHCl_2Br	219, 226, 334, 609, 739, 779, 1212, 1249, 3232
CHClBr_2	170, 204, 283, 571, 677, 758, 1188, 1228, 3233
CHFBr	339, 676, 820, 1189, 1323, 3236 <i>650, 1149, 1266 a)</i>
CFBr_2	178, 315, 384, 501, 817, 1176 <i>782, 1136 a)</i>
CFCIBr	233, 333, 446, 554, 878, 1182
CCl_2Br	228, 240, 339, 440, 845, 889 <i>835, 888 a)</i>
CClBr_2	179, 214, 303, 386, 793, 860 <i>783, 856 a)</i>

The experimental values of the vibrational frequencies are in italics. These values are taken from

^{a)} ref. 1S

Table 5S: Calculated MP2/6-311G(2d,2p) vibrational frequencies (in cm^{-1}) for transition states

Species	Vibrational frequencies (cm^{-1})
$\text{OH} + \text{CH}_2\text{FBr}$	2184i, 88, 128, 171, 323, 518, 740, 856, 1014, 1121, 1311, 1552, 3200, 3814
$\text{OH} + \text{CHFBr}_2$	2183i, 64, 104, 109, 174, 305, 340, 383, 754, 816, 881, 1074, 1114, 1539, 3813
$\text{OH} + \text{CHFCIBr}$	2220i, 71, 100, 116, 226, 322, 365, 455, 804, 839, 887, 1098, 1121, 1534, 3813
$\text{OH} + \text{CHCl}_2\text{Br}$	2174i, 30, 82, 108, 222, 228, 306, 423, 725, 775, 800, 876, 1109, 1380, 3808
$\text{OH} + \text{CHClBr}_2$	2173i, 32, 78, 102, 172, 207, 267, 388, 666, 761, 777, 869, 1091, 1366, 3808

Vibrational frequencies indicated in italics correspond to the hindered rotation of the -OH group

REFERENCE FOR SUPPORTING INFORMATION:

1S) Jacox, M.E. Vibrational and Electronic Energy Levels of Polyatomic Transient Molecules, J.Phys.Chem.Ref.Data, 1994, Monograph N°3.

Effect of Bromine Substitution on the Lifetimes and Ozone Depletion Potentials of Organic Compounds

Robert E. Huie, Vladimir L. Orkin, Florent Louis, Sergey N. Kozlov, and Michael J. Kurylo

*Physical and Chemical Properties Division,
National Institute of Standards and Technology
Gaithersburg, Maryland 20899-8381*

301-975-2559 robert.huie@nist.gov
301-975-4418 vladimir.orkin@nist.gov
33-3-20-43-63-32 flouis@pop.univ-lille1.fr
7 (095) 939-7318 kozlov@chph.ras.ru
202-358-0237 mkurylo@mtpe.hq.nasa.gov

INTRODUCTION

Although the bromofluorocarbon compounds known as halons are excellent fire suppressants, their production is being phased out due to the considerable danger they pose to the Earth's ozone layer. A number of non-brominated substances have been proposed and tested, but the effort to find replacements continues to return to bromine due to the chemical characteristics of this element as a chemically active flame suppressant. Thus, a number of classes of bromine-containing molecules have been proposed for investigation as to their fire-suppression characteristics. Before candidate replacements can be placed into service, it is important to establish their environmental effects, particularly the projected ozone depletion potential. Generally, these replacement compounds are designed to be reactive toward atmospheric hydroxyl radicals. This reaction leads to chemical transformations that ultimately lead to the removal of the bromine from the atmosphere. Additionally, photolysis of these compounds in the atmosphere will release Br and may further shorten their lifetimes. In order to quantitatively evaluate the impact of these compounds in the atmosphere, we have investigated the reactivity of several classes of reactants toward OH, both experimentally and computationally. Rate constants were determined over the temperature range of at least 250 K to 370 K. In addition, we have measured the absorption spectra of most of these compounds down to 160 nm. We have then utilized this information to derive predicted ozone depletion potentials.

Experimental Section

UV Absorption Cross-Section Measurements. The absorption spectra of the brominated compounds to be analyzed were measured over the wavelength range of 160-280 nm using a single beam apparatus consisting of a 1 m vacuum monochromator equipped with a 600 lines/mm grating and a photomultiplier. The radiation source was a deuterium lamp. Spectra were recorded at increments of 0.5 nm at spectral slit widths of 0.5 nm. The pressure inside the (16.9 ± 0.05) cm absorption cell was measured by a manometer at $T = (295 \pm 1)$ K. Absorption spectra of the evacuated cell and of the cell filled with a gas sample were alternately recorded several times, and the absorption cross sections were calculated from the differences. The

complete spectra were constructed from data taken over several overlapping wavelength ranges. Data over each range were obtained at several pressures to verify adherence to the Beer-Lambert absorption law. The overall instrumental error associated with uncertainties in the path length, pressure, temperature stability, and the measured absorbance was estimated to be less than 2% over most of the wavelength range, increasing to ca. 10-20 % at the long-wavelength ends of the spectra. Mixtures containing 2%, 10%, and 100% of the compounds under study were used at pressures in the cell ranging from 4 Pa to 120 kPa (0.03 - 900 Torr).

OH Reaction Rate Constant Measurements. The principal component of the flash photolysis-resonance fluorescence (FPRF) apparatus is a Pyrex reactor (of approximately 50 cm³ internal volume) thermostated with water or ethanol circulated through its outer jacket. Reactions were studied in argon carrier gas (99.9995% purity) at a total pressure of 13.33 kPa (100.0 Torr). Flows of dry argon, argon bubbled through water thermostated at 276 K, and reactant mixtures (containing 0.01%-0.1% of the reactant diluted with argon) were premixed and flowed through the reactor at a total flow rate between 0.6 and 1.4 cm³ s⁻¹, STP. The concentrations of the gases in the reactor were determined by measuring the mass flow rates and the total pressure with a manometer. Flow rates of argon, the H₂O/argon mixture, and reactant/inert gas mixtures were measured by calibrated mass flow meters. Hydroxyl radicals were produced by the pulsed photolysis (1-4 Hz repetition rate) of H₂O (introduced via the 276 K argon / H₂O bubbler) by a xenon flash lamp focused into the reactor. The radicals were then monitored by their resonance fluorescence near 308 nm, excited by a microwave-discharge resonance lamp (330 Pa or 2.5 Torr of a ca. 2% mixture of H₂O in UHP helium) focused into the reactor center. The resonance fluorescence signal was recorded on a computer-based multichannel scanner (channel width 100 μ s) as a summation of 2,000-5,000 consecutive flashes. The radical decay signal at each reactant concentration was analyzed as described previously [1] to obtain the first-order decay rate coefficient due to the reaction under study.

Computational Determinations of OH Kinetics. Fully optimized geometries, harmonic frequencies, and zero-point energy corrections, ZPE, of reactants, transition structures and products were computed with the second-order Møller-Plesset perturbation theory, UMP2, using the 6-311G(2d,2p) basis set. Electron correlation was calculated with the fourth-order Møller-Plesset perturbation theory in the space of single, double, triple and quadruple excitations with full annihilation of spin contamination, [2] PMP4(SDTQ). These single-point energy calculations were carried out with the 6-311G(3df,2p) basis set using the geometries previously optimized at the MP2/6-311G(2d,2p) level. All relative energies quoted and discussed in this paper include zero-point energy corrections with unscaled frequencies obtained at the MP2/6-311G(2d,2p) level.

Rate constants, $k(T)$, were computed using the following transition state theory expression [3]:

$$k(T) = \Gamma(T) \times \frac{k_B T}{h} \times \frac{Q^{TS}(T)}{Q^{OH}(T) Q^{CHXYZ}(T)} \times \exp\left(-\frac{\Delta E}{k_B T}\right) \quad (1)$$

Where: $Q^{OH}(T)$, $Q^{CHXYZ}(T)$, $Q^{TS}(T)$, are the total partition functions for the hydroxyl radical, halomethane of type CHXYZ, and transition state respectively at temperature T ; ΔE is the activation energy including zero-point energy and thermal corrections to the internal energy; k_B is Boltzman's constant, and h is Planck's constant. For all species, the total partition function can be cast in terms of the translational, (Q^T), rotational, (Q^R), electronic, (Q^e), and

vibrational, (Q_v^x), partition functions. In computing the electronic partition function for the OH radical, Q_e^{OH} , the multiplicity of the states $^2\Pi_{3/2}$ and $^2\Pi_{1/2}$ and the energy gap of 139.7 cm^{-1} between the low-lying electronic states have been taken into consideration. As in our previous work, the tunneling correction $\Gamma(T)$ in equation (1) is computed by the simple Wigner's formalism [4]:

$$\Gamma(T) = 1 + \frac{1}{24} \left(\frac{h\nu^*}{k_B T} \right)^2 \quad (2)$$

Where ν^* is the imaginary frequency at the saddle point and the other terms have the same meaning as in equation (1). The rate constant calculations over the temperature range 250-400 K were carried out using the TURBO-RATE program. [5]

Results and Discussion

UV Absorption Spectra All of the bromine-containing compounds absorb ultraviolet radiation strongly in the 195 nm – 215 nm region, where photodissociation in the lower stratosphere is most important. This reduces their atmospheric lifetimes, but contributes to the ozone depletion potential. The measured absorption cross sections for this region are utilized in our calculations of the ozone depletion potentials for these species. The results of our measurements on bromine-containing compounds are shown in Figures 1 – 3, along with some other gasses for comparison.

Figure 1. UV absorption spectra of bromopropanes and 2-bromo-1,1-difluoroethyl methyl ether

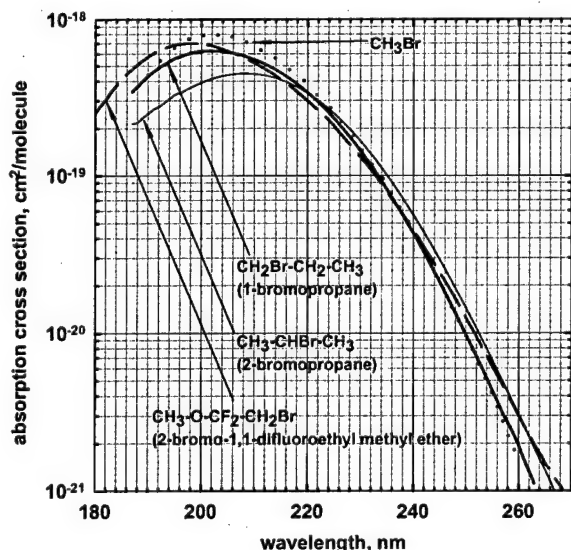


Figure 2. UV absorption spectra of selected Br-containing fluorinated alkenes and alkanes

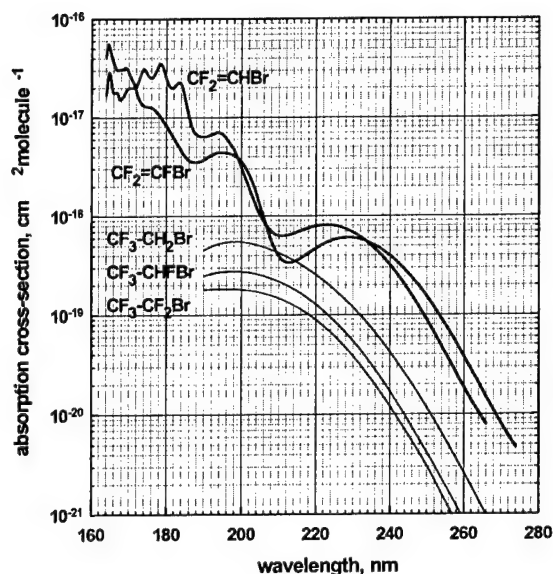
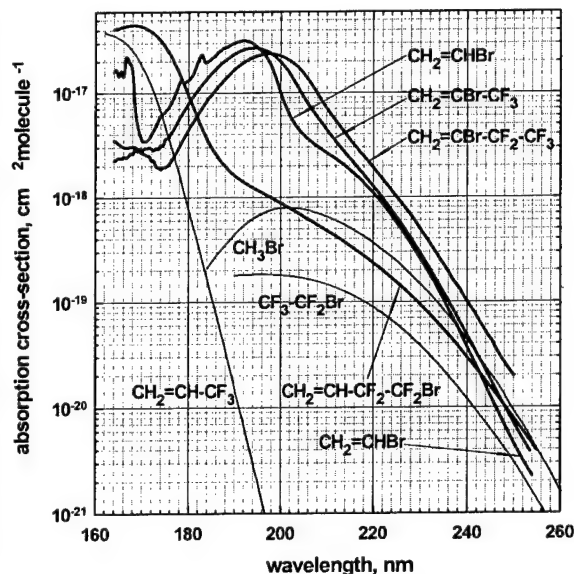


Figure 3. UV absorption spectra of selected Br-containing fluorinated alkenes and alkanes



Experimental Kinetics: The results of our measurements on the reactions of hydroxyl radicals with five bromofluoro-alkenes at different temperatures are presented in Figure 4. The derived Arrhenius parameters for the reactions are listed in Table 1. The effect of halogenation on alkene reactivity is quite complicated. Nevertheless, one can speculate on the correlation between reactivity and structure of these halogenated alkenes. Fluorination of one olefinic carbon tends to deactivate while fluorination of the second olefinic carbons tends to compensate that deactivation. This suggests that the alkene reactivity toward OH depends mainly on the geometrical localization of π -electron density. Bromination of the olefinic carbon increases the reactivity of fluorinated alkenes while Br on a remote carbon has essentially no effect (Figure 5).

Figure 4. Rate Constants for Reactions between OH and Br-containing Fluorinated Alkenes

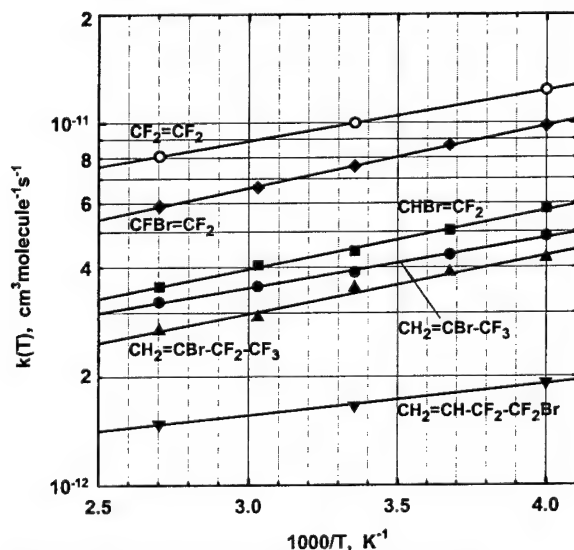
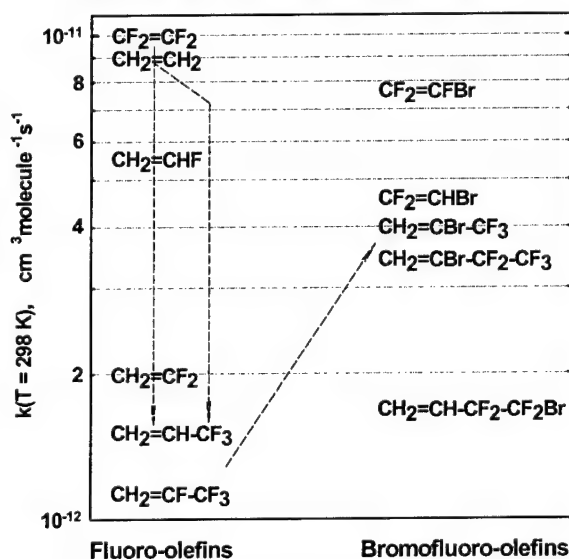


Figure 5. Effect of Bromination on Reactivity of Fluorinated Olefins toward OH

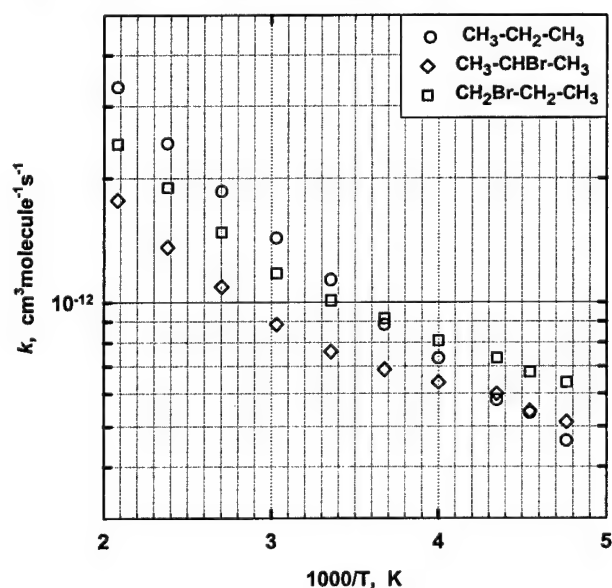


Arrhenius Parameters for OH Reactions of Br-containing Fluoroalkenes and their Estimated Environmental Parameters

Molecule	$A \times 10^{12}$, $\text{cm}^3 \text{molecule}^{-1} \text{s}^{-1}$	$E/R \pm$ $\Delta E/R$, K	$k(298) \times 10^{12}$ $\text{cm}^3 \text{molecule}^{-1} \text{s}^{-1}$	Atmospheric lifetime, days	ODP
$\text{CF}_2=\text{CF}_2$	3.39 ± 0.22	-323 ± 11	9.98 ± 0.02	1.1	
$\text{CFBr}=\text{CF}_2$	2.02 ± 0.12	-396 ± 18	7.62 ± 0.06	1.4	0.0022
$\text{CHBr}=\text{CF}_2$	$1.30^{+0.22}_{-0.18}$	-370 ± 47	4.53 ± 0.10	2.4	0.0015
$\text{CH}_2=\text{CBr}-\text{CF}_3$	$1.36^{+0.17}_{-0.14}$	-317 ± 34	3.94 ± 0.06	2.4	0.0034
$\text{CH}_2=\text{CBr}-\text{CF}_2-\text{CF}_3$	$0.98^{+0.35}_{-0.26}$	-369 ± 90	3.39 ± 0.14	3.1	0.0030
$\text{CH}_2=\text{CH}-\text{CF}_2-\text{CF}_2\text{Br}$	$0.85^{+0.15}_{-0.12}$	-201 ± 46	1.68 ± 0.05	6.7	0.0043

Atmospheric lifetimes and ODPs were estimated in the manner typically used for long-lived compounds. Such estimations assume a uniform tropospheric distribution that is not correct for short-lived compounds. ODPs were estimated using the calculated lifetime of CF_3Br equals to 65 years and its $\text{ODP}(\text{CF}_3\text{Br}) = 13$. [6]

Figure 6. Rate Constants for Reactions of OH with 1-bromopropane, 2-bromopropane, and propane

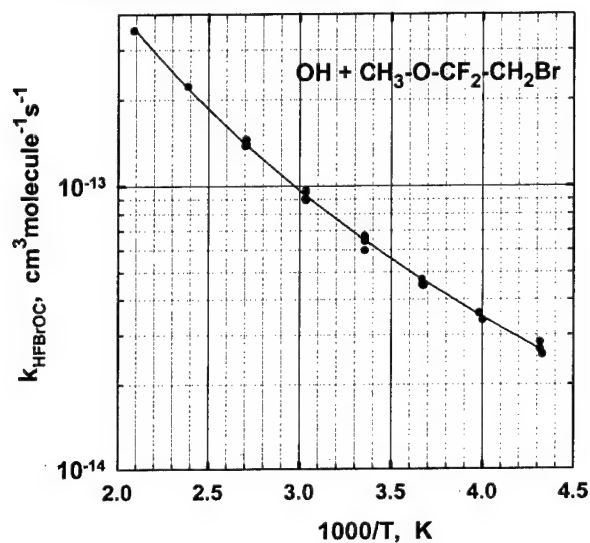


The reactivity of OH toward both 1- and 2-bromopropane has been determined over the temperature range 210 K to 480 K. The Arrhenius plots presented in Figure 6 show curvature due to the different rate constants for abstraction from the different types of C-H bonds in the molecules. In Table 2, we present the Arrhenius parameters for the temperature range below 298 K.

Table 2. Arrhenius Parameters for OH Reactions of propane and bromopropanes

Molecule	$A \times 10^{12}$, $\text{cm}^3 \text{molecule}^{-1} \text{s}^{-1}$	E/R , K	$k(298) \times 10^{12}$ $\text{cm}^3 \text{molecule}^{-1} \text{s}^{-1}$	Atmospheric lifetime, days	ODP
$\text{CH}_3\text{CH}_2\text{CH}_2\text{Br}$	3.04	329	1.01	14	0.015
$\text{CH}_3\text{CHBrCH}_3$	1.90	275	0.76	19	0.018

Figure 7. The Rate Constants for the Reaction between
OH and 2-bromo-1,1-difluoroethyl methyl ether



In Figure 7 we present our results on the kinetics of the reaction of OH with the bromine-substituted fluoroether $\text{CH}_3\text{OCF}_2\text{CH}_2\text{Br}$. The Arrhenius plot is clearly curved, which we ascribe to abstraction at the two different C-H sites. The results can be represented by the expression $k = 5.24 \times 10^{-14} (T/298)^{3.77} \exp(+ (63 \pm 202)/T) \text{ cm}^3 \text{ molec}^{-1} \text{ s}^{-1}$.

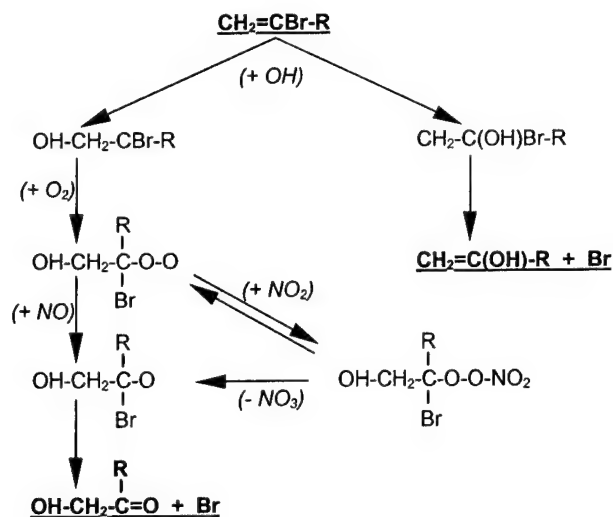
Computational Kinetics: The computational screening approach was applied to a series of halogenated methanes for which reliable kinetic data were available. [7] By this means, we were able to demonstrate that the chosen level of theory could provide calculated rate constants that were within better than factors of three of the experimental values, and typically within better than a factor of two. The results of these calculations are presented in Table 3 for the bromine-containing methanes. [8]

Table 3. Calculated Arrhenius Parameters for Reactions with OH at the PMP4(STDQ)/6-311G(3df,2p) Level of Theory, Estimated Atmospheric Lifetimes, and ODPs

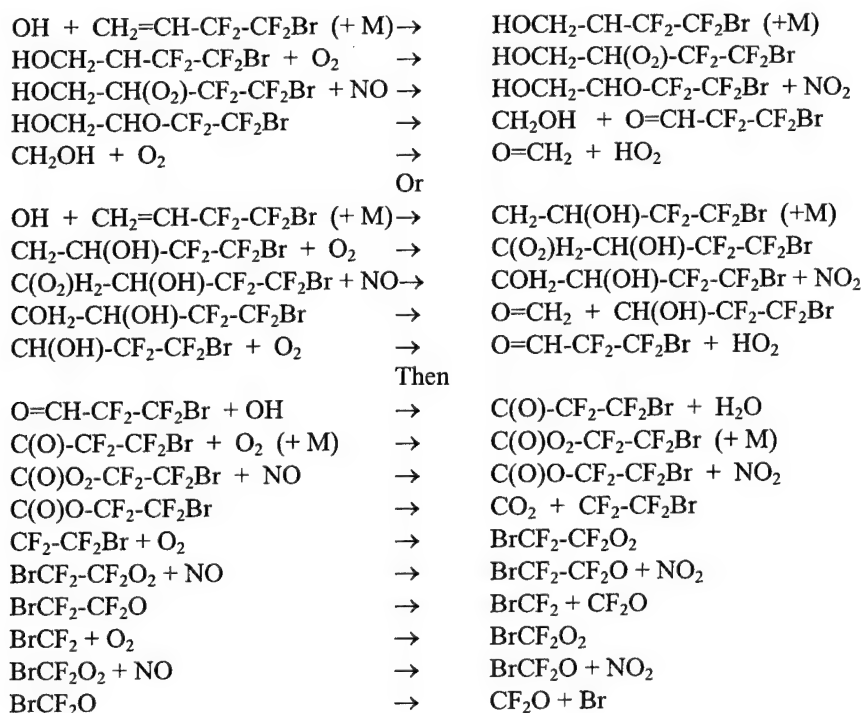
Molecule	$A \times 10^{12}$, $\text{cm}^3 \text{molecule}^{-1} \text{s}^{-1}$	E/R K	$k(298) \times 10^{14}$ $\text{cm}^3 \text{molecule}^{-1} \text{s}^{-1}$	Atmospheric lifetime, years	ODP
CH ₃ Br	5.4	1610	2.4	2.5	1.2
CHF ₂ Br	1.5	1550	1.0	6.0	1.6
CH ₂ FBr	3.8	1440	3.0	1.9	0.59
CH ₂ ClBr	2.2	945	9.2	0.52	0.23
CHFCIBr	2.2	920	6.8	0.70	0.27
CH ₂ Br ₂	2.5	995	8.9	0.55	0.43
CHFBBr ₂	1.6	825	10.0	0.46	0.30
CHCl ₂ Br	0.8	330	26.4	0.15	0.047
CHClBr ₂	0.8	250	34.6	0.11	0.08

An interesting observation is that whereas more heavily substituted methanes have lower pre-exponential factors, this is more than made up in their lower values of E/R . Thus, the predicted lifetimes decrease from 2.5 years for CH₃Br to 0.11 years for CHClBr₂, with the calculated ODP values decreasing from 1.2 to 0.08. In our comparison between experimental and computational results, we found that the rate constants for the faster reactions seemed to be somewhat overestimated. Thus, we would expect that the actual rate constants for the faster reactions ($k_{298} > 10^{-13} \text{ cm}^3 \text{ molec}^{-1} \text{ s}^{-1}$) to be somewhat lower and the lifetimes and ODPs larger.

Fate of the Bromine: General mechanisms for atmospheric degradation of fluorinated Br containing alkenes has been developed based on the analysis of available kinetic data. When bromine is substituted on an olefinic carbon, the scheme below suggests that it is ejected early in the reaction.



When bromine resides on a carbon removed from the double bond, the mechanism is somewhat more complex, as illustrated below for decomposition of $\text{CH}_2=\text{CH-CF}_2\text{-CF}_2\text{Br}$:



References

- [1] Orkin, V. L.; Huie, R. E.; Kurylo, M. J. *J. Phys. Chem.* **1996**, *100*, 8907-8912.
- [2] (a) Schlegel, H. B. *J. Chem. Phys.* **1986**, *84*, 4530. (b) Schlegel, H. B. *J. Phys. Chem.* **1988**, *92*, 3075 (c) Sosa, C.; Schlegel, H. B. *Int. J. Quantum Chem.* **1986**, *29*, 1001. (d) Sosa, C.; Schlegel, H. B. *Int. J. Quantum Chem.* **1987**, *30*, 155.
- [3] (a) Johnston, H. S. *Gas Phase Reaction Rate Theory*; The Roland Press Company: New York, 1966. (b) Laidler, K.J. *Theories of Chemical Reaction Rates*, McGraw-Hill: New York, 1969. (c) Weston, R.E.; Schwartz, H.A. *Chemical Kinetics*, Prentice-Hall: New York, 1972. (d) Rapp, D. *Statistical Mechanics*, Holt, Reinhard, and Winston: New York, 1972. (e) Nikitin, E.E. *Theory of Elementary Atomic and Molecular Processes in Gases*, Claredon Press: Oxford, 1974. (f) Smith, I.W.M. *Kinetics and Dynamics of Elementary Gas Reactions*, Butterworths: London, 1980. (g) Steinfeld, J.I.; Francisco, J.S.; Hase, W.L. *Chemical Kinetics and Dynamics*, Prentice-Hall: New Jersey, 1989.
- [4] Wigner, E.P. *Z.Phys.Chem.* **1932**, *B19*, 203.
- [5] Rate constants calculated with the Turbo-Rate module in the beta version of the TURBO-OPT geometry optimization package, developed by C. Gonzalez and Tom Allison, National Institute of Standards and Technology, Gaithersburg, MD.
- [6] *Scientific Assessment of Ozone Depletion: 1998*, Global Ozone Research and Monitoring Project, Report No. 44; World Meteorological Organization: Geneva, Switzerland, 1999.
- [7] (a) Louis, F.; Gonzalez, C.A.; Huie, R. E.; Kurylo, M. J. *J. Phys. Chem. A* **2000**, *104*, 2931. (b) Louis, F.; Gonzalez, C.A.; Huie, R. E.; Kurylo, M. J. *J. Phys. Chem. A* **2000**, *104*, 8773.
- [8] Louis, F.; Gonzalez, C.A.; Huie, R. E.; Kurylo, M. J. *J. Phys. Chem. A* **2001**, *105*, 1599.

Photochemistry of Bromine-Containing Fluorinated Alkenes: Reactivity toward OH and UV Spectra

Vladimir L. Orkin,* Florent Louis,[#] Robert E. Huie, and Michael J. Kurylo

Physical and Chemical Properties Division, National Institute of Standards and Technology,
Gaithersburg, Maryland 20899

Received: December 5, 2001; In Final Form: July 30, 2002

The rate constants for the reactions of OH radicals with the fluorinated alkenes containing one Br atom ($\text{CFBr}=\text{CF}_2$, $\text{CHBr}=\text{CF}_2$, $\text{CH}_2=\text{CBr}-\text{CF}_3$, $\text{CH}_2=\text{CBr}-\text{CF}_2-\text{CF}_3$, and $\text{CH}_2=\text{CH}-\text{CF}_2-\text{CF}_2\text{Br}$), as well as $\text{CF}_2=\text{CF}_2$, were measured using the flash photolysis resonance fluorescence technique over the temperature range 250–370 K to give the following Arrhenius expressions: $k_{\text{C}_2\text{F}_3\text{Br}}(T) = (2.02^{+0.13}_{-0.12}) \times 10^{-12} \exp\{(396 \pm 18)/T\} \text{ cm}^3 \text{ molecule}^{-1} \text{ s}^{-1}$; $k_{\text{C}_2\text{HF}_2\text{Br}}(T) = (1.30^{+0.22}_{-0.18}) \times 10^{-12} \exp\{(370 \pm 47)/T\} \text{ cm}^3 \text{ molecule}^{-1} \text{ s}^{-1}$; $k_{\text{C}_3\text{H}_2\text{F}_3\text{Br}}(T) = (1.36^{+0.17}_{-0.14}) \times 10^{-12} \exp\{(317 \pm 34)/T\} \text{ cm}^3 \text{ molecule}^{-1} \text{ s}^{-1}$; $k_{\text{C}_4\text{H}_2\text{F}_3\text{Br}}(T) = (0.98^{+0.35}_{-0.26}) \times 10^{-12} \exp\{(369 \pm 90)/T\} \text{ cm}^3 \text{ molecule}^{-1} \text{ s}^{-1}$; $k_{\text{C}_4\text{H}_3\text{F}_4\text{Br}}(T) = (0.85^{+0.15}_{-0.12}) \times 10^{-12} \exp\{(201 \pm 46)/T\} \text{ cm}^3 \text{ molecule}^{-1} \text{ s}^{-1}$; $k_{\text{C}_2\text{F}_4}(T) = (3.39^{+0.22}_{-0.12}) \times 10^{-12} \exp\{(323 \pm 11)/T\} \text{ cm}^3 \text{ molecule}^{-1} \text{ s}^{-1}$. Ultraviolet absorption spectra of these brominated fluoroalkanes and bromoethene were measured between 164 and 276 nm. On the basis of these results, the atmospheric lifetimes were estimated to be 1.4, 2.4, 2.8, 3.2, 7.0, and 1.1 days, respectively. The general pattern of haloalkene reactivity toward OH is discussed.

Introduction

Despite their excellence as fire suppressants, the production of bromofluorocarbons (Halons) is being phased out because of the danger they pose to the Earth's stratospheric ozone layer. A number of nonbrominated substances have been proposed and tested, but the effort to find replacements continues to return to bromine-containing compounds because of the properties of bromine as a chemically active flame suppressant. One class of suppressants currently under consideration is the family of bromofluoroalkenes.¹ The presence of a carbon–carbon double bond is expected to render these substances highly reactive toward the hydroxyl radical, OH, resulting in an extremely short tropospheric lifetime, thereby limiting their delivery of bromine to the stratosphere where it can participate in ozone-destroying catalytic reactions. To quantify their atmospheric lifetimes, we have investigated the reactivity toward OH of five singly brominated fluoroalkenes, chosen to represent a variety of possible relative placements of bromine, fluorine, and hydrogen in relation to the double bond: $\text{CFBr}=\text{CF}_2$, $\text{CHBr}=\text{CF}_2$, $\text{CH}_2=\text{CBr}-\text{CF}_3$, $\text{CH}_2=\text{CBr}-\text{CF}_2-\text{CF}_3$, and $\text{CH}_2=\text{CH}-\text{CF}_2-\text{CF}_2\text{Br}$. Rate constants were measured over the temperature range 250 to 370 K. We also investigated the reactivity of $\text{CF}_2=\text{CF}_2$ toward OH over this temperature range. In addition, we have measured the ultraviolet absorption spectra of all of these compounds and bromoethene, $\text{CHBr}=\text{CH}_2$ down to 164 nm.

Experimental Section

Detailed descriptions of the apparatuses and the experimental methods used to measure the rate constants for the reactions of

the various fluorinated alkenes with OH and the alkene absorption spectra are given in previous papers.^{2–4} Therefore, only brief descriptions are given here.²³

OH Reaction Rate Constant Measurements. The principal component of the flash photolysis–resonance fluorescence (FPRF) apparatus is a Pyrex reactor (of approximately 50 cm³ internal volume) thermostated with water or ethanol circulated through its outer jacket. Reactions were studied in argon carrier gas (99.9995% purity) at a total pressure of 13.33 kPa (100.0 Torr). Flows of dry argon, argon bubbled through water thermostated at 276 K, and fluoroalkene mixtures (containing 0.01%–0.1% of the reactant diluted with argon) were premixed and flowed through the reactor at a total flow rate between 0.6 and 1.4 cm³ s^{−1}, STP. The concentrations of the gases in the reactor were determined by measuring the mass flow rates and the total pressure with a MKS Baratron manometer. Flow rates of argon, the H₂O/argon mixture, and reactant/inert gas mixtures were measured by calibrated Tylan mass flow meters. Hydroxyl radicals were produced by the pulsed photolysis (1–4 Hz repetition rate) of H₂O (introduced via the 276 K argon/H₂O bubbler) by a xenon flash lamp focused into the reactor. The radicals were then monitored by their resonance fluorescence near 308 nm, excited by a microwave-discharge resonance lamp (330 Pa or 2.5 Torr of a ca. 2% mixture of H₂O in UHP helium) focused into the reactor center. The resonance fluorescence signal was recorded on a computer-based multichannel scanner (channel width 100 μs) as a summation of 1000–5000 consecutive flashes. The radical decay signal at each reactant concentration was analyzed as described by Orkin et al.³ to obtain the first-order decay rate coefficient due to the reaction under study. At each temperature, the rate constant was determined from the slope of the decay rate versus haloalkene concentration plot using at least seven different concentrations.

All samples, except tetrafluoroethene, were used as supplied after several freeze/pump/thaw cycles. Bromoethene (CHBrCH_2 ,

* To whom correspondence should be addressed. Also associated with the Institute of Energy Problems of Chemical Physics, Russian Academy of Sciences, Moscow 117829, Russia.

[#] Present address: Laboratoire de Physicochimie des Processus de Combustion, UMR CNRS 8522, Université des Sciences et Technologies de Lille, 59655 Villeneuve d'Ascq Cedex, France.

TABLE 1: Rate Constants Measured for the Reactions of OH with Haloalkenes

<i>T</i> , K	<i>k</i> (<i>T</i>), ^a 10 ⁻¹² cm ³ molecule ⁻¹ s ⁻¹ (haloalkene concentration range, 10 ¹³ molecule/cm ³)					
	CF ₂ =CF ₂	CFBr=CF ₂	CHBr=CF ₂	CH ₂ =CBr-CF ₃	CH ₂ =CBr-CF ₂ -CF ₃	CH ₂ =CH-CF ₂ -CF ₂ Br
250	12.3 ± 0.20 (0.39–2.96)	9.79 ± 0.22 (0.39–2.96)	5.79 ± 0.15 (0.77–6.60)	4.87 ± 0.08 (0.78–4.52)	4.23 ± 0.10 (1.56–5.40)	1.92 ± 0.06 (3.12–15.2)
272		8.67 ± 0.21 (0.36–2.72)	5.05 ± 0.10 (1.43–5.44)	4.33 ± 0.15 (1.43–5.44)	3.87 ± 0.10 (0.35–4.48)	
298	10.0 ± 0.15 (0.65–2.48)	7.59 ± 0.15 (0.33–3.05)	4.43 ± 0.08 (0.65–6.09)	3.88 ± 0.15 (1.31–7.59)	3.51 ± 0.07 (0.66–5.23)	1.65 ± 0.04 (2.62–21.9)
330		6.63 ± 0.13 (0.59–2.51)	4.06 ± 0.05 (1.19–5.52)	3.55 ± 0.10 (0.59–5.50)	2.92 ± 0.06 (3.36–11.0)	
370	8.09 ± 0.10 (0.26–2.45)	5.89 ± 0.37 (0.26–1.53)	3.55 ± 0.05 (1.06–4.92)	3.22 ± 0.08 (2.11–9.82)	2.68 ± 0.08 (2.11–9.82)	1.48 ± 0.03 (2.63–17.7)

^a Uncertainties represent statistical levels of confidence of 95% and do not include an estimated uncertainty of 4% associated with possible systematic errors.

99.5% purity, Matheson Gas Products). 1-bromo-2,2-difluoroethene (CHBrCF₂, 99.5+% purity, Ozone, St. Petersburg, Russia), and bromotrifluoroethene (CFBrCF₂, 99.5+% purity, Ozone, St. Petersburg, Russia) were used without any further purification. Tetrafluoroethene (CF₂CF₂, Union Carbide Corp.) was ca. 98% purity stabilized with ca. 1% of α -pinene with hexafluorocyclopropane (1%) and CO₂ (0.2%) as the main impurities. 2-Bromo-3,3,3-trifluoropropene (CH₂CBrCF₃) and 2-bromo-3,3,4,4-pentafluoro-1-butene (CH₂CBrCF₂CF₃) were at least 98% purity with corresponding bromine-free fluorinated alkenes as the main impurities (SynQuest Labs., Inc.). They could also contain corresponding 1-bromoalkenes and 1,2-dibromoalkanes as minor impurities. 4-Bromo-3,3,4,4-tetrafluoro-1-butene (CH₂CHCF₂CF₂Br, SynQuest Labs., Inc.) was at least 98% purity with CH₂CHCF₂CF₂Cl and 2-methoxyethanol (CH₃-O-CH₂-CH₂OH) as possible impurities. The presence of the above-mentioned halogenated hydrocarbon impurities could not result in a noticeable overestimation of the measured rate constant because they are less reactive than the target compound. There are two impurities that cause concern: α -pinene and CH₃-O-CH₂-CH₂OH. Their OH reaction rate constants at room temperature are ca. 6×10^{-11} and 1.1×10^{-11} cm³ molecule⁻¹ s⁻¹, respectively,⁵ and exceed the measured reaction rate constants of the target compounds, C₂F₄ and CH₂-CHCF₂CF₂Br. A sample of CF₂CF₂ was purified by passing through a -100 °C cold trap to decrease the α -pinene concentration from ca. 1% to below 0.03% (determined by UV absorption analysis near 220 nm). GC analysis of a CH₂CHCF₂-CF₂Br sample for the presence of 2-methoxyethanol indicated less than ca. 0.1% of this impurity. Thus, these impurity levels are low enough to result in no noticeable overestimation of the measured rate constants (less than 0.2% and 1% for C₂F₄ and CH₂CHCF₂CF₂Br, respectively).

UV Absorption Cross Section Measurements. The absorption spectra of the bromofluoroalkenes were measured over the wavelength range of 160–280 nm using a single beam apparatus consisting of a 1-m vacuum monochromator equipped with a 600 lines/mm grating. The radiation source was a Hamamatsu L1385 deuterium lamp, and the detector was a Hamamatsu R166 photomultiplier. Spectra were recorded at increments of 0.5 nm at a spectral slit width of 0.5 nm. The pressure inside the 16.9 ± 0.05 cm absorption cell was measured by a MKS Baratron manometer at *T* = 295 ± 1 K. Absorption spectra of the evacuated cell and of the cell filled with a gas sample were alternately recorded several times, and the absorption cross sections at the wavelength λ were calculated as

$$\sigma(\lambda) = \frac{\ln\{I_0(\lambda)/I_{[HA]}(\lambda)\}}{[HA]L}$$

where [HA] is the concentration of haloalkene in the absorption cell with the optical path length *L*. *I*₀(λ) and *I*_[HA](λ) are the radiation intensities measured after the absorption cell when the haloalkene concentration was zero and [HA], respectively. The complete spectrum of each compound was constructed from data taken over several overlapping wavelength ranges. Data over each spectral range were obtained at several pressures to verify adherence to the Beer–Lambert absorption law. The coincidence of the contiguous parts of spectra taken over overlapping wavelength ranges was usually better than ca. 1%. The overall instrumental error associated with uncertainties in the path length, pressure, temperature stability, and measured absorbance was estimated to be less than 2% over most of the wavelength range, increasing to ca. 10%–20% at the long-wavelength ends of the spectra because of increased uncertainty in measuring low absorbance values. Different manometrically prepared mixtures containing 2%, 10%, and 100% of haloalkenes were used at total pressures in the cell ranging from 4 Pa to 120 kPa (0.03–900 Torr). There was no difference in the absorption cross sections obtained with different mixtures, and their use allowed a wider dynamic range in absorption measurements.

Results and Discussion

Kinetics. Rate constants measured for the reactions of hydroxyl radicals with the five bromofluoroalkenes and CF₂=CF₂ at different temperatures are listed in Table 1. The data are presented graphically in Figure 1, and the derived Arrhenius parameters are listed in Table 2, along with available data from the literature. To the best of our knowledge, there are no other results available on the reactivity of the bromofluoroalkenes studied in the present work. The CF₂=CF₂ reaction was studied at room temperature in two previous investigations^{6,7} (see Table 2). A previous measurement from our laboratory⁶ coincides with the present result. Acerboni et al.⁷ measured the reaction by a relative rate technique with two different reference reactions. While their reported average value of the rate constant exceeds the present results, the quoted uncertainty is much larger than the disagreement.

The effect of fluorination on alkene reactivity is quite complicated. Nevertheless, one can speculate on the correlation between reactivity and structure of these halogenated alkenes. The room-temperature rate constants for the reactions of these and some other bromine/fluorine-substituted alkenes with the hydroxyl radical are listed in Table 3. Asymmetric fluorination of the olefinic carbon atom tends to lessen reactivity, whereas

TABLE 2: Arrhenius Parameters for OH Reactions of Br-Containing Fluoroalkenes and Their Estimated Atmospheric Lifetimes^a

molecule	$A \times 10^{12}$, $\text{cm}^3 \text{ molecule}^{-1} \text{ s}^{-1}$	$E/R \pm \Delta E/R$, K	$k(298) \times 10^{12}$ $\text{cm}^3 \text{ molecule}^{-1} \text{ s}^{-1}$	atmospheric lifetime, days ^b
$\text{CF}_2=\text{CF}_2$	3.39 ± 0.22	-323 ± 11	9.98 ± 0.15 10.2 ± 0.5^6 11.3 ± 3.3^7	1.1
$\text{CFBr}=\text{CF}_2$	2.02 ± 0.12	-396 ± 18	7.62 ± 0.15	1.4
$\text{CHBr}=\text{CF}_2$	$1.30^{+0.22}_{-0.18}$	-370 ± 47	4.53 ± 0.10	2.4
$\text{CH}_2=\text{CBr}-\text{CF}_3$	$1.36^{+0.17}_{-0.14}$	-317 ± 34	3.94 ± 0.15	2.8
$\text{CH}_2=\text{CBr}-\text{CF}_2-\text{CF}_3$	$0.98^{+0.35}_{-0.26}$	-369 ± 90	3.39 ± 0.14	3.2
$\text{CH}_2=\text{CH}-\text{CF}_2-\text{CF}_2\text{Br}$	$0.85^{+0.15}_{-0.12}$	-201 ± 46	1.68 ± 0.05	7.0

^a Uncertainties represent statistical levels of confidence of 95% and do not include estimated systematic errors. ^b Atmospheric lifetimes were estimated in the manner typically used for long-lived compounds. Such estimations assume a uniform tropospheric distribution that is not correct for short-lived compounds.

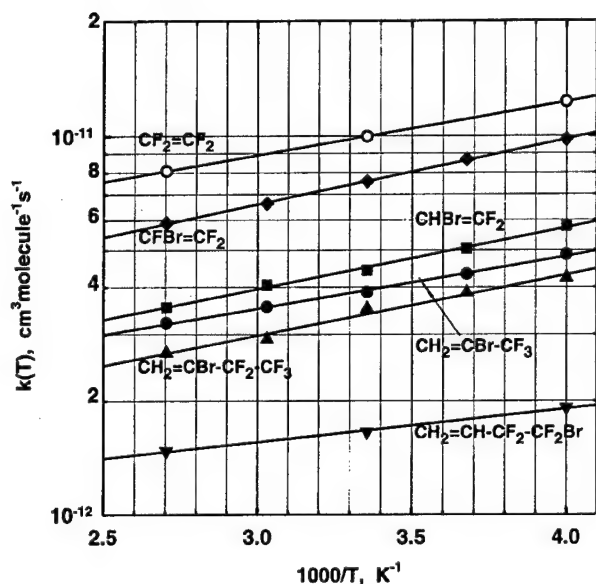


Figure 1. Arrhenius plot showing the average rate constants for the reactions of OH with halogenated alkenes obtained at each temperature. The solid lines are the least-squares fits to the data points with the Arrhenius parameters presented in Table 2.

TABLE 3: Hydroxyl Radical Reactivity toward Haloalkenes

molecule	$k(298) \times 10^{12}$, $\text{cm}^3 \text{ molecule}^{-1} \text{ s}^{-1}$	ref
$\text{CH}_2=\text{CH}_2$	9.0	20
$\text{CH}_2=\text{CHF}$	5.5	21
$\text{CH}_2=\text{CF}_2$	2.0	22
$\text{CF}_2=\text{CF}_2$	10.	this work
$\text{CHBr}=\text{CH}_2$	7.0	21
$\text{CFBr}=\text{CF}_2$	7.6	this work
$\text{CHBr}=\text{CF}_2$	4.5	this work
$\text{CH}_2=\text{CH}-\text{CH}_3$	30.	20
$\text{CH}_2=\text{CH}-\text{CF}_3$	1.5	6
$\text{CH}_2=\text{CF}-\text{CF}_3$	1.1	6
$\text{CF}_2=\text{CF}-\text{CF}_3$	2.2	6
$\text{CH}_2=\text{CBr}-\text{CF}_3$	3.9	this work
$\text{CH}_2=\text{CBr}-\text{CF}_2-\text{CF}_3$	3.4	this work
$\text{CH}_2=\text{CH}-\text{CF}_2-\text{CF}_2\text{Br}$	1.7	this work

further fluorination (yielding more symmetric substitution) compensates for the original deactivation. This can be seen from the reactivities of CH_2CH_2 , CH_2CF_2 , CHFCH_2 , and CF_2CF_2 . This suggests that the alkene reactivity toward OH depends mainly on the geometrical localization of π -electron density. The π -electron localization in the center of the $\text{C}=\text{C}$ bond ($\text{CH}_2=\text{CH}_2$, $\text{CF}_2=\text{CF}_2$) promotes the OH addition reaction,

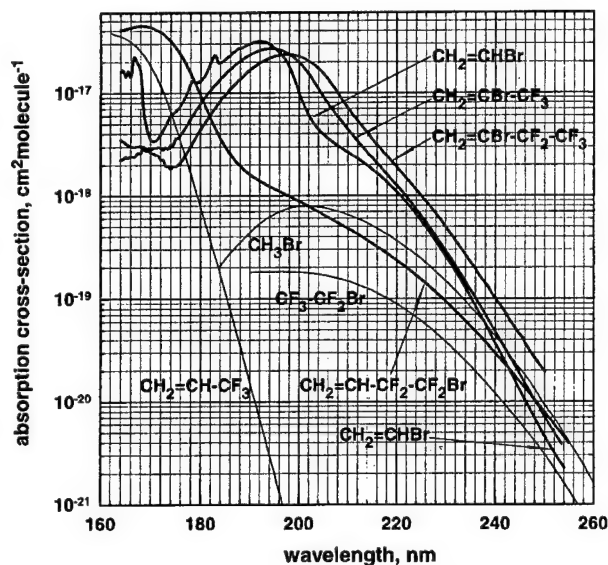


Figure 2. Ultraviolet absorption spectra of several $\text{CH}_2=\text{CBr}-$ containing haloalkenes and $\text{CH}_2=\text{CH}-\text{CF}_2-\text{CF}_2\text{Br}$ at $T = 295 \text{ K}$. Absorption spectra of CH_3Br ,⁸ $\text{CF}_3-\text{CF}_2\text{Br}$,⁹ and $\text{CH}_2=\text{CH}-\text{CF}_3$ ⁶ are shown for comparison purposes.

while the shift of the electron density toward the carbon atom (due to the high electron affinity of the F atom) obstructs it. It is interesting that the $-\text{CF}_3$ group adjacent to the double bond causes an even more pronounced deactivating effect than the F-atom despite the smaller electron affinity of $-\text{CF}_3$ and longer distance from a $\text{C}=\text{C}$ double bond. This suggests the importance of a geometrical factor, as well as the electron affinity of the substitute, on the delocalization of π -electrons.

Bromination of the olefinic carbon located between the double bond and a fluorinated alkyl group increases the reactivity of fluorinated $\text{C}_{n \geq 3}$ alkenes, while Br on a remote carbon has essentially no effect. This suggests that the large electron rich Br atom shields the deactivating adjacent $-\text{CF}_3$ ($-\text{C}_2\text{F}_5$) group.

Ultraviolet Spectra. The ultraviolet absorption spectra of the halogenated alkenes obtained in this work are presented in Figures 2 and 3. The spectral data are provided in the Supporting Information and at www.nist.gov/kinetics/spectra/index.htm. These UV spectra reflect the interaction between π -electrons of the $\text{C}=\text{C}$ double bond and the electrons of the bromine atom. The $\text{CH}_2=\text{CBr}-$ group has a very strong absorption with a maximum at 190–200 nm (see spectra for CH_2CHBr , $\text{CH}_2\text{-CBrCF}_3$, and $\text{CH}_2\text{CBrCF}_2\text{CF}_3$), which suppresses the distinctive shorter wavelength absorption of $\text{CH}_2=\text{CH}-$ group (see spectrum for CH_2CHCF_3 in Figure 2). The absorption in the

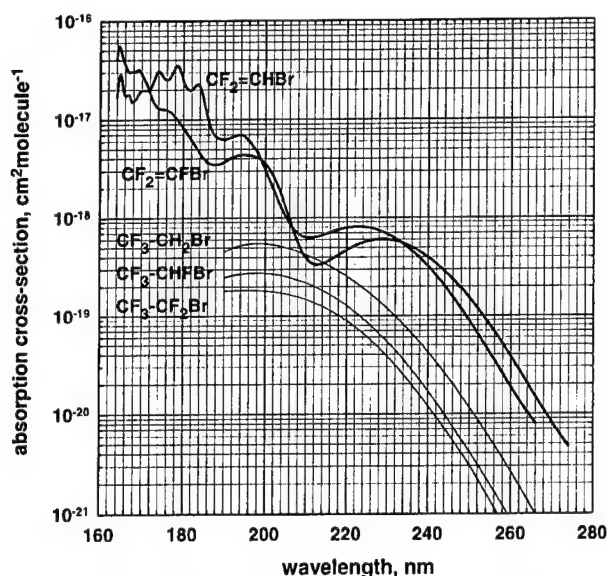


Figure 3. Ultraviolet absorption spectra of $\text{CF}_2=\text{CFBr}$ and $\text{CF}_2=\text{CHBr}$ at $T = 295$ K. Absorption spectra of bromofluoroalkanes^{9,10} are shown for comparison purposes.

maximum is about 1.5 orders of magnitude higher than that of a bromoalkane such as CH_3Br ⁸ and is the strongest absorption exhibited by any brominated hydrocarbon in the region of the stratospheric transparency window near 200 nm. In contrast, the spectrum of $\text{CH}_2=\text{CH}-\text{CF}_2-\text{CF}_2\text{Br}$ appears to be a superposition of absorption by a fluoroalkene⁶ (such as $\text{CH}_2=\text{CHCF}_3$) and a bromofluoroalkane (such as $\text{CF}_3\text{CF}_2\text{Br}$). The absorption spectra of Br-containing fluorinated ethenes ($\text{CHBr}=\text{CF}_2$ and $\text{CFBr}=\text{CF}_2$) are presented in Figure 3. In contrast with the $\text{CH}_2=\text{CBr}-$ group, they exhibit a less-pronounced absorption at 190–200 nm while showing much stronger absorption at the shorter wavelengths. Their longest wavelength absorption bands are of slightly higher intensity than those of bromofluoroethanes^{9,10} and are about 20–30 nm red-shifted (see Figure 3).

Atmospheric Implications. The atmospheric lifetimes of the alkenes under study can be estimated on the basis of the photochemical properties obtained in the present work. All of the compounds are very reactive toward OH, while their absorption cross sections for tropospheric UV radiation (above 290 nm) are negligible. Therefore, the reactions with hydroxyl radicals in the troposphere dictate their atmospheric lifetimes. A simple scaling procedure has proven to be valid for relatively long-lived compounds that are well-mixed throughout the troposphere. For such chemicals, lifetimes can be estimated using the equation¹¹

$$\tau_i^{\text{OH}} = \frac{k_{\text{MC}}(270)}{k_i(270)} \tau_{\text{MC}}^{\text{OH}}$$

where τ_i^{OH} and $\tau_{\text{MC}}^{\text{OH}}$ are the atmospheric lifetimes of the compound of interest and methyl chloroform (MC), respectively, due to reactions with hydroxyl radicals in the troposphere only and $k_i(270)$ and $k_{\text{MC}}(270) = 5.78 \times 10^{-15} \text{ cm}^3 \text{ molecule}^{-1} \text{ s}^{-1}$ (ref 8) are the rate constants for the reactions of OH with these substances at $T = 270$ K. The value of $\tau_{\text{MC}}^{\text{OH}}$ was obtained following the procedure used by Prinn et al.¹² from the measured lifetime of MC, $\tau_{\text{MC}} = 4.8$ years, when an ocean loss of 85 years and a stratospheric loss of 37 years are taken into account. Applying this method to the alkenes of this study yields the

estimated atmospheric lifetimes listed in Table 2. As can be seen, the lifetimes derived here are very short, much shorter than the characteristic time of mixing processes in the troposphere, and hence are only crude estimates. The correct residence time of the compounds in the atmosphere will depend on the emission location and season, as well as local atmospheric conditions. Nevertheless, these estimations give a useful scaling among these alkenes and demonstrate that they are extremely short-lived in the atmosphere.

Note that these calculated lifetimes reflect the globally averaged sink for a compound due to its reaction with OH in the troposphere and, therefore, lie between the shortest local lifetimes in the tropical region and longest ones at high latitudes. Such lifetimes have clear physical meaning for long-lived chemicals that are well mixed in the troposphere following their emission. Such lifetimes can be used for quantitative analysis of chemical concentrations in the atmosphere. In the case of short-lived compounds, these calculated parameters should lie between the atmospheric lifetimes in the tropical and high latitude areas. Calculation of the entire range of real atmospheric lifetimes requires detailed 3-D modeling. In two recent papers, 3-D modeling was performed to study the atmospheric fate of 1-bromopropane, a short-lived compound with an estimated lifetime of 14.4 days using the above-mentioned scaling procedure. The detailed calculations resulted in lifetime ranges of 8–24 days¹³ and 9–19.5 days¹⁴ with the shorter values corresponding to tropical emission and the longer ones to emission at higher latitudes.

Using these rough lifetime estimates together with the measured UV absorption spectra, one can calculate approximate ozone depletion potentials (ODPs) for these chemicals. On the basis of an ODP for CF_3Br of 13 and a lifetime of 65 years,¹⁵ ODP values considerably smaller than 0.01 are obtained for the bromofluoroalkenes studied. The determination of the correct ODP values requires 3D modeling calculations that consider local emission conditions. Moreover, based on the shortness of the lifetimes of the alkenes themselves, correct ODP values must take into account the lifetimes of any bromine-containing products resulting from the tropospheric oxidation of the alkenes. Therefore, it is important to estimate the total lifetime of Br atoms in the form of volatile degradation products produced in the oxidation processes initiated by the reactions of OH with Br-containing fluoroalkenes.

We can speculate on a possible degradation mechanism for Br-containing fluorinated alkenes in the atmosphere. It is worthwhile to point out that the production of a relatively long-lived bromine-containing degradation product is not likely for a compound with a brominated olefinic carbon (i.e., all of the bromoalkenes studied in the present work, except $\text{CH}_2=\text{CH}-\text{CF}_2-\text{CF}_2\text{Br}$). Because of the relatively weak C–Br bond, the Br atom can be quickly ejected to form either a carbonyl ($\text{C}=\text{O}$) or a hydroxyalkene ($\text{C}=\text{C}-\text{OH}$), depending on which olefinic carbon acquired OH in the initial addition reaction. Note that analogous processes are known in the oxidation of chlorinated compounds. Thus, $\text{C}=\text{O}$ formation and Cl atom release are a part of kinetic scheme for the decomposition of hydrochlorofluoroalkanes (HCFCs) in the atmosphere.¹⁶ Along similar lines, the release of Cl atom following the reaction of OH with *trans*-1,2-dichloroethene ($\text{CHCl}=\text{CHCl}$) has been directly observed.¹⁷ In accordance with the kinetic scheme shown in Figure 4, the Br atom will probably be released immediately after the initial reaction between OH and brominated alkene in the lower troposphere (probably within minutes in the case of the $\text{C}=\text{O}$ formation channel). Furthermore,

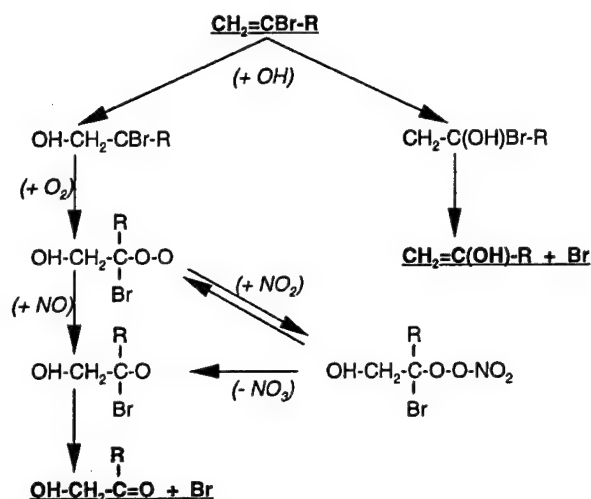


Figure 4. Kinetic scheme for the degradation of bromoalkenes of the form $\text{C}=\text{C}-\text{Br}$ in the atmosphere.

haloalkylperoxynitrate formation cannot significantly increase the lifetime of bound bromine and therefore its transport to the stratosphere because of the short lifetime of such compounds due to thermal decomposition.^{18,19}

Acknowledgment. This work was supported by the Upper Atmosphere Research Program of the National Aeronautics and Space Administration and by the Next Generation Fire Suppression Technology Program, funded by the Department of Defense Strategic Environmental Research and Development Program under MIPR Number W74RDV73243630.

Supporting Information Available: The ultraviolet absorption cross sections of halogenated alkenes are presented in Table 4. This material is available free of charge via the Internet at <http://pubs.acs.org>.

References and Notes

- (1) *Proceedings, Halon Options Technical Working Conference*; University of New Mexico: Albuquerque, NM, May 2–4, 2000.
- (2) Kurylo, M. J.; Cornett, K. D.; Murphy, J. L. *J. Geophys. Res.* **1982**, *87*, 3081–3085.
- (3) Orkin, V. L.; Huie, R. E.; Kurylo, M. J. *J. Phys. Chem.* **1996**, *100*, 8907–8912.

- (4) Orkin, V. L.; Khamaganov, V. G.; Guschin, A. G.; Huie, R. E.; Kurylo, M. J. *J. Phys. Chem.* **1997**, *101*, 174–178.
- (5) Mallard, W. G.; Westley, F.; Herron, J. T.; Hampson, R. F.; Frizzel, D. H. *NIST Chemical Kinetics Database*, version 6.0; NIST: Gaithersburg, MD, updated 1997.
- (6) Orkin, V. L.; Huie, R. E.; Kurylo, M. J. *J. Phys. Chem. A* **1997**, *101*, 9118–9124.
- (7) Acerboni, G.; Jensen, N. R.; Rindone, B.; Hjorth, J. *Chem. Phys. Lett.* **1999**, *309*, 364–368.
- (8) DeMore, W. B.; Sander, S. P.; Golden, D. M.; Hampson, R. F.; Kurylo, M. J.; Howard, C. J.; Ravishankara, A. R.; Kolb, C. E.; Molina, M. J. *Chemical Kinetics and Photochemical Data for Use in Stratospheric Modeling*, Evaluation No. 12; JPL Publication 97-4; Jet Propulsion Laboratory, California Institute of Technology: Pasadena, CA, 1997.
- (9) Molina, L. T.; Molina, M. J.; Rowland, F. S. *J. Phys. Chem.* **1982**, *86*, 2672–2676.
- (10) Orkin, V. L.; Kasimovskaya, E. E. *J. Atmos. Chem.* **1995**, *21*, 1–11.
- (11) Spivakovsky, C. M.; Logan, J. A.; Montzka, S. A.; Balkanski, Y. J.; Foreman-Fowler, M.; Jones, D. B. A.; Horowitz, L. W.; Fusco, A. C.; Brenninkmeijer, C. A. M.; Prather, M. J.; Wofsy, S. C.; McElroy, M. B. *J. Geophys. Res.* **2000**, *105*, 8931–8980.
- (12) Prinn, R. G.; Weiss, R. F.; Miller, B. R.; Huang, A.; Alyea, F. N.; Cunnold, D. M.; Fraser, P. J.; Hartley, D. E.; Simmonds, P. G. *Science* **1995**, *269*, 187–192.
- (13) Bridgeman, C. H.; Pyle, J. A.; Shallcross, D. E. *J. Geophys. Res.* **2000**, *105* (D21), 26493–26502.
- (14) Wuebbles, D. J.; Patten, K. O.; Johnson, M. T.; Kotamarthi, R. J. *Geophys. Res.* **2001**, *106* (D13), 14551–14571.
- (15) *Scientific Assessment of Ozone Depletion: 1998*; Global Ozone Research and Monitoring Project, Report No. 44; World Meteorological Organization: Geneva, Switzerland, 1999.
- (16) *Scientific Assessment of Ozone Depletion: 1991*; Global Ozone Research and Monitoring Project, Report No. 25; World Meteorological Organization: Geneva, Switzerland, 1991.
- (17) Canosa-Mas, C. E.; Dillon, T. J.; Sidebottom, H.; Thompson, K. C.; Wayne, R. P. *Phys. Chem. Chem. Phys.* **2001**, *3*, 542–550.
- (18) Atkinson, R. Gas-phase tropospheric chemistry of organic compounds. *J. Phys. Chem. Ref. Data Monogr.* **1994**, *2*, 1–216.
- (19) *Scientific Assessment of Ozone Depletion: 1994*; Global Ozone Research and Monitoring Project, Report No. 37; World Meteorological Organization: Geneva, Switzerland, 1995.
- (20) Atkinson, R.; Baulch, D. L.; Cox, R. A.; Hampson, R. F., Jr.; Kerr, J. A.; Rossi, M. J.; Troe, J. *J. Phys. Chem. Ref. Data* **1999**, *28*, 191–393.
- (21) Perry, R. A.; Atkinson, R.; Pitts, J. N., Jr. *J. Chem. Phys.* **1977**, *67*, 458–462.
- (22) Howard, C. J. *J. Chem. Phys.* **1976**, *65*, 4771–4777.
- (23) Certain commercial equipment, instruments, or materials are identified in this article to adequately specify the experimental procedure. Such identification does not imply recognition or endorsement by the National Institute of Standards and Technology, nor does it imply that the material or equipment identified is necessarily the best available for the purpose.

OH Reactivity and UV Spectra of Propane, *n*-Propyl Bromide, and Isopropyl BromideSergey N. Kozlov,[†] Vladimir L. Orkin,^{*,‡} Robert E. Huie, and Michael J. Kurylo

Physical and Chemical Properties Division, National Institute of Standards and Technology, Gaithersburg, Maryland 20899

Received: August 6, 2002; In Final Form: November 12, 2002

The rate constants for the reactions of OH radicals with the 1-bromopropane, 2-bromopropane, and propane were measured using the flash photolysis resonance fluorescence technique over the temperature range between 210 and 480 K. Arrhenius plots exhibit a noticeable curvature, and the rate constants can be represented using a three-parameter modified Arrhenius expression over the temperature range of the experiments with ca. 2% precision. Such a fit also describes the available high-temperature data for propane quite well. The best three-parameter fits to the data are: $k_{\text{C}_3\text{H}_8}(T) = 1.96 \times 10^{-12} \times (T/298)^{1.83} \times \exp\{-167/T\} \text{ cm}^3 \text{ molecule}^{-1} \text{ s}^{-1}$; $k_{\text{nPB}}(T) = 2.99 \times 10^{-13} \times (T/298)^{2.79} \times \exp\{+369/T\} \text{ cm}^3 \text{ molecule}^{-1} \text{ s}^{-1}$; and $k_{\text{iPB}}(T) = 1.66 \times 10^{-13} \times (T/298)^{2.95} \times \exp\{+461/T\} \text{ cm}^3 \text{ molecule}^{-1} \text{ s}^{-1}$. For the low temperature range of atmospheric interest, the reaction rate constants can be accurately presented by standard Arrhenius expressions. Based on the available low-temperature data the following rate constants can be recommended for the purpose of atmospheric modeling: $k_{\text{C}_3\text{H}_8}(T < 300 \text{ K}) = 8.66 \times 10^{-12} \times \exp\{-615/T\} \text{ cm}^3 \text{ molecule}^{-1} \text{ s}^{-1}$; $k_{\text{nPB}}(T < 300 \text{ K}) = 3.03 \times 10^{-12} \times \exp\{-330/T\} \text{ cm}^3 \text{ molecule}^{-1} \text{ s}^{-1}$; $k_{\text{iPB}}(T < 300 \text{ K}) = 1.77 \times 10^{-12} \times \exp\{-260/T\} \text{ cm}^3 \text{ molecule}^{-1} \text{ s}^{-1}$. Atmospheric lifetimes were estimated to be ca. 14, 14, and 19 days for $\text{CH}_3\text{CH}_2\text{CH}_3$, $\text{CH}_2\text{BrCH}_2\text{CH}_3$, and $\text{CH}_3\text{CHBrCH}_3$, respectively. The ultraviolet absorption spectra of these bromopropanes were measured between 164 and 270 nm.

Introduction

Brominated alkanes are the primary source gases for bromine in the stratosphere where bromine participates in the catalytic destruction of ozone. The production of industrial bromine containing halocarbons is consequently being phased out under the provisions of the Montreal Protocol and its Amendments. Nevertheless, a few Br-containing compounds are still in use or are under consideration for use in industrial applications due to their possible environmental acceptability as a result of their extremely short residence times in the atmosphere. One of them, $\text{CH}_2\text{Br}-\text{CH}_2-\text{CH}_3$ (1-bromopropane, *n*-propyl bromide, nPB) is an industrial cleaning solvent. Previous kinetic studies^{1–4} of the reaction of nPB with hydroxyl radicals and atmospheric model calculations^{5–7} indicated its atmospheric lifetime to be as short as 8–34 days. However, the spread among the available kinetic data at room temperature and above was ca. 30%, and the temperature dependence was not well determined. While the present work was in progress, new rate constant measurements and a reaction mechanism study⁸ was conducted that decreased these uncertainties. Taking into account the practical importance of this reaction and the possibility of curvature of the Arrhenius temperature dependence due to different reaction sites available for OH attack, we investigated the reaction of OH + *n*-propyl bromide over a wide temperature range (210–480 K) in order to better assess the temperature dependence of the rate constant.

The rate constants for reactions of OH with $\text{CH}_3-\text{CHBr}-\text{CH}_3$, (2-bromopropane, isopropyl bromide, iPB) and propane ($\text{CH}_3-\text{CH}_2-\text{CH}_3$) were also investigated over the same tem-

perature interval. The isopropyl bromide reaction has been investigated in some of the earlier mentioned studies.^{1,2,4}

The reaction of OH with propane has been intensively studied over the past 35 years⁹ and its value at room temperature is well established. There are also four fairly recent studies at temperatures below 300 K by different research groups using different experimental methods including pulse techniques,^{10,11} a flow technique (high-pressure turbulent flow),¹² and a relative technique.¹³ Thus, this reaction presents a good opportunity to examine measurement accuracy in the determination of OH reaction rate constants for very reactive hydrohalocarbons. Thus, we report the results of our measurements of the OH + propane reaction obtained over a temperature interval that includes low temperatures of atmospheric interest and extends far enough above the room temperature to be compared with the results of higher temperature measurements.

While the reactions with hydroxyl radicals dictate the residence time of bromoalkanes in the atmosphere, their photolysis in the stratosphere also releases Br atoms that trigger the destruction of stratospheric ozone. To complete the photochemical information related to the atmospheric fate of bromopropanes, we have measured their ultraviolet absorption spectra between 164 and 270 nm.

Experimental Section

Detailed descriptions of the apparatus and the experimental methods used to measure the rate constants for the reactions with OH and absorption spectra of the bromopropanes are given in previous papers.^{14–17} Therefore, only brief descriptions are given here.

OH Reaction Rate Constant Measurements. The principal component of the flash photolysis–resonance fluorescence (FPRF) apparatus is a Pyrex reactor (of approximately 50 cm³ internal volume) thermostated with methanol, water, or mineral

* Corresponding author.

[†] Present address: Institute of Chemical Physics, Russian Academy of Sciences, Moscow, 117334, Russia.

[‡] Also associated with the Institute of Energy Problems of Chemical Physics, Russian Academy of Sciences, Moscow, 117829, Russia.

TABLE 1: Molar Concentration of the Main Detected Impurities in Bromopropane Samples^a

compound					
<i>n</i> -propyl bromide			isopropyl bromide		
main impurities	original sample (99%)	after GC purification	main impurities	99.2% sample	99.8+ % sample
propene	0.007%		propene	0.16% ^b	
acetone	0.02%		acetone		0.05%
chloropropane	0.02%		<i>i</i> -propanol	0.20%	0.09%
propanol	0.09%		bromoethane	0.01%	
isopropyl bromide	0.17%	0.01%	di- <i>i</i> -propyl ether	0.021%	0.017%
di- <i>n</i> -propyl ether	0.34%	0.005%	<i>n</i> -propyl bromide	0.04%	0.05%
toluene	0.02%		1,2-dibromopropane	0.1%	0.09%
1-bromopentane	0.04%				
1,2-dibromopropane	0.03%				

^a The italicized values were obtained without direct calibration of GC with the sample of the compound by accepting the sensitivity to closest analogues. ^b The result of analysis of liquid phase. Approximately 5% of propene was detected in the vapor phase of this sample.

oil circulated through its outer jacket. Reactions were studied in argon carrier gas (99.9995% purity) at a total pressure of 4.00 kPa (30.0 Torr). Flows of dry argon, argon bubbled through water thermostated at 276 K, and (bromo)propane mixtures (containing 0.05% or 0.1% of the reactant diluted with argon) were premixed and flowed through the reactor at a total flow rate between 0.3 and 0.6 cm³ s⁻¹, STP. Flow rates of argon, the H₂O/argon mixture, and reactant/inert gas mixtures were measured by Tylan mass flow meters calibrated for each gas mixture. The concentrations of the gases in the reactor were calculated from the flow rates and the total pressure measured with a MKS Baratron manometer.

Uncertainties due to systematic effects in our measurements can be associated with such procedures as the absolute calibration of the MKS Baratron manometer (which measures the pressure in the reaction cell), the calibrations of the three Tylan mass flow meters (argon, argon/water, and reactant mixture flows), and the temperature stability and measurements in the reaction cell. The stated accuracy of the reaction cell manometer (ca. 0.1%) was verified by its absolute calibration. The manometers used to prepare the reactant mixtures were intercalibrated and their linearity was found to be accurate to within ca. 0.2%. All mass flow meters were calibrated by measuring the rate of pressure change in the reaction cell (an additional volume was connected for larger flow rates) isolated from the vacuum pump. These calibrations were usually reproducible within 0.5–1%. The determination of the reactant concentration in the cell only requires relative gas flow rates and one absolute pressure measurement. In addition, we verified the composition of the bromopropane mixtures in the storage bulbs by comparing the measured UV absorption between 166 and 171 nm for the mixture with that for a corresponding amount of pure bromopropane. For example, the absorption of 25 Torr of 0.100% mixture of *n*BP in argon was compared with the absorption of 0.0250 Torr of pure *n*BP. Such comparison revealed no difference within the precision of these absorption measurements (estimated as ca. 0.5%). The uncertainty of the temperature in the reaction cell was around 0.3 K between 250 and 370 K. This increased to about 1 K at the low temperature end and to about 2 K at the high temperature end of the temperature range used in this study due primarily to temperature fluctuations. The relative error that can be introduced by the gas temperature fluctuations is decreased essentially by the opposite temperature dependencies of the reactant concentration and the measured rate constant. To quantify the combined uncertainty associated with our experimental procedure, we added the square root of the sum-of-the-squares of the flow meter calibration uncertainties to the other uncertainties mentioned above. Thus we estimate the expanded uncertainty due to possible instrumental effects to be ca. 4% (95% confidence interval).

Hydroxyl radicals were produced by the pulsed photolysis (1–4 Hz repetition rate) of H₂O (introduced via the 276 K argon/H₂O bubbler) by a xenon flash lamp focused into the reactor. Earlier studies with this apparatus indicated that the initial OH concentration was of the order of 10¹¹ molecule/cm³. The initial concentration was increased by up to a factor of between 4 and 20 by variation in the flash intensity and/or H₂O concentration. The variation in flash intensity and H₂O concentration serves as a diagnostic for kinetic errors associated with the reactions of OH with either primary reaction products or with products from the possible photolysis of the reactant.¹⁶ No statistically significant difference was observed in the rate constants obtained over most of the range of this variation. Differences of up to 5% could be obtained only at the highest concentration of H₂O coupled with the highest flash intensity. Nevertheless, all kinetic experiments were conducted at lowest values of both the flash energy and H₂O concentration.

The OH radicals were monitored by their resonance fluorescence near 308 nm, excited by a microwave-discharge resonance lamp (330 Pa or 2.5 Torr of a ca. 2% mixture of H₂O in UHP helium) focused into the reactor center. The resonance fluorescence signal was recorded on a computer-based multichannel scanner (channel width 100 μs) as a summation of 500 to 5000 consecutive flashes. The resonance fluorescence decay at each reactant concentration was analyzed as described by Orkin et al.¹⁵ to obtain the first-order decay rate coefficient (10 to 350 s⁻¹) due to the reaction under study. At each temperature the rate constant was determined from the slope of a plot of the decay rate versus (bromo) propane concentration. The concentration ranges and number of determinations used at each temperature are given in Table 2.

UV Absorption Cross Section Measurements. The absorption spectra of undiluted bromopropanes and methyl bromide (measured for comparison) were obtained over the wavelength range of 164 nm to 270 nm using a single-beam apparatus consisting of a 1-m vacuum monochromator equipped with a 600 lines/mm grating. The radiation source was a Hamamatsu L1385 deuterium lamp, and the detector was a Hamamatsu R166 photomultiplier. Spectra were recorded at increments of 0.5 nm at a spectral slit width of 0.5 nm. The pressure inside the 16.9 ± 0.05 cm absorption cell was measured by a MKS Baratron manometer at *T* = 295 ± 1 K. Absorption spectra of the evacuated cell and of the cell filled with a gas sample were alternately recorded several times, and the absorption cross sections at the wavelength λ were calculated as

$$\sigma(\lambda) = \frac{\ln\{I_0(\lambda)/I_{[\text{BP}]}(\lambda)\}}{[\text{BP}] \times L}$$

where [BP] is the concentration of bromopropane in the

TABLE 2: Rate Constants Measured in the Present Work for the Reactions of OH with *n*- and *i*-Bromopropane and Propane^a

temp, K	CH ₂ Br-CH ₂ -CH ₃	CH ₃ -CHBr-CH ₃	CH ₃ -CH ₂ -CH ₃
	$k(T),^b 10^{-13} \text{ cm}^3 \text{ molecule}^{-1} \text{ s}^{-1}$		
210	6.40 ± 0.24 0.33–1.5 (13)	5.1 ± 0.3 0.33–1.8 (10)	4.6 ± 0.2 0.66–2.3 (11)
220	6.78 ± 0.40 0.62–2.2 (4)	5.45 ± 0.10 0.32–2.2 (14)	5.39 ± 0.07 0.33–2.2 (8)
230	7.33 ± 0.18 0.32–2.1 (12)	6.00 ± 0.10 0.16–2.8 (35)	5.79 ± 0.09 0.32–2.1 (17)
250	8.08 ± 0.08 0.56–2.6 (12)	6.37 ± 0.10 0.29–2.5 (25)	7.32 ± 0.12 0.29–2.0 (17)
272	9.15 ± 0.09 0.51–2.4 (12)	6.87 ± 0.10 0.26–2.4 (30)	8.84 ± 0.16 0.26–1.8 (15)
298	10.1 ± 0.15 0.26–1.8 (28)	7.58 ± 0.12 0.24–1.6 (17)	11.3 ± 0.2 0.12–0.82 (22)
330	11.8 ± 0.2 0.42–1.5 (8)	8.85 ± 0.20 0.13–1.5 (21)	14.3 ± 0.3 0.24–0.84 (8)
370	14.8 ± 0.5 0.19–1.3 (7)	10.9 ± 0.2 0.11–1.2 (27)	18.6 ± 0.5 0.22–7.5 (9)
420	19.0 ± 0.3 0.12–0.83 (18)	13.5 ± 0.3 0.13–1.6 (24)	24.3 ± 0.4 0.20–1.0 (20)
480	24.2 ± 0.5 0.081–0.68 (28)	17.7 ± 0.3 0.16–1.6 (41)	33.4 ± 0.7 0.16–1.1 (16)

^a The italicized values represent reactant concentration range, 10^{14} molecule/cm³ (number of points in parentheses). ^b Uncertainties represent statistical levels of confidence of 95% and do not include an estimated uncertainty of 4% associated with possible systematic errors.

absorption cell with the optical path length L . $I_0(\lambda)$ and $I_{[\text{BP}]}(\lambda)$ are the radiation intensities measured after the absorption cell when the bromopropane concentration was zero and [BP], respectively. The complete spectrum of each compound was constructed from data taken over several overlapping wavelength ranges. Data over each spectral range were obtained at 5 to 6 pressures of each bromoalkane to verify adherence to the Beer–Lambert absorption law. The total range of reactant pressures used for these measurements was 6.7 Pa to 20 kPa (0.05 Torr to 150 Torr). The coincidence of the contiguous parts of spectra taken over overlapping wavelength ranges was usually better than ca. 1%. The overall instrumental error associated with uncertainties in the path length, pressure, temperature stability, and the measured absorbance was estimated to be less than 2% over most of the wavelength range (up to 250 nm), increasing to ca. 10–20% above 250 nm due to increased uncertainty in measuring low absorbance values.

Reactants. The sample of *n*-propyl bromide (99% stated purity) and two samples of isopropyl bromide (99.2% and 99.8% stated purity) were obtained from Sigma-Aldrich Co. The sample of propane was obtained from MG Scientific gases. Our GC-MS and GC-FID analysis of the propane sample revealed ca. 0.04% of isobutane, the only reactive impurity presented in noticeable amount. The presence of isobutane at such a low level can result in an overestimation of the measured rate constant by only 0.2% at the lowest temperature in this study.⁹ Propene and ethene are the most undesirable reactive impurities that can be present in propane, since their OH reaction rate constants are approximately $3 \times 10^{-11} \text{ cm}^3 \text{ molecule}^{-1} \text{ s}^{-1}$ and $1.5 \times 10^{-11} \text{ cm}^3 \text{ molecule}^{-1} \text{ s}^{-1}$, respectively at 210 K.⁹ Fortunately, their presence can be easily detected by their extremely strong absorption near 170 nm.¹⁸ Therefore, in addition to GC analysis, we also measured the absorption spectrum of the propane sample between 165 and 175 nm in order to check for the possible presence of alkenes. Based on the results of UV absorption measurements, we conclude that the concentration of neither ethene nor propene exceeds 0.003% in the sample of propane. This level of alkene impurities cannot

cause any noticeable overestimation of the measured rate constant. Therefore, we used this sample without further purification after several freeze/pump/thaw cycles.

We analyzed the samples of nPB and iPB using GC-MS and GC coupled with a thermoconductivity detector. Results of these analyses are presented in Table 1. The GCs were calibrated by direct injections of the chemicals whose impurity levels could cause the greatest kinetic concern: propene, acetone, propanol, 2-propanol, toluene, and di-*n*-propyl ether. Other impurities should have an OH reactivity comparable with that of the bromopropanes under study and, therefore, cannot result in any noticeable overestimation of the measured rate constants. Another possible complication in the study of brominated compounds is contamination with molecular bromine, which is very reactive toward OH radicals.⁹ Fortunately, because Br₂ absorbs visible light, even a contamination level as low as ca. 0.01% is readily visible with the naked eye in transparent liquid samples. Analysis of the liquid samples of bromopropanes using a spectrophotometer revealed no absorption near 400 nm, thereby allowing us to estimate the bromine concentration to be less than ca. 0.002%. All experiments were performed with mixtures prepared from the liquid phase of the samples to ensure the absence of errors due to any impurities.

To eliminate errors associated with the presence of the reactive impurities we purified the nPB sample using a preparative scale gas chromatograph. Results of GC analyses of the purified sample are presented in Table 1. The residual impurities cannot result in any overestimation of the measured rate constant, and this purified sample was used for both kinetic and spectral measurements. In the case of iPB, we performed diagnostic measurements with both samples of different purity. At 220 K where the kinetic effect of impurities would be the greatest, the rate constant obtained using the 99.2% purity sample was about 10% larger than that obtained using the 99.8+% purity sample. This difference could be quantitatively assigned to OH reactions with the impurities at the abundances listed in Table 1 (with propene contributing approximately 80% of this difference and *i*-propanol the remainder). Consequently, all of the kinetic (and spectral) data reported here for iPB were obtained using mixtures prepared from the liquid phase of the 99.8+% purity sample. For both the kinetic and spectral measurements all bromopropane samples were used after outgassing by several freeze/pump/thaw cycles.

Results and Discussion

The rate constants obtained for the title reactions are presented in Table 2. Figure 1a shows the data obtained for propane along with the results of previous studies that were conducted below room temperature. The data obtained for *n*-propyl bromide and isopropyl bromide are presented graphically in Figures 2 and 3, respectively, along with those available from the literature. All three figures clearly illustrate that the Arrhenius plots for these reactions exhibit noticeable curvature over the temperature range of our study.

OH + CH₃-CH₂-CH₃. Arrhenius curvature has been reported by all groups who studied this reaction below room temperature using absolute techniques. A three-parameter fit to our data yields the following expression:

$$k_{\text{C}_3\text{H}_8}(T) = 1.96 \times 10^{-12} \times (T/298)^{1.83} \times \exp\{-167/T\} \text{ cm}^3 \text{ molecule}^{-1} \text{ s}^{-1} \quad (1)$$

This expression gives the rate constants that are within 1.7% of the values measured in the present work and reported in Table

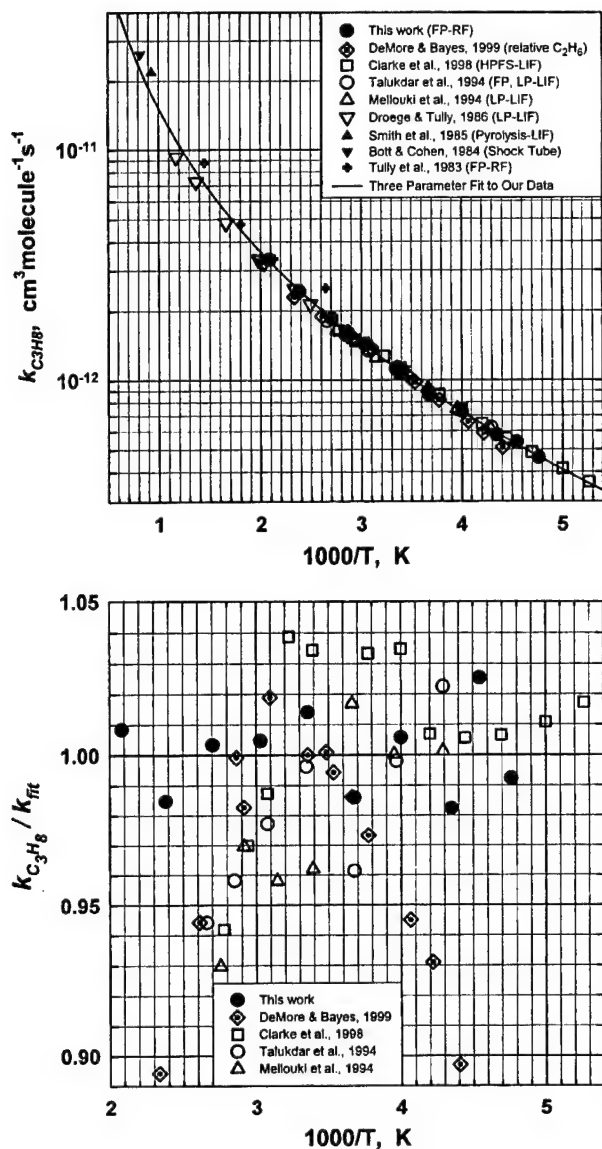


Figure 1. (a) Arrhenius plot for the reaction of OH with propane. (b) Rate constants for the reaction of OH with propane normalized to a three-parameter fit to the data from the present work.

2 (except for $k_{\text{C}_3\text{H}_8}$ (220 K), which is 2.5% higher). These deviations are smaller than the 95% statistical confidence intervals of individual determinations (again, except for $k_{\text{C}_3\text{H}_8}$ (220 K), which has the 95% confidence interval of 1.2%). Although derived from data below 480 K one can see from Figure 1a that this three-parameter fit reasonably describes the results of the higher temperature measurements including the latest and most comprehensive study,¹⁹ which was performed over the temperature interval between 293 and 854 K and probably supersedes the earlier results from the same laboratory²⁰ (less than 4% deviation below 430 K, which increases up to 16% at 854 K). This extrapolation agrees even with the available results of measurements at highest temperatures $T = 1075 \text{ K}$ ²¹ and $T = 1220 \text{ K}$ ²² (deviations are 25% and 16% respectively, well within the uncertainty of measurements).

Figure 1b shows all of the low-temperature data available in the literature normalized to the rate constants calculated from eq 1. One can see that the results of all absolute measurements below ca. 350 K agree with the above presentation to better than ca. 4% and their spread in Figure 1b is essentially random.

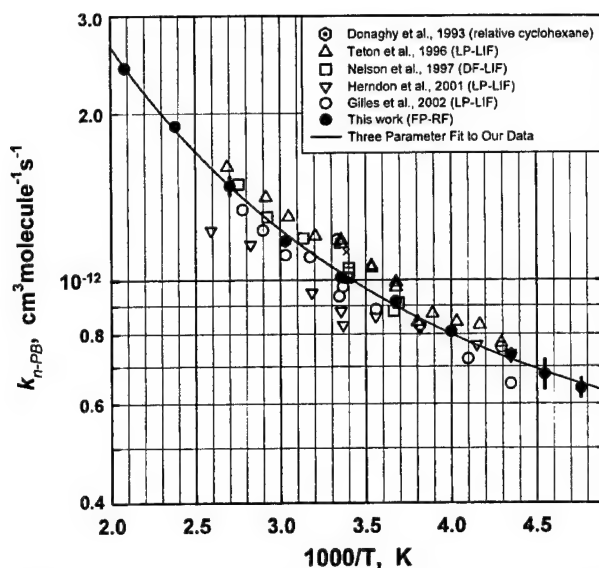


Figure 2. Arrhenius plot for the reaction of OH with *n*-propyl bromide.

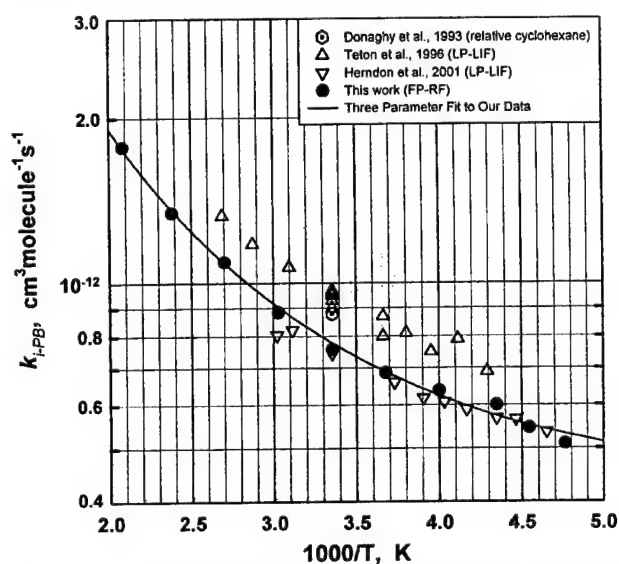


Figure 3. Arrhenius plot for the reaction of OH with isopropyl bromide.

The results of the relative rate measurements¹³ show no Arrhenius curvature and agree with the absolute data near room temperature with differences increasing to 10–11% at both lower and higher temperatures. This is seen from a parabolic shape of these data as presented in Figure 1b, which is suggestive of possible systematic errors in the measurements. For example, while the results of relative measurements accumulate the uncertainty of the reference reaction ($\text{OH} + \text{C}_2\text{H}_6$ in this particular case) along with their own possible instrumental error, no simple renormalization of the relative rate data will bring them into coincidence with the absolute studies. Recalculating the ratios reported in ref 13 using the rate constant for the reference reaction from the latest $\text{OH} + \text{C}_2\text{H}_6$ study performed over a temperature interval mainly below room temperature¹² decreases the low-temperature deviation to less than 7% while increasing the discrepancy above room temperatures. This is because all studies of the $\text{OH} + \text{C}_2\text{H}_6$ rate constant show essentially linear behavior of the Arrhenius plots as do the rate constant ratios ($k_{\text{C}_3\text{H}_8}/k_{\text{C}_2\text{H}_6}$) obtained in ref 13. We, thus, conclude that the rate constant for the reaction between

OH and propane has been well established by absolute measurement techniques over the temperature range of atmospheric interest and that the relative rate data from ref 13 underestimate the Arrhenius curvature.

Our data on the OH reaction with propane between 298 and 210 K can be represented by the standard Arrhenius expression with $k(298 \text{ K}) = 1.10 \times 10^{-12} \text{ cm}^3 \text{ molecule}^{-1} \text{ s}^{-1}$ and $E/R = 624 \text{ K}$.

All of the literature data below room-temperature yield about the same E/R factors (613 K,¹⁰ 613 K,¹¹ and 608 K¹²), except those obtained by a relative rate technique¹³ that yields $E/R = 745 \text{ K}$. Based on a combined fit to the data obtained at and below room temperature using absolute techniques, we recommend the following Arrhenius expression for use in atmospheric modeling:

$$k_{\text{C}_3\text{H}_8}(T < 300 \text{ K}) = 8.66 \times 10^{-12} \exp\{-615/T\} \text{ cm}^3 \text{ molecule}^{-1} \text{ s}^{-1} \quad (2)$$

OH + CH₂Br-CH₂-CH₃. The results obtained in the present work for the reaction between OH and *n*-propyl bromide are shown in Figure 2 together with existing literature data. A three-parameter fit to our data results in the following expression:

$$k_{\text{nPB}}(T) = 2.99 \times 10^{-13} \exp\{+369/T\} \times (T/298)^{2.79} \text{ cm}^3 \text{ molecule}^{-1} \text{ s}^{-1} \quad (3)$$

which gives the rate constants that are within 2% of the measured values reported in Table 2. Our results lie in the middle of the complete database for this reaction. Despite their higher scatter, most of the previously reported data are within 10% of the best fit to our results. In particular, our results are in very good agreement with the results of the discharge flow-LIF study reported in ref 3. A very recent paper by Gilles et al.⁸ reports new results obtained between 230 and 360 K that probably supersede the previously reported data from the same laboratory⁴ and are in better agreement with our data. As with propane, the data at and below room temperature are reasonably represented by a standard Arrhenius expression. A fit to the complete data set over this temperature region yields the expression

$$k_{\text{nPB}}(T < 300 \text{ K}) = 3.03 \times 10^{-12} \exp\{-330/T\} \text{ cm}^3 \text{ molecule}^{-1} \text{ s}^{-1} \quad (4)$$

This expression provides values for $k_{\text{nPB}}(298 \text{ K})$ and E/R identical with those obtained in this work and can be recommended for atmospheric modeling purposes. Using the parameterization of the NASA Panel for Data Evaluation, we recommend $k_{\text{nPB}}(298 \text{ K}) = 1.00 \times 10^{-12} \text{ cm}^3 \text{ molecule}^{-1} \text{ s}^{-1}$ and $E/R = 330 \text{ K}$ with an uncertainty factor (1 σ) of

$$f_{\text{nPB}}(T) = 1.1 \times \exp\left\{50 \times \left|\frac{1}{T} - \frac{1}{298}\right|\right\} \quad (5)$$

OH + CH₃-CHBr-CH₃. An Arrhenius plot for this reaction also exhibits noticeable curvature and a three-parameter fit to our data results in the following expression:

$$k_{\text{iPB}}(T) = 1.66 \times 10^{-13} \exp\{+461/T\} \times (T/298)^{2.95} \text{ cm}^3 \text{ molecule}^{-1} \text{ s}^{-1} \quad (6)$$

which gives rate constants that are within 4% of the values measured in the present work and reported in Table 2. The result

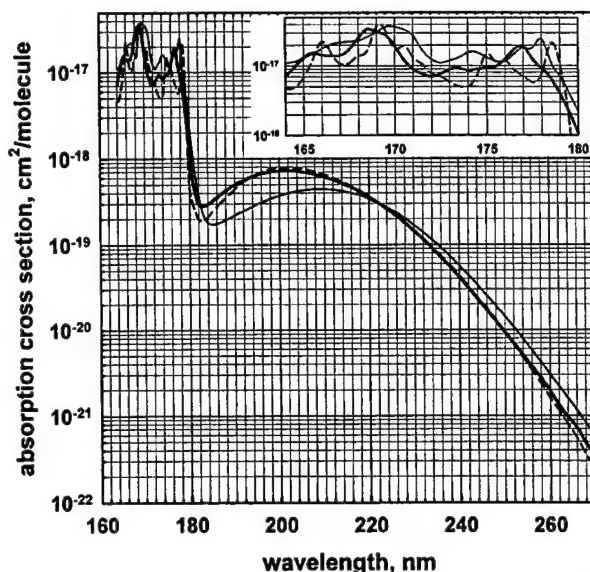


Figure 4. Ultraviolet absorption spectra for *n*-propyl bromide (solid thick line), isopropyl bromide (solid thin line), and methyl bromide (dashed line).

of this fit is shown in Figure 3 along with our data and data from the literature.

Our results for this reaction are in very good agreement with those reported in ref 4, the agreement being better than 4.5%, except at the highest temperature reported in ref 4 where it is 11%. The results of two other studies^{1,3} are systematically higher and the discrepancy with our data is greater than in the case of the CH₂Br-CH₂-CH₃ reaction.

The data at and below room temperature can be represented by a standard Arrhenius expression. A combined fit to our data and those from ref 4 yield the following expression, which is recommended for atmospheric modeling purposes:

$$k_{\text{iPB}}(T < 300 \text{ K}) = 1.77 \times 10^{-12} \exp\{-260/T\} \text{ cm}^3 \text{ molecule}^{-1} \text{ s}^{-1} \quad (7)$$

Using the parameterization of the NASA Panel for Data Evaluation, this corresponds to $k_{\text{iPB}}(298 \text{ K}) = 7.4 \times 10^{-13} \text{ cm}^3 \text{ molecule}^{-1} \text{ s}^{-1}$ and $E/R = 260 \text{ K}$, with an uncertainty factor (1 σ) of

$$f_{\text{iPB}}(T) = 1.15 \times \exp\left\{50 \times \left|\frac{1}{T} - \frac{1}{298}\right|\right\} \quad (8)$$

Ultraviolet Spectra. The ultraviolet absorption spectra of bromopropanes obtained in this work are presented in Figure 4 along with the spectrum of CH₃Br for comparison. We measured the CH₃Br spectrum between 164 and 180 nm and accepted the latest recommendation²³ between 180 and 270 nm. All three spectra look alike and have the same features at the shortest wavelengths characterizing the C-Br band absorption in alkanes. Table 3 lists the measured absorption cross sections with a step of 2 nm over the stratospheric transparency window near 200 nm. The detailed absorption cross sections over entire wavelength range are available in the Supporting Information and at www.nist.gov/kinetics/spectra/index.htm.

Atmospheric Implications. The atmospheric lifetimes of singly brominated propanes can be estimated based on the photochemical properties obtained in the present work. These compounds are very reactive toward OH while their absorption cross sections for tropospheric UV radiation (above 290 nm)

TABLE 3: Absorption Cross Sections of Bromopropanes between 180 and 230 nm at $T = 295$ K

wavelength, nm	absorption cross section, 10^{-19} , cm ² /molecule	
	CH ₂ Br-CH ₂ -CH ₃	CH ₃ -CHBr-CH ₃
180	10.85	22.02
182	2.99	3.65
184	2.95	1.82
186	3.56	1.76
188	4.27	1.94
190	4.98	2.21
192	5.65	2.48
194	6.25	2.80
196	6.70	3.13
198	7.02	3.43
200	7.18	3.73
202	7.26	3.99
204	7.12	4.20
206	6.88	4.35
208	6.52	4.42
210	6.10	4.42
212	5.65	4.36
214	5.15	4.22
216	4.66	4.01
218	4.14	3.74
220	3.58	3.41
222	3.08	3.07
224	2.60	2.71
226	2.18	2.36
228	1.78	2.02
230	1.44	1.68

are negligible (i.e., they are $<10^{-22}$ cm²/molecule and the chemicals are not photolyzed in the troposphere). However, accurate values of the shorter wavelength UV cross sections are required for calculating bromine release from nPB and iPB in the stratosphere and the ozone depletion potentials of such compounds.

The reactions with hydroxyl radicals in the troposphere thus dictate the atmospheric lifetimes of propane, *n*-propyl bromide, and isopropyl bromide. A simple scaling procedure has been proved to be valid for relatively long-lived compounds that are well mixed throughout the troposphere. For such chemicals, lifetimes can be estimated using the equation²⁴

$$\tau_i^{\text{OH}} = \frac{k_{\text{MC}}(272)}{k_i(272)} \cdot \tau_{\text{MC}}^{\text{OH}} \quad (9)$$

where τ_i^{OH} and $\tau_{\text{MC}}^{\text{OH}} = 5.9$ years are the atmospheric lifetimes of the compound of interest and methyl chloroform (MC), respectively, due to reactions with hydroxyl radicals in the troposphere only, and $k_i(272)$ and $k_{\text{MC}}(272) = 6.0 \times 10^{-15}$ cm³ molecule⁻¹ s⁻¹ (ref 23) are the rate constants for the reactions of OH with these substances at $T = 272$ K. The value of $\tau_{\text{MC}}^{\text{OH}} = 5.9$ years was obtained following the procedure used by Prinn et al.²⁵ from the measured lifetime of MC, $\tau_{\text{MC}} = 4.8$ years, when an ocean loss of 85 years and a stratospheric loss of 37 years are taken into account. Applying this method to the title compounds of this study yields the estimated atmospheric lifetimes of 14 days, 14 days, and 19 days for propane, *n*-propyl bromide, and isopropyl bromide, respectively. As can be seen, the lifetimes derived here are very short, much shorter than the characteristic time of mixing processes in the troposphere and hence are only crude estimates. The correct residence time of the compounds in the atmosphere will depend on the geographical location and season of the emissions as well as local atmospheric conditions. Some results of detailed atmospheric modeling can be found in the recent publications.^{6,7} Neverthe-

less, the presented estimations demonstrate that these chemicals are very short-lived ones, give reasonable average values of their lifetimes and a useful scaling among such compounds.

Acknowledgment. This work was supported by the Upper Atmosphere Research Program of the National Aeronautics and Space Administration. Certain commercial equipment, instruments, or materials are identified in this article in order to adequately specify the experimental procedure. Such identification does not imply recognition or endorsement by the National Institute of Standards and Technology, nor does it imply that the material or equipment identified are necessarily the best available for the purpose.

Supporting Information Available: The ultraviolet absorption cross sections of nBP and iBP are presented in Table 4. This material is available free of charge via the Internet at <http://pubs.acs.org>.

References and Notes

- (1) Donaghy, T.; Shanahan, I.; Hande, M.; Fitzpatrick, S. *Int. J. Chem. Kinet.* **1993**, *25*, 273–284.
- (2) Teton, S.; El Boudali, A.; Mellouki, A. *J. Chim. Phys.* **1996**, *93*, 274–282.
- (3) Nelson, D. D., Jr.; Wormhoudt, J. C.; Zahniser, M. S.; Kolb, C. E.; Ko, M. K. W.; Weisenstein, D. K. *J. Phys. Chem. A* **1997**, *101*, 4987–4990.
- (4) Herndon, S. C.; Gierczak, T.; Talukdar, R. K.; Ravishankara, A. R. *Phys. Chem. Chem. Phys.* **2001**, *3*, 4529–4535.
- (5) Wuebbles, D. J.; Jain, A. K.; Patten, K. O.; Connell, P. S. *Atmos. Environ.* **1998**, *32*, 107–113.
- (6) Bridgeman, C. H.; Pyle, J. A.; Shallcross, D. E. *J. Geophys. Res.* **2000**, *105*, D21, 26, 493–26, 502.
- (7) Wuebbles, D. J.; Patten, K. O.; Johnson, M. T.; Kotamarthi, R. *J. Geophys. Res.* **2001**, *106*, D13, 14551–14571.
- (8) Gilles, M. K.; Burkholder, J. B.; Gierczak, T.; Marshall, P.; Ravishankara, A. R. *J. Phys. Chem. A* **2002**, *106*, 5358–5366.
- (9) Mallard, W. G.; Westley, F.; Herron, J. T.; Hampson, R. F.; Frizzel, D. H. NIST Chemical Kinetics Database, Version 6.0; NIST: Gaithersburg MD, updated 1997.
- (10) Talukdar, R. K.; Mellouki, A.; Gierczak, T.; Barone, S.; Chiang, S.-Y.; Ravishankara, A. R. *Int. J. Chem. Kinet.* **1994**, *26*, 973–990.
- (11) Mellouki, A.; Teton, S.; Laverdet, G.; Quilgars, A.; Le Bras, G. *J. Chim. Phys.* **1994**, *91*, 473–487.
- (12) Clarke, J. S.; Kroll, J. H.; Donahue, N. M.; Anderson, J. G. *J. Phys. Chem. A* **1998**, *102*, 9847–9857.
- (13) DeMore, W. B.; Bayes, K. D. *J. Phys. Chem.* **1999**, *103*, 2649–2654.
- (14) Kurylo, M. J.; Cornett, K. D.; Murphy, J. L. *J. Geophys. Res.* **1982**, *87*, 3081–3085.
- (15) Orkin, V. L.; Huie, R. E.; Kurylo, M. J. *J. Phys. Chem.* **1996**, *100*, 8907–8912.
- (16) Orkin, V. L.; Khamaganov, V. G.; Guschin, A. G.; Huie, R. E.; Kurylo, M. J. *J. Phys. Chem.* **1997**, *101*, 174–178.
- (17) Orkin, V. L.; Louis, F.; Huie, R. E.; Kurylo, M. J. *J. Phys. Chem. A* **2002**, *106*, 10195–10199.
- (18) Orkin, V. L.; Huie, R. E.; Kurylo, M. J. *J. Phys. Chem.* **1997**, *101*, 9118–9124.
- (19) Droge, A. T.; Tully, F. P. *J. Phys. Chem.* **1986**, *90*, 1949–1954.
- (20) Tully, F. P.; Ravishankara, A. R.; Carr, K. *Int. J. Chem. Kinet.* **1983**, *15*, 1111–1118.
- (21) Smith, G. P.; Fairchild, P. W.; Jeffries, J. B.; Crosley, D. R. *J. Phys. Chem.* **1985**, *89*, 1269–1278.
- (22) Bott, J. F.; Cohen, N. *Int. J. Chem. Kinet.* **1984**, *16*, 1557–1566.
- (23) Sander, S. P.; Friedl, R. R.; Golden, D. M.; Huie, R. E.; Kurylo, M. J.; Orkin, V. L.; Ravishankara, A. R.; Kolb, C. E.; Molina, M. J.; Finlayson-Pitts, B. J.; Moortgat, G. K. *Chemical Kinetics and Photochemical Data for Use in Atmospheric Studies, Evaluation No. 14*; JPL Publication 02-XX; Jet Propulsion Laboratory, California Institute of Technology: Pasadena, CA, 2002.
- (24) Spivakovsky, C. M.; Logan, J. A.; Montzka, S. A.; Balkanski, Y. J.; Foreman-Fowler, M.; Jones, D. B. A.; Horowitz, L. W.; Fusco, A. C.; Brenninkmeijer, C. A. M.; Prather, M. J.; Wofsy, S. C.; McElroy, M. B. *J. Geophys. Res.* **2000**, *105*, 8931–8980.
- (25) Prinn, R. G.; Weiss, R. F.; Miller, B. R.; Huang, A.; Alyea, F. N.; Cunnold, D. M.; Fraser, P. J.; Hartley, D. E.; Simmonds, P. G. *Science* **1995**, *269*, 187–192.

The OH Reactivity and UV Spectra of Propane, n-Propyl Bromide, and Isopropyl Bromide.

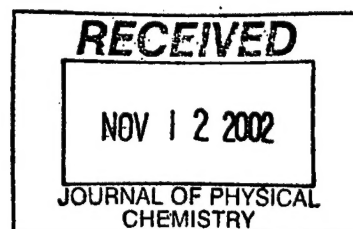
Sergey N. Kozlov, Vladimir L. Orkin, Robert E. Huie, and Michael J. Kurylo

Supporting Materials

Table 4. Absorption cross sections of bromopropanes between 164 nm and 270 nm at T = 295 K.

Wavelength, nm	Absorption cross section, 10 ⁻²⁰ , cm ² /molecule	
	CH ₂ BrCH ₂ CH ₃	CH ₃ CHBrCH ₃
164.0	707	1111
164.5	953	1146
165.0	1296	1290
165.5	1534	1495
166.0	1432	1773
166.5	1407	2044
167.0	1419	2174
167.5	1733	2246
168.0	2519	2319
168.5	3427	2634
169.0	3142	3075
169.5	2806	3713
170.0	1917	3681
170.5	1218	3391
171.0	894	2746
171.5	763	1685
172.0	706	1253
172.5	764	1103
173.0	890	1195
173.5	925	1322
174.0	863	1574
174.5	898	1565
175.0	931	1330
175.5	980	1181
176.0	1246	1175
176.5	1730	1484
177.0	1903	1829
177.5	1264	1815
178.0	927	2459
178.5	667	1145
179.0	397	707

SUPPLEMENTARY MATERIAL



REVISED

179.5	219	408
180.0	108.5	220.2
180.5	62.5	126.7
181.0	43.4	76.9
181.5	34.1	51.2
182.0	29.9	36.5
183.0	28.1	22.35
184.0	29.5	18.24
185.0	32.4	17.37
186.0	35.6	17.62
187.0	39.0	18.43
188.0	42.7	19.42
189.0	46.4	20.68
190.0	49.8	22.06
191.0	53.3	23.46
192.0	56.5	24.83
193.0	59.6	26.35
194.0	62.5	27.99
195.0	64.9	29.69
196.0	67.0	31.3
197.0	68.8	32.8
198.0	70.2	34.3
199.0	71.2	35.9
200.0	71.8	37.3
201.0	72.7	38.6
202.0	72.6	39.9
203.0	72.0	41.0
204.0	71.2	42.0
205.0	70.1	42.8
206.0	68.8	43.5
207.0	67.2	43.9
208.0	65.2	44.2
209.0	63.2	44.3
210.0	61.0	44.2
211.0	58.9	44.0
212.0	56.5	43.6
213.0	54.1	43.0
214.0	51.5	42.2
215.0	48.9	41.2
216.0	46.6	40.1
217.0	44.0	38.8
218.0	41.4	37.4
219.0	38.6	35.8
220.0	35.8	34.1

221.0	33.2	32.4
222.0	30.8	30.7
223.0	28.4	28.9
224.0	26.0	27.1
225.0	23.9	25.3
226.0	21.8	23.6
227.0	19.8	21.9
228.0	17.83	20.2
229.0	16.05	18.43
230.0	14.40	16.82
232.0	11.62	13.97
234.0	9.11	11.45
236.0	7.08	9.21
238.0	5.46	7.30
240.0	4.10	5.68
242.0	3.09	4.39
244.0	2.30	3.35
246.0	1.72	2.54
248.0	1.28	1.918
250.0	0.93	1.444
252.0	0.688	1.072
254.0	0.506	0.789
256.0	0.374	0.577
258.0	0.277	0.421
260.0	0.195	0.305
262.0	0.134	0.222
264.0	0.096	0.160
266.0	0.073	0.116
268.0	0.048	0.082
270.0	0.034	0.060